UMI Number: 9730405

UMI
300 North Zeeb Road
Ann Arbor, MI 48103

ABSTRACT

THE FATIGUE PROBLEMS OF CRACKS SUBJECTED TO OBLIQUELY INCIDENT STRESS WAVES

by
I-Chung Weng

Catastrophic failure of aircraft and other structures are often caused by undetected cracks. Fracture mechanics has been developed to augment traditional static and fatigue design. In the static theory of fracture mechanics, extensive treatment has been given to the stress distribution around sharp cracks and notches under various loading conditions. Previous works on the problems of dynamic loadings are not accurate in dealing with singularities at high frequencies. The numerical solutions become unrealistic at high frequencies in many practical applications.

To address the need to obtain the stress intensity factor in high frequency dynamic loading situations, we studied the use of dislocation to represent a crack by a continuous distribution of dislocation singularities. This study focused on the configuration of finite crack located in an infinite isotropic elastic solid which is subjected to harmonic shear waves. The most important contribution of this thesis is a new approach which is based on the development of dynamic dislocation model to investigate the dynamic problems of cracks, particularly the dynamic interaction between a surface crack and screw dislocations; dynamic interaction between a free surface and an internal crack; crack propagation under dynamic loadings. With this approach, we are able to derive the exact analytical expression for stress intensity factor at any given frequencies.

Results of the present investigation show the dynamic stress intensity factors will increase as the wave number (a measure of frequency of loadings) increases and the maximum value is about 25% more than the static stress intensity factor. At relatively high frequencies, the stress intensity factor drops rapidly beyond the first maximum value and exhibits oscillations of approximately constant period as wave number increases. This conclusion can be used to predict the useful life of a component at which consists of the crack propagation phase. The stress intensity factors at both sides of a finite crack have been performed for different inclined angle θ. The results show the right side stress intensity factor is bigger than the left side's when $0 < \theta < \pi/2$ or $3\pi/2 < \theta < 2\pi$.

The dynamic interaction between screw dislocations and a surface crack has been investigated. It has been found, under the periodic dynamic stress, the surface crack can be repelled by the dislocation with proper direction of the applied stress and the negative Burgers vector of the dislocation.

Simulation results of the dislocation model for an internal crack show that free surface effect plays a very important role in crack propagation. The stress intensity factors at crack tip which is nearest to the free surface suffer a sharp increase. It indicates that an internal crack close to a free surface could easily be extended to a surface crack.

At the end, an analysis of the scattering of horizontally shear waves by a finite extending uniformly crack has been carried out by using the dislocation method. It is found that the peaks of dynamic stress intensity factor decrease at normal incidence and almost the same magnitude for incident angles equal to 0 and π as propagation velocity increases.

THE FATIGUE PROBLEMS OF CRACKS SUBJECTED TO OBLIQUELY INCIDENT STRESS WAVES

by
I-Chung Weng

A Dissertation
Submitted to the faculty of
New Jersey Institute of Technology
in Partial Fulfillment of the Requirements for the Degree of
Doctor Philosophy

Department of Mechanical Engineering

May 1997

APPROVAL PAGE

THE FATIGUE PROBLEMS OF CRACKS SUBJECTED TO OBLIQUELY INCIDENT STRESS WAVES

I-Chung Weng

Dr. Zhiming Ji, Dissertation Advisor | Date
Associate Professor of Mechanical Engineering, NJIT

Dr. Bernard Koplik, Committee Member | Date
Professor and Chairman of Mechanical Engineering, NJIT

Dr. Benedict C. Sun, Committee Member | Date
Associate Professor of Engineering Technology, NJIT

Dr. Rong-Yaw Chen, Committee Member | Date
Professor of Mechanical Engineering, NJIT

Dr. Ansel C. Ugural, Committee Member | Date
Professor of Mechanical Engineering, NJIT

BIOGRAPHICAL SKETCH

Author: I-Chung Weng

Degree: Doctor of Philosophy

Date: May 1997

Undergraduate and Graduate Education:

- Doctor of Philosophy in Mechanical Engineering
  New Jersey Institute of Technology, Newark, NJ, USA, 1997

- Master of Science in Mechanical Engineering
  Stevens Institute of Technology, Hoboken, NJ, USA, 1993

- Bachelor of Mechanical Engineering
  Feng Chia University, Taichung, Taiwan, 1987

Major: Mechanical Engineering

Presentations and Publications:

I. C. Weng and Z. Ji,
"The Dynamic Stress Intensity Factor of Surface and Internal Crack Subjected to Obliquely Shear Waves," A Critical Link: Diagnosis to Prognosis for MFPT Society, pp. 553-562, April 1997.

I. C. Weng and Z. Ji,
"The Dynamic Interaction Between a Screw Dislocation and a Surface Crack," Proceeding of *25th CSCE Annual Conference,* Sherbrooke, Quebec, May 27-30 1997.

I. C. Weng and Z. Ji,
"The Dynamic Stress Intensity Factor of a Moving Crack Subjected to Obliquely Incident Shear Waves," *2nd JIMEC '97,* Jordan, June 1-5 1997.

This dissertation is dedicated to my family who always give me
their love, patience, courage and support in moments
of frustration, difficulties and despair

ACKNOWLEDGMENT

I would like to express my appreciation and sincere gratitude to my research advisor, Dr. Zhiming Ji, for his valuable patient guidance, counsel, and friendship throughout this research.

I am very grateful to Dr. R. Chen for his support at the moment of frustration. I also express my special thanks to Dr. B. Koplic, Dr. A. Ugural, Dr. B. Sun for their suggestions to improve this dissertation. I am also thankful to the Mechanical Engineering Department, New Jersey Institute of Technology for providing me with support during my Doctoral program.

Specially, I thank my wife Victoria for her patience, comfort, and support in the darkest moments of my life. I also extend my thanks to my parents for their support throughout my life, without them, my efforts are useless.

Finally, I extend my thanks to THE LORD. He leads me beside quiet waters, he restores my soul. He guides me in paths of rightness for his name's sake. I will fear no evil, for he is with me.

TABLE OF CONTENTS

TABLE OF CONTENTS
(Continued)

Chapter | Page

TABLE OF CONTENTS
(Continued)

LIST OF TABLES

Table **Page**

LIST OF FIGURES

LIST OF FIGURES
(Continued)

LIST OF FIGURES
(Continued)

LIST OF SYMBOLS

S	strain energy density factor
K	stress intensity factor
W	strain energy density
$\overset{n}{T_i}$	traction vector
u_i , x_i	displacement components
s	path around the dislocation distribution
$D(s)$	density function
b	Burgers vector
ν	Poisson ratio
$p(x)$	internal pressure
w_k	the anti-plane displacement component
w_0	the amplitude of the applied wave
ω	the frequency of the applied wave
θ	the angle of incidence measured from the x-axis
α	wave number
c	shear wave velocity given by $(\mu/\rho)^{1/2}$
μ	shear modulus
ρ	mass density
w^*	the imaginary component of w_k
σ^*	anti-plane stress
$d(r)$	total displacement at point (x, y) when a shear wave is incident normally on the screw dislocation

LIST OF SYMBOLS
(Continued)

u	the amplitude of the screw dislocation
J_0 , J_2	the zeroth and the second order of the first kind of Bessel function
J, Y	polynomials defined in Eqs. 2.13a, 2.13.b
$A_1(s)$	power series defined in Eq. 2.17a
$A_2(s)$	power series defined in Eq. 2.17b
Y_0 ,Y_2	the zeroth and the second order of the second kind of Bessel function
$p(x)$	phase lag
γ	the Euler constant
K_{III}	the stress intensity factor of tearing mode
$T_n(x)$	the first kind of Chebyshev Polynomial
$U_n(s)$	the second kind of Chebyshev Polynomial
A_{mn} ,B_{mn} C_{mn} , η_m ν_m	integrals defined in Eqs. 2.20a, 2.20b
A, B, C	matrix defined in Eq. 2.22
$\vec{\eta}$, $\vec{\nu}$	vectors defined in Eq. 2.22
K^L_{III}	left side stress intensity factor
$p_1(s)$	phase lag of the surface crack modeled by a continuous distribution of screw dislocation
$p_2(x_0)$	phase lag of the dislocation at $(x_0, 0)$
L	crack length

LIST OF SYMBOLS
(Continued)

$\vec{a}', \vec{a}''$	vectors defined in Eqs. 3.8a, 3.8b
$\chi, \varepsilon, \xi, \eta$	polynomials defined in Eqs. 3.2a, 3.2b
$\vec{b}', \vec{b}''$	vectors defined in Eqs. 3.8a, 3.8b
$\vec{R}, \vec{f}, \vec{g}$	vectors defined in Eqs. 3.5a, 3.5b, 3.10
K_S	stress intensity factor due to stress field of the dislocation
K_C	stress intensity factor due to the applied SH waves
G_{III}	crack extension force
x_0	distance from crack tip to the screw dislocation
$p_2(x_1)$ $p_2(x_2)$	phase lags of screw dislocations at $(x_1, 0)$ and $(x_2, 0)$
χ_1, ξ_1, χ_2 ξ_2	polynomials defined in Eqs. 3.15a, 3.15.b
$\vec{a}''', \vec{b}'''$	vectors defined in Eqs. 3.18a, 3.18b
$\vec{f}_1, \vec{f}_2$ $\vec{g}_1, \vec{g}_2$	vectors defined in Eqs. 3.18a, 3.18b
$\vec{R}_1, \vec{R}_2$	vectors defined in Eqs. 3.21a, 3.21b
$S(x)$	stress field of normalized length of a surface crack
σ_a	applied stress
$S'(x)$	stress field of normalized length of an internal crack
$E(\kappa)$	first kind of complete elliptic integrals

LIST OF SYMBOLS
(Continued)

$G(\kappa)$	second kind of complete elliptic integrals
$\lvert H_{III}\rvert^{R}$	stress intensity factors at right-hand of the internal crack
$\lvert H_{III}\rvert^{L}$	stress intensity factors at left-hand of the internal crack
X, Y, Z	moving coordinate system
x, y, z	stationary coordinate system
M^*	Mach number
ω^*	apparent circular frequency
φ	apparent incidence angle
β, λ, ε	dimensionless coefficient defined in Eq. 5.2
c_2	crack propagation speed
ϑ , r_2, ϕ_2	coefficients defined in Eqs. 5.14a, 5.14b, 5.15
τ_{φ}	maximum circumferential shear stress

PREFACE

In traditional material science and machine design, materials are normally assumed to be homogeneous, especially for the purpose of predicting the life cycle of structures. However, the engineering materials do contain microcracks from which failure starts. In general, there are many factors that cause the cracks to grow in machine body, such as high temperature, continuous loading or impact loading etc. Sometimes, the growth of crack may destroy the machine structure during general use. So design based on homogeneity assumption of material is not sufficient when the failure caused by the growth of cracks is to be considered. Therefore, most of the times, the traditional material science can deal with most of the engineering problems, but the fracture mechanics must be considered when the machine structure contains the microcracks.

Previous works on the crack problems have been focused mostly on the specific configurations with static loadings - infinite crack, semi-infinite crack, Griffith crack and so on. Early experimental work points to strong correlation between the growth of cracks and cyclic stress intensity factor range. Since loadings in most of the practical applications are dynamic, solutions for the static problems have limited usage.

The present research work uses the dislocation models to simulate the cracks under dynamic loading conditions. Under harmonic loading, a crack is known to extend in an unstable manner whenever the stress intensity factor exceeds a critical value. The stress intensity factors are calculated based on the crack size and location, stress magnitude and direction, and material properties such as shear modulus and mass density. The result can be used to predict the useful life of a component at any frequencies.

Simulation results of the model are compared with that other previous works at low frequencies to ensure its correctness. This dissertation is organized as follows:

Chapter 1: A brief introduction on research in fracture mechanics including scientific and historic background.

Chapter 2: Development of dislocation model for the surface crack and finite crack subjected to dynamic loadings.

Chapter 3: Extension of the concept of dislocation model to analyze the dynamic interaction between a surface crack and multi screw dislocations.

Chapter 4: Extension of the concept developed in Chapter 2 to analyze the dynamic interaction between an internal crack and the free surface.

Chapter 5: Extension of the concept of dislocation model to derive stress intensity factors of a moving crack (crack propagation).

Chapter 6: Conclusion of the present research work and includes recommendations for further research and improvements are discussed in this chapter.

CHAPTER 1

INTRODUCTION

Fracture mechanics methodology is based on the assumption that all engineering materials contain cracks from which failure starts. Cracks result in high stress elevation in the neighborhood of the crack tip, which should receive particular attention since it is at that point that further crack growth takes place. Many of the conventional criteria, such as maximum normal stress, critical stress intensity factor or energy release rate, etc., had some limited success in analyzing the simpler crack problems, but are found to be inadequate and often invalid for the more complex situations. Their works are limited in the elasticity and linearity of material or structure behavior and symmetry between load and crack orientation. There remains much to be done in dynamic problems that can be employed to assure the safety of engineering structures.

1.1 Background of Research

From the viewpoint of fracture mechanics, the knowledge of the state of the stress and displacement around the crack point is one of the key requirements for a fracture strength analysis of structural members weakened by flaws. First, Irwin (1957) proposed a mathematical crack model classifying the near stress field into three fracture models. Any deformation of the crack surface can result from a superposition of these basic deformation modes. He is also the first to recognize the general applicability of the singular stress field and introduced the concept of the stress intensity factor to measure the strength of the stress field.

In the static elasticity, extensive treatment has been given to problems involving the stress distribution around sharp cracks and notches under various loading conditions. As an instance of application to fracture mechanics, the two dimensional elliptical hole solution became the basis of almost all present day theories of brittle fracture. For example, Mal, Loeber and Sih (1969) made a detailed study of the displacement and the stress fields in the vicinity of the crack due to an incident antiplane shear wave. Although Mal showed that his method can be extended to yield information on the near field as well as the far field at any given frequencies, it is still very difficult to derive the exact solutions due to mathematical complexity. Thesher and Smith (1972) computed the stress intensity factor of a part-through circular segment in a plate. Also due to mathematical complexity, previous works on the dynamics problem have been limited mostly to some special configurations, such as a semi-infinite crack or an array of infinite collinear cracks. Jain and Kanwal (1972) used the approximation method to find out the stress distributions of two cracks of equal length, which lied on the same plane under SH loading. Their results are valid only at low and intermediate frequencies (wave number $\alpha<2$, see section 2.3 for the definition of wave number) where α is the wave number. Takakuda (1983) used the Boundary Integration method to derive the stress intensity factors from two randomly located parallel cracks. Ju and Chen (1992) presented statistical micromechanical formulations to investigate effective elastic moduli of two dimensional brittle solids with interacting slit microcracks. Karim and Awal (1992) used a hybrid finite element method to analyze the guided waves scattering in a plate containing multiple cracks at arbitrary orientations. Numerical results show the effects of cracks in a form of changes impulse shapes of the displacements on the surface of the plate. But the size of the finite element zone to be considered has been found to be independent of the wavelength of the input waves within the low frequency considered. Mikata (1993) investigated reflection and transmission of elastic waves by a period array of coplanar cracks. The results are limited to this special configuration and valid at low frequencies ($\alpha < 1.9$). Although Meguid and Wang (1994) analyzed the dynamic interaction of a main crack with an arbitrary located and oriented microcrack based upon the use of self-consistent iterative procedure and integral transform techniques which were performed by previous application, the procedure showed the difficulties with solving the Fourier transforms resulted from the wave equations.

Freund (1974) presented the Wiener-Hopf method to derive the stress intensity factors due to normal impact loading of an semi-infinite crack. He divided the displacements of the semi-infinite crack surface into two parts. One comes from the stress distribution along the crack surface and second is due to the displacements of dislocation climbing. From the stress distribution of the semi-infinite crack, he found out that the displacements due to stress distribution along the crack surface is not equal to zero. This result contradicts with the boundary condition that requires displacements to be zero at the crack surface because of symmetry. Thus, Freund used a superposition method to adjust the displacements of dislocation climbing so that the total displacements at that position satisfy the boundary condition. This superposition method is used as a foundation in this dissertation for developing an effective method to get the solutions of the stress intensity factors for cracks located in an elastic infinite isotropic elastic solid which is subjected to harmonic shear waves.

1.2 Classical Concepts in Fracture Mechanics

One of the important items to be considered in the design of engineering structures is stress analysis. Through this analysis, the magnitude and direction of the stresses and strains at various points of the structure are known. Then criterion of failure is selected for determining the type of material to be used for each element of the structure. The traditional approach is to design the structural element such that the applied stresses are kept below the yield strength of the material with proper safety factor. Such an approach is adequate for low strength and medium strength material provided that the materials are free from mechanical defects. It is now a common knowledge that the conventional design criteria cannot adequately describe the failure of high strength material because they are particularly sensitive to the presence of flaws or mechanical defects that are inherent in the material. Although the concept of stress concentration has been acknowledged in the calculation of stresses in the vicinity of holes, notches and other types of geometric discontinuities, nevertheless, the "stress concentration factor" itself is not a criterion of failure. This factor merely indicates the ratio of the elevation of the local stress to that of the applied stress.

In the case of a mathematically sharp crack, the stress concentration at the crack tip is very high and becomes infinite. This result is obviously of no use to the designer who adopts the traditional failure criterion since the magnitude of the crack tip stresses is always many times greater than that of the yield stress. The estimation on the remaining life of cracked parts requires a new discipline which is not covered by the conventional theories of failure. In practice, many structures have failed by unstable crack propagation at normal stress levels considerably less than the yield strength of the material. Such failures indicate that flaws can greatly influence the load carrying capacity of the structure. The cause of the problem is that many of these flaws cannot be detected either during the time of manufacturing or the life span of the structure. It is apparent that defects which cannot be avoided in many of the engineering materials cause a distribution of the stresses which must be accounted for in the prediction of the load at failure.

1.2.1 Stress Concentration

The first attempt to put forth a rational theory of fracture mechanics was made by Griffith (1921) who laid down the condition under which a small crack in a solid becomes unstable. His analytical model is based on the elasticity solution of an elongated cavity in the form of an ellipse. The idea is to focus attention on the stress distribution around a cavity. Referring to Figure 1.1, the maximum stress σ_m occurs at the apex of the major axis.

1.2.2 Stress Intensity Factor

Linear fracture mechanics technology has been rapidly gaining acceptance as an effective tool in design for the prevention of brittle fracture. A basic assumption in applying this technology is that all engineering materials possess flaws or mechanical defects no matter how carefully they were fabricated. The idea is to focus attention in a small region around the tip of the crack where fracture is most likely to take place and to ensure that the surrounding material has adequate toughness. This provides the designer with an extra material parameter for measuring the resistance of a material against fracture in addition to the conventional material property data such as yield strength. Such quantity was briefly refereed to as fracture toughness. The stress intensity factor can be interpreted as the critical value of the intensity of the stress field in the immediate vicinity of a sharp crack tip as shown in Figure 1.2. When the load or crack size is kept below the point of unstable crack extension, the magnitude of this stress field is measured by the so-called "stress intensity factor" K:

$$\begin{aligned}
\sigma_x &= \frac{K}{\sqrt{2\pi r}}\cos\frac{\theta}{2}\left(1-\sin\frac{\theta}{2}\sin\frac{3\theta}{2}\right)+\ \ldots \\
\sigma_y &= \frac{K}{\sqrt{2\pi r}}\cos\frac{\theta}{2}\left(1+\sin\frac{\theta}{2}\sin\frac{3\theta}{2}\right)+\ \ldots \\
\tau_{xy} &= \frac{K}{\sqrt{2\pi r}}\cos\frac{\theta}{2}\sin\frac{\theta}{2}\cos\frac{3\theta}{2}+\ \ldots
\end{aligned} \tag{1.1}$$

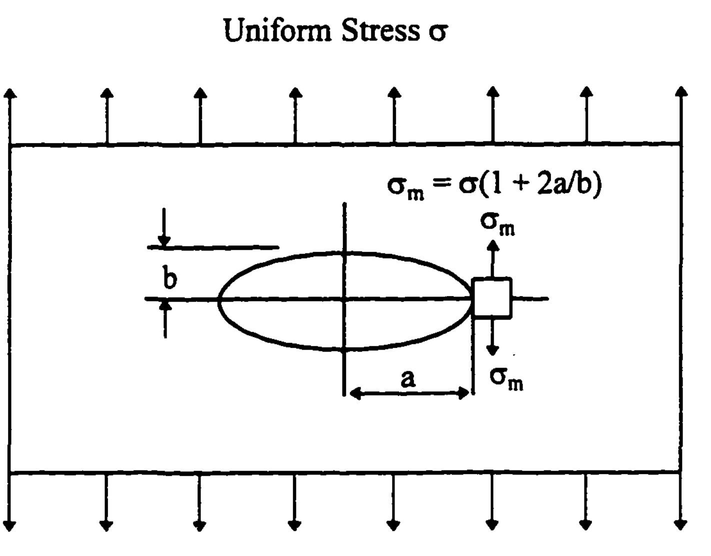

Figure 1.1 Elliptical cavity

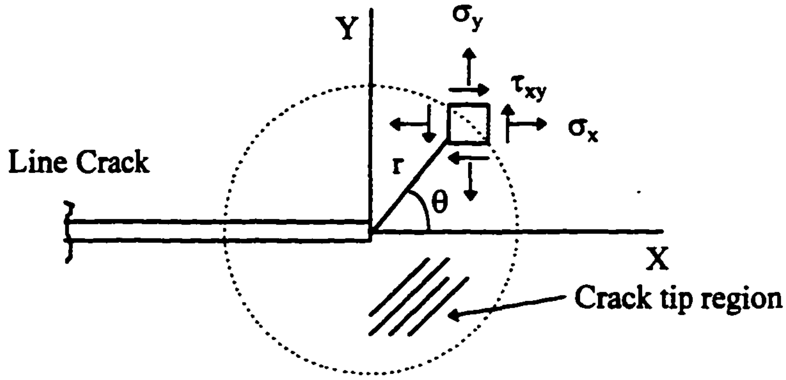

Figure 1.2 Stress element near crack tip

1.2.3 The Strain Energy Density Concept

Sih (1973) proposed a theory of fracture mechanics based on the field strength of the local strain energy density which marks a fundamental departure from the classical and current concepts. The theory requires no calculation on the energy release rate and thus possesses the advantage of being able to treat all mixed mode crack extension problems. Also it is for the description of failure of a material element by yielding . However, it was later realized many materials failure is due to fatigue damage. As a result, it is limited on the applications of dynamic loadings. This theory is developed on the basis of a strain energy density factor S for a material element at a finite distance r_0 from the point of failure initiation (Figure 1.3). Note that S is defined by:

$$S = r_0 \frac{dW}{dV} \tag{1.2}$$

where $\frac{dW}{dV}$ is the strain energy density function per unit volume. The strain energy density concept displays two fundamental hypotheses on crack initiation and direction.

Hypothesis (1): The crack will spread in the direction of maximum potential energy density.

Hypothesis (2): Crack extension occurs when the strain energy density factor reaches a critical value.

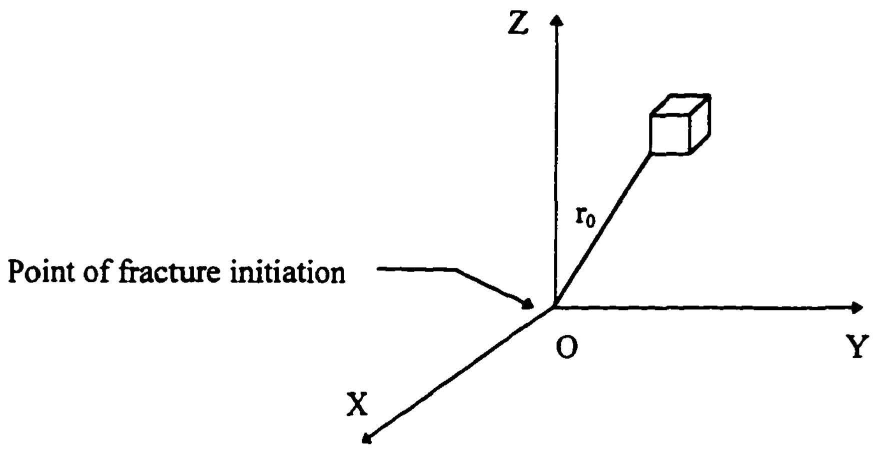

Figure 1.3 Spherical core region surrounding point O of failure initiation and a material element outside the core region.

1.3 Crack Modeling

Consider a plane crack extending through the thickness of a flat plate and let the crack plane occupy the plane XZ and the crack front be parallel to the Z-axis. Place the origin of the system OXYZ at the midpoint of the crack front. It was first pointed out by Irwin (1957) who proposed a mathematical crack model classifying the near stress field into three fracture models. Any deformation of the crack surface can result from a superposition of these basic deformation modes, which are defined as follows:

(a) *Opening mode*, I. The crack surfaces separate symmetrically with respect to the planes XY and XZ (Figure 1.4a).

(b) *Sliding mode*, II. The crack surfaces slide relative to each other symmetrically with respect to the plane XY and skew-symmetrically with respect to the plane XZ (Figure 1.4b).

(c) *Tearing mode*, III. The crack surfaces slide relative to each other skew-symmetrically with respect to the plane XY and XZ (Figure 1.4c).

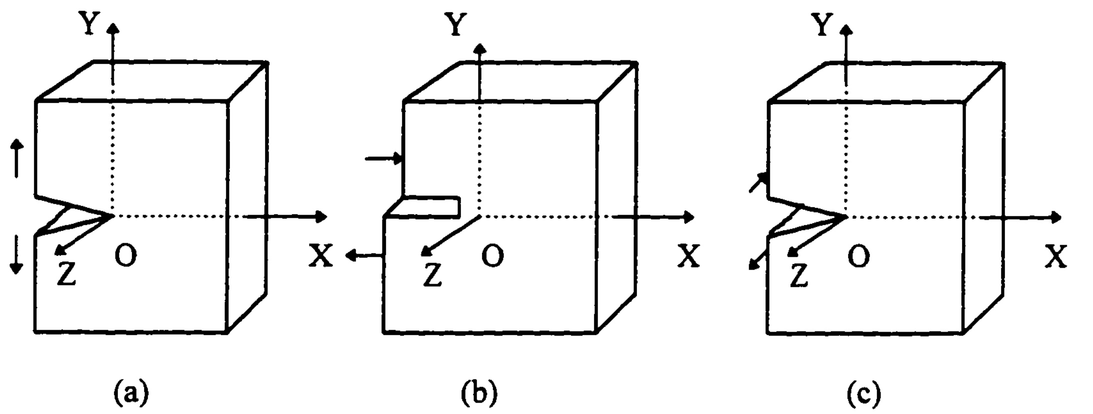

Figure 1.4 The three basic modes of crack extension. (a) Opening mode, I. (b) sliding mode, II, and (c) tearing (or antiplane) mode, III.

1.3.1 J-Integral Fracture Criterion

The mathematical formulation of conservation laws applicable in elastostatics in the form of path independent integrals of some functions of the elastic field over the bounding surface of a closed region originates from the work of Rice (1968). The path independent nature of the integral allows the integration path to be taken close to or sufficiently far from the crack tip. For the particular case of the two-dimensional plane elastic problem, consider the integral:

$$J = \int_{c} W dn_i - \int \overset{n}{T_i} \frac{\partial u_i}{\partial x_i} ds \qquad (1.3)$$

Where W is the strain energy density, $\overset{n}{T_i}$ and n_i are the traction vector and normal vector directed at a point on the contour c surrounding the crack tip respectively, u_i and x_i are displacement components and s is a measure of arc length along c. The path independence of J implies that plastic deformation being an irreversible process must be excluded from the system. For ductile fracture, there are too many fundamentally unsolved difficulties concerning the association of J. Even for the elastic case, it is limited to two dimensions.

1.3.2 Crack Opening Displacement Criterion

The critical crack opening displacement (COD) was proposed by Wells (1961) for the study of crack initiation in situations where significant plastic deformation precedes fracture. Under such conditions it is argued that the stresses around the crack tip reach the critical value and therefore fracture is controlled by the amount of plastic strain. One measure of the crack tip plastic strain is the separation of the crack faces or crack opening displacement. It is expected that crack extension begins when the crack opening displacement reaches some critical value which is characteristic of the material at a given temperature, plate thickness, strain rate and environmental conditions. Early experimental evidence suggested that COD gives a reasonable prediction of global instability if the amount of yielding near the crack tip is sufficiently small. In general, this criteria seems to be applicable only when the crack tip stress is perturbed only slightly from linear elasticity.

1.3.3 Eigenfunction Expansion Method

The method of eigenfunction expansion introduced by Williams (1957) is the most direct way of finding the structure of the stress field in the neighborhood of the crack tip. Followed the method of complex potentials, he expressed the displacements and the stresses components in plane elasticity problems as two unknown complex potentials and solved them from strain energy concepts. Stress intensity factors for a number of edge crack specimens are obtained by Strawley and Gross (1966), using the eigenfunction expansion solution.

1.3.4 Conformal Mapping Method

In many crack problems involving complicated geometry, it is convenient to use conformal transformation where the physical problem is mapped to a region with a unit circle or to a half plane. The method was used extensively by Bowei (1964) who developed polynomial mapping approximations to complicated configurations involving cracks in finite plates and emanating from the boundary of circular holes.

1.4 Interaction of Elastic Waves with A Crack

There are two closely related crack problems in elastodynamic which are important in the field of fracture mechanics. These are the problems of a stationary and moving crack subjected to loads that vary with time. The load may be periodic in time or applied suddenly to the elastic body. As in all crack problems, the detailed stress field near the crack tip must be known before any fracture analyses could be performed. If the crack is stationary, it is desirable to predict the level of applied stress at which the crack begins to spread.

Ang and Knopoff (1964) obtained approximate expressions for the displacement produced at large distances from the crack due to obliquely incident longitudinal and shear waves under the assumption that the wave lengths are large compared to the crack width. Loeber and Sih (1968) made a detailed study of the displacement and the stress fields. Unfortunately, their results are valid only at low and intermediate frequencies. Although Mal (1969) used two Helmholtz equations which satisfied the Riemann-Hilbert problem to determine the diffraction of normally incident longitudinal and antiplane shear waves on a Griffith crack and showed his method can be extended to yield information on the near field as well as the far field at any given frequencies, it is still very difficult to derive the exact solutions due to mathematical complexity. Jain and Kanwal (1972) used the approximation method to find out the stress distributions of two equal length of cracks which lied on the same plane under SH (antiplane shear wave) loading.

Freund (1974) presented the Wiener-Hopf method to derive the stress intensity factors due to normal impact loading of an semi-infinite crack. Stone and Ghosh (1980) found out the diffraction of antiplane shear waves by an edge crack. They inserted the displacements due to the incident, reflected, and scattered waves into wave equation to satisfy the boundary conditions. Furthermore, Takakuda (1983) used the Boundary

Integration method to derive the stress intensity factors of two randomly located parallel cracks.

1.5 Objective and Scope of Research

In contrast to static mechanics, both mathematical and experimental difficulties are encountered in the efforts to understand dynamic fracture phenomena. In recent years a considerable amount of research has been directed towards the solution of problems involving wave reflection by cracks in elastic media in an effort to improve an understanding of the behavior of material failure under dynamic loadings. In conventional studies of a single surface crack subjected to uniformly dynamics loading, the solution can be obtained by integral transform methods together with the direct application of the wave equations which satisfy the boundary conditions. However, the wave equations can not be applied to an internal crack due to the effect of the free surface. In other words, earlier works on dynamics problems are limited to the special configurations.

The main approach of the present study is to provide a dislocation model based on the mirror image with respect to the free surface of a surface crack or an internal crack, and verify these models by appropriate other works and computer simulation. It has been developed to determine the stress intensity factors at the crack tip in a semi-infinite isotropic elastic solid which is subjected to periodic cyclic loadings. This model represents a crack by a continuous distribution of dislocation singularities. With this goal, a few applications to solve the interaction between a crack and dislocations under dynamic loadings have been developed. Dynamic results obtained for these dislocation models have been compared with the earlier work at low frequencies. Following research results are presented in this thesis:

- Considering the dislocation concept applied to static crack problem and the works of Lee (1986), we represent a mirrored surface crack subjected to SH (horizontal polarized shear waves) with an array of screw dislocations. Similarly, we model the cracks subjected to P (primary waves) or SV (vertical polarized shear waves) with two arrays of edge dislocations: one vibrates on its glide plane and the other along its climbing direction. By using the conformal mapping technique and the numerical solution for edge crack subjected to anti-plane shear and inplane waves, the distribution densities of the dislocations as well as the phase lags are expressed as a system of singular integral equations, which contains Bessel functions.

- The above dislocation model is extended to investigate the dynamic interaction between the surface cracks and screw dislocations. The effects of the wave number, the input incident angle and the dislocation on the stress intensity factor are presented. In this model, the stable position as well as the strain energy are also considered in analyzing the drag and repelled forces between cracks and dislocations.

- Dislocation model for a moving crack has been developed. The effects of the wave number, the input incident angle and Mach number on the stress intensity factors are studied.

- Computer simulations: A crack model has been developed in NISA ENDURE program for analyzing the fatigue performance and fracture characteristics of engineering structures which operates on Crack Opening Displacement and J Integral theories. The singularities of the crack tip are also presented from the results of displacements and stress distributions. This results can be used to verify the results of dislocation models developed on superposition method. Some results reported in previous works have also been used for comparing the presented models and NISA simulations.

CHAPTER 2

STATIONARY DYNAMIC DISLOCATION MODEL

2.1 Introduction

Early fracture mechanics researchers considered dynamic effects, but only for the special case of single crack problem. More recently, fracture mechanics has been extended to include the interaction of two randomly oriented and located crack problems. Most of newer approached are based on generalizations of the wave equations. Loeber and Sih (1968) displayed a detailed study of the displacement and the stress fields in the vicinity of the crack due to an incident antiplane shear wave. Their studies provided two Helmholtz equations which satisfied the Riemann-Hilbert conditions. They obtained two dual integral equations through Fourier transformation. Then a Fredholm integral equation of the second kind was derived for the two dual equations to determine reflected field. Due to mathematical complexity, previous works on the dynamics problem have been limited mostly to the special configurations, like the model of a semi-infinite crack or an array of infinite collinear cracks. Problems become more complicated when the equations of static equilibrium are replaced by the dynamic equations of motion. A part of the present study is focused to develop an analytical model to calculate the dynamic stress intensity factors at the crack tips. This study is an extension of previous work on static problems (see Chapter 2.2.1) which investigates the reflected waves for a screw dislocation under inclined shear waves. These reflected waves are due to the inhomogeneity of dislocation density. Previous works on this subject showed that if the input stress waves are SH waves, the reflected waves would also be SH waves. This result is equivalent to that produced from a crack. Thus the deformation at a crack can be modeled as a continuously distributed screw dislocation under SH waves.

The key problem is to find the proper density function of dislocation such that the fundamental solutions satisfy the boundary condition. The above discussion shows that the chosen dislocation model depends primarily on the type of input dynamics waves. From Eshelby's study (1949), we model the cracks subjected to P (primary waves) or SV (vertical polarized shear waves) shown in Figure 2.1 with two arrays of edge dislocations: one vibrates on its glide plane and the other along its climbing direction.

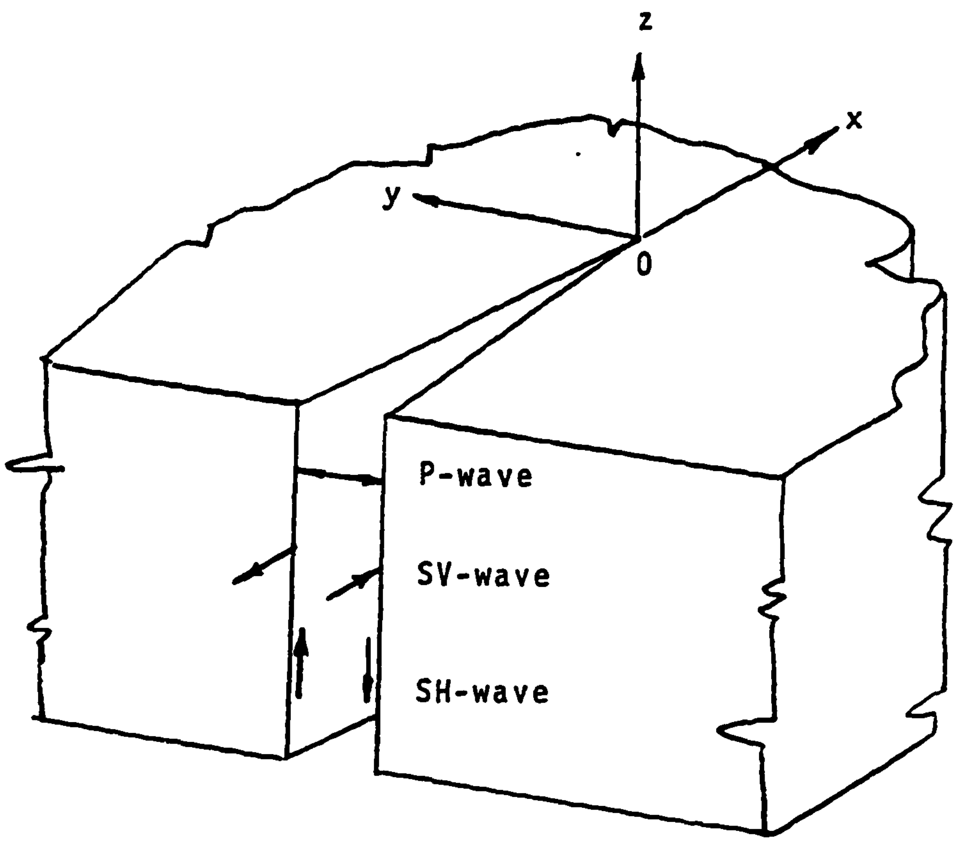

Figure 2.1 Three distinct types of input waves

Unfortunately, there are still many unsolved stress and displacement fields of reflected P and SV waves for edge dislocations. In this thesis, we consider a crack modeled as a continuously distributed screw dislocation under SH waves. This chapter presents a dislocation model based on the mirror image with respect to the free surface of a surface crack has been developed to determine the stress intensity factors at the crack tip in a semi-infinite isotropic elastic solid which is subjected to periodic cyclic loadings. The theoretical concepts developed in this study can be extended to derive the stress intensity factors of a surface crack interacting with multi screw dislocations and a moving crack problems. The research presented in this chapter has been partly reported in (Weng and Ji, 1997a).

2.2 Dislocation Concept

The best description of a dislocation is obtained from a study of its formation in the crystalline. As shown in Figure 2.2, (a) is a perfect, undeformed simple cubic lattice. Cut this lattice along any of the planes indicated in the auxiliary cubes. Let the atoms on one side of the cut shift in a direction parallel to the cut surface through a distance equal to one atom spacing. Then rejoin the atoms on either side of the cut. The lattice structure itself actually is almost perfect except near the lines AA. The line imperfections AA in the lattice are dislocation lines. The various types of dislocation lines are shown in Figure 2.2(b), (c), (d). If the atoms over the cut surface are shifted in a direction perpendicular to the line AA, an edge dislocation is created in the lattice (see Figure 2.2b); if the shift is parallel to AA, a screw dislocation is produced (shown in Figure 2.2c). The stress around the screw dislocation is everywhere a pure shear.

In order to describe the character of dislocation lines, a Burgers vector was introduced by J. M. Burgers (1932). Consider a screw dislocation shown in Figure 2.3. The starting point and the end point (the atoms shown solid) are one and the same atom in the case of the circuit that does not include the dislocation. However the starting point and ending points will not the same if the circuit enclose the dislocation. Thus there is closure failure in this circuit. The Burgers vector, pointing from the end point of the circuit to its beginning point, is defined to be the closure failure. In this case the closure failure leads to a vector 'b' parallel to the dislocation line. The dislocation loop could have been in any arbitrary shape. the only requirement is that the loop be closed. If a circular dislocation loop is made by shifting the atoms parallel to the plane of the loop, the character of each dislocation segment of the loop varies continuously from pure edge to mix to screw dislocation. It should be noted that segments on opposite sides of the loop are the same type of dislocation but have opposite sign.

2.2.1 Static Dislocation Model

When the concept of dislocation method applied to static problem, the crack is modeled by a continuous distribution of dislocations with the density function D(s). The density of the distribution is determined by satisfying boundary conditions. For cracks within elastic medium, a Burgers vector of D(s)ds is used as the Burgers vector of an infinitesimal dislocation of density D(s) at location x = s. By analogy with the definition of a physical dislocation, the Burgers vector of a continuous dislocation is given by :

$$b = \int D(s)ds \tag{2.1}$$

where s is a path around the dislocation distribution.

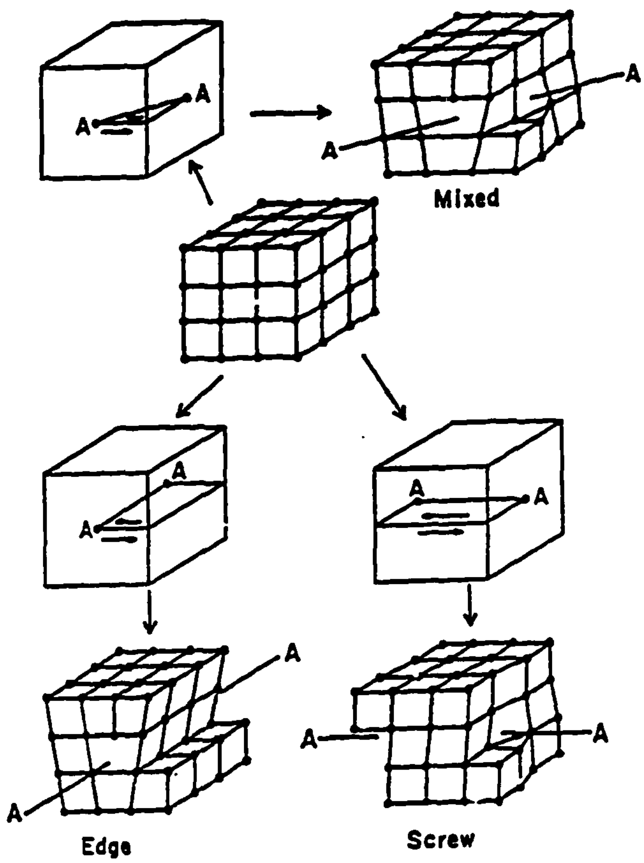

Figure 2.1 The creation of an edge, a screw dislocation

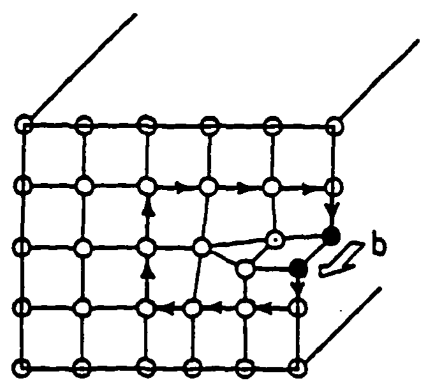

Figure 2.2 Burgers circuit around screw dislocation

Consider a crack in an infinite solid opened by an internal pressure p(x). The opening of the crack can be represented by an continuous dislocation of density D(s) lying along y = 0, |x| < a and having a Burgers vector b = $\int D(s)ds$. The dislocation causes stresses along y = 0 of

$$\sigma_y = -\sigma_x = \frac{2\mu}{\pi(1+\kappa)} \int_{-a}^{+a} \frac{D(s)ds}{(x-s)} \tag{2.2}$$

where $\kappa = (3 - 4\nu)$ in plane strain or $(3 - \nu)/(1 + \nu)$ in plane stress, ν is Poisson ratio, and μ is shear modulus. The boundary conditions on y = 0 are $\sigma_y = -p(x)$ for |x| < a and $\tau_{xy} = 0$ for all x. These conditions can be satisfied, using Eq. 2.2 by ensuring that

$$p(x) + \frac{2\mu}{\pi(1+\kappa)} \int_{-a}^{+a} \frac{D(s)ds}{(x-s)} = 0 \tag{2.3}$$

The solution of Eq. 2.3 for D(s) enables us to determine the stress intensity factor.

2.3 Theory of Dynamic Model

Surface cracks have been subjected to many studies and are well understood. For comparison purpose, we start our dynamic dislocation model with a surface crack. Consider a rectangular Cartesian coordinate system located at a free surface and normalize all lengths with respect to the width of the surface crack such that the surface crack occupies the region $0 \le x \le 1$, $y = 0$, $-\infty < z < \infty$, as shown in Fig. 2.4. The crack under investigation is defined as: A surface crack of infinite length ($-\infty < z < \infty$) and finite width lied in the xz plane of a homogeneous, isotropic, elastic, semi-infinite solid. It is assumed that the displacement components u_i and v_i in the x and y directions are quite small compared to that in anti-plane direction (z direction) and are considered to be negligible. Normally, the harmonic shear wave has a displacement field polarized in the plane perpendicular to y direction, i.e., the xz-plane. The shear wave can be further decomposed into two waves, one with a displacement vector parallel to the x-axis (SV), and the other with displacement vector parallel to the z-axis (SH).

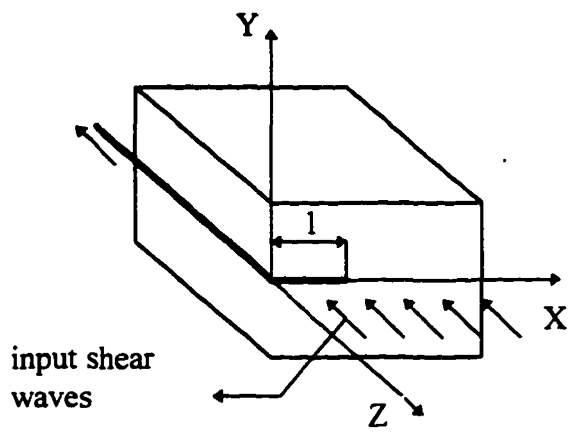

Figure 2.4 Surface crack $(0 \leq x \leq 1)$

For the case of harmonic shear waves (SV, SH) impinging on a semi-infinite crack lying along the x-axis, Sih (1968) found out the in anti-plane displacement component of the incident field at point (x, y) can be expressed as:

$$w_k = w_0 \exp\{-i[\alpha(x\cos\theta + y\sin\theta) - \omega t]\}$$

$$= w_0 \cos[\alpha(x\cos\theta + y\sin\theta) - \omega t] - i w_0 \sin[\alpha(x\cos\theta + y\sin\theta) - \omega t] \qquad (2.4)$$

where w_0 and ω are the amplitude and frequency of the applied wave, w_k is the anti-plane displacement component, θ is the angle of incidence measured from the x-axis and $\alpha = \omega/c$ is the wave number, with c being the shear wave velocity given by $(\mu/\rho)^{1/2}$. μ is the shear modulus and ρ the mass density. Table 2.1 gives the shear wave velocity of three materials for example. The displacement w_k can be decomposed into real (SV) and imaginary (SH) components which are parallel to x-axis and y-axis respectively. This study concentrates on the stress intensity factor of mode III. The anti-plane stress under SH waves can be derived from the equation $\tau = -\mu\partial w^{\bullet}/\partial y$ and $w^{\bullet}$ by taking the imaginary component of Eq. 2.4:

$$\sigma^{\bullet} = \sigma_0 \sin\theta \cos[\alpha(x\cos\theta + y\sin\theta) - \omega t] \tag{2.5}$$

where $\sigma_0 = w_0\mu\alpha$, $\sigma^{\bullet}$ is the anti-plane stress. According to the theories of dislocation-modeling technique and complex variable method (Juang and Lee, 1986), the problem is now equivalent to that of a mirror image of the surface crack with respect to the free surface. The problem is now changed to a finite crack of length 2 in an infinite medium as shown in Fig. 2.5.

Table 2.1 Shear wave velocity of materials

Material	steel(mild)	titanium	iron(cast)
c (km/sec)	3.2	3.1	3.2

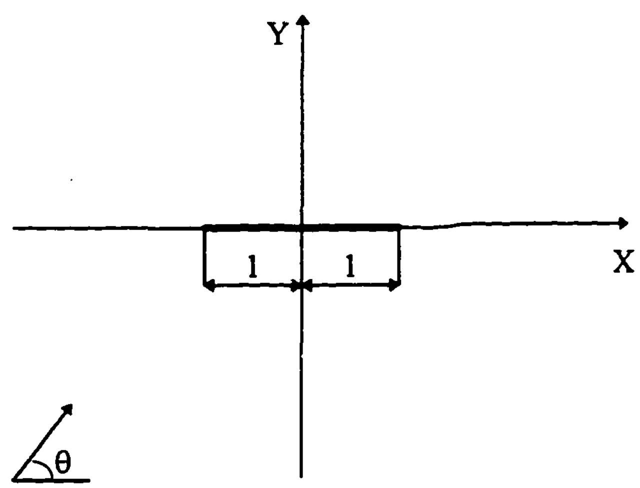

SH wave on xz plane

Figure 2.5 A surface crack and its image

Now, the surface crack is modeled by a continuous distribution of a screw dislocation parallel to the z axis. When the input shear waves meet this dislocation, these waves are reflected due to the inhomogeneity of dislocation density. Previous works on this subject showed that if the input stress waves are SH waves, the reflected waves would also be SH waves. This result is equivalent to that produced from a crack. Thus the deformation at a crack can be modeled as a continuous distribution of screw dislocation under SH waves. From Eshelby's study (1949), the total displacement at point (x, y) when a shear wave is incident normally on the screw dislocation is:

$$d(r) = \frac{\alpha bu}{4}\left(\frac{2}{\pi\alpha r}\right)^{1/2}\cos[\omega t+p(r)]\sin\theta \qquad (2.6)$$

where $r = (x^2+y^2)^{1/2}$, u is the amplitude of the screw dislocation and b is the Burger's vector. Another approach related to the interaction of screw dislocations and sound waves was studied by Nabarro (1951). He derived the total displacement as follows:

$$d(r) \approx \left(\frac{2}{\pi\alpha r}\right)^{1/2} Au\cos[\omega t+p(r)]\sin\theta \qquad (2.7)$$

Comparing Eqs. 2.6, and 2.7, we can get $A \approx \alpha b/4$. Nabarro showed that the scattered wave may be represented by Bessel functions of order 1. The anti-plane displacement is:

$$w(r) = Au\sin\theta\{J_1(\alpha|r|)\cos[\omega t+p(r)] + Y_1(\alpha|r|)\sin[\omega t+p(r)]\} \qquad (2.8)$$

Since the total surface traction should be zero along the crack surface, the input inclined shear stress must equal to the scattered stress. Inserting Eq. 2.8 into $\tau = -\mu\partial w(x)/\partial y$, the anti-plane stress wave released along y = 0 plane as :

$$\sigma_d(x) = B\alpha^2\{[J_0(\alpha|x|) + J_2(\alpha|x|)]\cos[\omega t+p(x)] + [Y_0(\alpha|x| + Y_2(\alpha|x|)]\sin[\omega t+p(x)]\} \qquad (2.9)$$

where $B = -bu\mu/8$, $p(x)$ is the phase lag, and J_0 and J_2 are the zeroth order and the second order of the first kind of Bessel function respectively. Similarly, Y_0 and Y_2 are the zeroth order and the second order of the second kind of Bessel function.

Using the concept of dislocation method applied to static problem, similar formulations can be made for dynamic problems. The total stress wave released from the screw dislocation from $-1 \le x \le 1$ can be expressed as the convolution of the density function and the released stress wave:

$$\sigma_T = \int_{-1}^{1} D(s)\,\sigma_d(x-s)ds = \int_{-1}^{1} D(s)\,B\alpha^2\{[J_0(\alpha|x-s|)+J_2(\alpha|x-s|)]\cos[\omega t+p(s)]+[Y_0(\alpha|x-s|)$$

$$+Y_2(\alpha|x-s|)]\sin[\omega t+p(s)]\}ds \tag{2.10}$$

From Eq. 2.5, stress σ^* along the crack surface (y=0 plane) is $\sigma^* = \sigma_0\sin\theta\cos(\alpha x\cos\theta-\omega t)$. Since the total surface traction should be zero along the crack surface, we have $\sigma_T + \sigma^* = 0$ along the $y = 0$ plane. Therefore,

$$\int_{-1}^{1} D\,B\alpha^2\{[J_0(\alpha|x-s|) + J_2(\alpha|x-s|)]\cos[\omega t+p(s)] + [Y_0(\alpha|x-s|) + Y_2(\alpha|x-s|)]\sin[\omega t+p(s)]\}ds$$

$$= -\sigma_0\sin\theta\cos(\alpha x\cos\theta-\omega t) \tag{2.11}$$

After expanding $\cos[\omega t+p(s)]$, $\sin[\omega t+p(s)]$, and $\cos(\alpha x\cos\theta-\omega t)$, Eq. 2.11 may be expressed as:

$$\int_{-1}^{1} D(s)A\alpha^2\,[\,J\cos\omega t\cos p(s) + Y\sin\omega t\cos p(s) - J\sin\omega t\sin p(s) + Y\cos\omega t\sin p(s)\,]ds$$

$$= -\sigma_0\sin\theta\cos(\alpha x\cos\theta)\cos\omega t - \sigma_0\sin\theta\sin(\alpha x\cos\theta)\sin\omega t \tag{2.12}$$

From the coefficients of $\sin\omega t$ and $\cos\omega t$, we divide Eq 2.12 into two parts:

$$\int_{-1}^{1} D(s)\, B\alpha^2[Y\cos p(s) - J \sin p(s)]ds = -\sigma_0 \sin\theta \sin(\alpha x \cos\theta) \tag{2.13a}$$

$$\int_{-1}^{1} D(s)\, B\alpha^2[J\cos p(s) + Y\sin p(s)]ds = -\sigma_0 \sin\theta \cos(\alpha x \cos\theta) \tag{2.13b}$$

where $J = J_0(\alpha|x\text{-}s|) + J_2(\alpha|x\text{-}s|)$ and $Y = Y_0(\alpha|x\text{-}s|) + Y_2(\alpha|x\text{-}s|)$. There are two unknown functions D(s) and p(s) in Eqs. 2.13a, 2.13b. To make the problem easier to solve, we replace D(s) and p(s) with another two functions, $A_1(s)$ = D(s)Bcosp(s) and $A_2(s)$ = D(s)Bsinp(s). Since there is singularity in Y when the value of x approaches to s, we must separate Y into singular and regular parts. Expanding Eq. 2.13a and 2.13b (Appendix A), we have:

$$-4/\pi\,(s)\int_{-1}^{1} A_1/(x\text{-}s)^2 ds + 2\alpha^2/\pi \int_{-1}^{1} A_1(s) J \ln(\alpha|x\text{-}s|)ds + \int_{-1}^{1}\alpha^2\,[A_1(s)f(x,s) - A_2(s)J]ds$$

$$= -\sigma_0 \sin\theta \sin(\alpha x\cos\theta) \tag{2.14a}$$

$$-4/\pi \int_{-1}^{1} A_2(s)(/(x\text{-}s)^2 ds + 2\alpha^2/\pi \int_{-1}^{1} A_2(s) J\ln(\alpha|x\text{-}s|)ds + \int_{-1}^{1}\alpha^2\,[A_2(s)f(x,s) + A_1(s)J]ds$$

$$= -\sigma_0 \sin\theta \cos(\alpha x\cos\theta) \tag{2.14b}$$

where $f(x,s) = -1/\pi + 2/\pi[(\gamma\text{-}\ln 2)J_0(\alpha|x\text{-}s|) - \ln 2 J_2(\alpha|x\text{-}s|)]$

$$-2/\pi \sum_{j=0}^{\infty}(-1)^j\,(\alpha/2)^{2j+2}(x\text{-}s)^{2j+2}\left[\frac{\Psi(j+1)+\psi(j+3)}{2\,j!(2+j)!} - \frac{\Psi(j+2)+\gamma}{[(j+1)!]^2}\right],$$

with the Euler constant $\gamma \cong 0.577215665$, and $\Psi(j) = -\gamma + \sum_{k=1}^{j-1}(1/k)$, $j > 1$. Our problem is now to find unknown functions $A_1(s)$ and $A_2(s)$ that satisfy Eqs. 2.14a, 2.14b and would converge when x approaches s. The dynamic stresses around a small circle centered at the crack tip ($r_2 \to 2a$ and $\phi_2 \to 0$) under shear waves can be expressed as:

$$\tau_{yz} = \frac{K_{III}}{\sqrt{2r_i}} \cos(\phi_i/2) \tag{2.15a}$$

$$\tau_{xz} = -\frac{K_{III}}{\sqrt{2r_i}} \sin(\phi_i/2) \tag{2.15b}$$

where r_i and ϕ_i ($i = 1, 2$) are shown in Fig. 2.6. K_{III} is the stress intensity factor for tearing mode. That means the stress intensity factors at the tip of the crack rely on existence of the $r^{1/2}$ stress singularity.

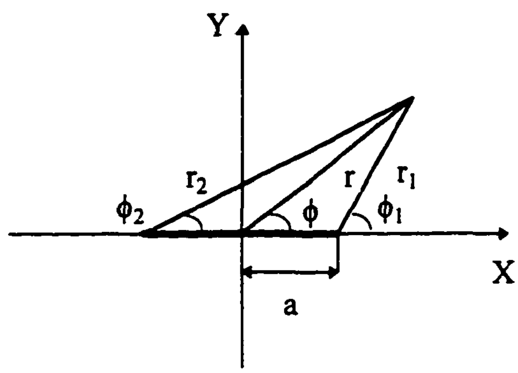

Figure 2.6 Definitions of r_i and ϕ_i

To determine the $A_1(s)$ and $A_2(s)$ in Eqs. 2.14a and 2.14b, it is necessary to solve the singularities in both $\int_{-1}^{1} A_1(s)/(x-s)^2 ds$ and $\int_{-1}^{1} A_2(s)/(x-s)^2 ds$. According to the Simpson integration method, the integration of f(x) can be expressed as follows:

$$\int_a^b f(x)dx \approx \sum_{k=1}^{n} f(x_k)(\Delta x)_k \tag{2.16}$$

where $(\Delta x)_k = S_n$ (b-a), and S_n is defined as: $\left\{ \begin{array}{ll} n \text{ is odd} & S_n = (b-a)\{\frac{1}{2}, 1, 1, \ldots, \frac{1}{2}\} \\ n \text{ is even} & S_n = (b-a)\{1, 4, 2, 4, \ldots 2, 4\} \end{array} \right.$,. With this observation, the $A_1(s)$ and $A_2(s)$ can be expressed in terms of the $(1-s^2)^n$. From above equations, we can assume $A_1(s)$ and $A_2(s)$ contain the term $(1-s^2)^{1/2}$. In order to converge the values of $A_1(s)$ and $A_2(s)$, we express the $A_1(s)$ and $A_2(s)$ in power series forms:

$$A_1(s) = (1-s^2)^{1/2} \sum_{n=0}^{\infty} a_n U_n(s) \tag{2.17a}$$

$$A_2(s) = (1-s^2)^{1/2} \sum_{n=0}^{\infty} b_n U_n(s) \tag{2.17b}$$

where $U_n(s)$ is the second kind of Chebyshev Polynomial. The definitions of $U_n(s)$ is based on Rivlin (1974):

$$T_n(\cos\varphi) = \cos(n\varphi),\ x = \cos(\varphi),\ U_{n-1}(s) = \frac{T'(x)}{n} = \frac{\sin(n\varphi)}{\sin(\varphi)} \tag{2.18}$$

where $T_n(x)$ is the first kind of Chebyshev Polynomial. According to Eq. 2.18, the $U_n(s)$ converges faster than traditional power series method. With this method, we can deal with more complicated power series problems. Integrating both sides of Eqs. 2.14a and 2.14b and substituting $A_1(s)$ and $A_2(s)$ from Eqs. 2.17a and 2.17b, we have:

$$\sum_{n=0}^{\infty} a_n \{-4/\pi \int_{-1}^{1} U_m(x)(1-x^2)^{1/2} \int_{-1}^{1} \frac{U_n(s)}{(x-s)^2}(1-s^2)^{1/2}\, ds dx + \alpha^2 \int_{-1}^{1} U_m(x)(1-s^2)^{1/2}$$

$$\int_{-1}^{1} [\frac{2}{\pi} J \ln(\alpha|x-s|) + f(x,s)] U_n(s)(1-s^2)^{1/2}\, ds dx\} - \sum_{n=0}^{\infty} b_n \alpha^2 \int_{-1}^{1} U_m(x)(1-x^2)^{1/2} \int_{-1}^{1} J U_n(s)(1-$$

$$s^2)^{1/2} ds dx = -\int_{-1}^{1} U_m(x)(1-x^2)^{1/2} [\sigma_0 \sin\theta \sin(\alpha x \cos\theta)] dx \tag{2.19a}$$

$$\sum_{n=0}^{\infty} b_n \{-4/\pi \int_{-1}^{1} U_m(x)(1-x^2)^{1/2} \int_{-1}^{1} \frac{U_n(s)}{(x-s)^2}(1-s^2)^{1/2}\, ds dx + \alpha^2 \int_{-1}^{1} U_m(x)(1-s^2)^{1/2}$$

$$\int_{-1}^{1}[\frac{2}{\pi}J\ln(\alpha|x-s|)+f(x,s)]U_n(s)(1-s^2)^{1/2}dsdx\}+\sum_{n=0}^{\infty}a_n\alpha^2\int_{-1}^{1}U_m(x)(1-x^2)^{1/2}\int_{-1}^{1}JU_n(s)(1-$$

$$s^2)^{1/2}dsdx = -\int_{-1}^{1}U_m(x)(1-x^2)^{1/2}[\sigma_0\sin\theta\cos(\alpha x\cos\theta)]dx \qquad (2.19b)$$

where m = 0, 1, 2, 3, ..., M, ...∞ and n = 0, 1, 2 3, ..., N, ..., ∞. Since U_n does not vanish when n approaches ∞, a_n and b_n should converge to zero as n approaches ∞. Therefore we assume that the problem can be approximated with the following series:

$$\sum_{n=0}^{N}[(A_{mn}+B_{mn})a_n - C_{mn}b_n] = \eta_m \quad (m = 0, 1, ..M) \qquad (2.20a)$$

$$\sum_{n=0}^{N}[C_{mn}a_n + (A_{mn}+B_{mn})b_n] = \nu_m \quad (m = 0, 1, ..M) \qquad (2.20b)$$

where $A_{mn} = -4/\pi\int_{-1}^{1}U_m(x)(1-x^2)^{1/2}\int_{-1}^{1}\frac{U_n(s)}{(x-s)^2}(1-s^2)^{1/2}dsdx = \begin{cases} 0 & m\neq n \\ 2(n+1)\pi & m=n \end{cases}$

$$B_{mn} = \alpha^2\int_{-1}^{1}U_m(x)(1-s^2)^{1/2}\int_{-1}^{1}[\frac{2}{\pi}J\ln(\alpha|x-s|)+f(x,s)]U_n(s)(1-s^2)^{1/2}dsdx$$

$$C_{mn} = \alpha^2\int_{-1}^{1}U_m(x)(1-x^2)^{1/2}\int_{-1}^{1}JU_n(s)(1-s^2)^{1/2}dsdx$$

$$\eta_m = -\int_{-1}^{1}U_m(x)(1-x^2)^{1/2}[\sigma_0\sin\theta\sin(\alpha x\cos\theta)]dx$$

$$\nu_m = -\int_{-1}^{1}U_m(x)(1-x^2)^{1/2}[\sigma_0\sin\theta\cos(\alpha x\cos\theta)]dx$$

Appendix B provides the Eqs. 2.20a and 2.20b of integral terms in the above equations. Eqs. 2.20a and 2.20b contain 2(N+1) unknown coefficients a_n and b_n with

2(M+1) equations. To solve for a_n and b_n (n = 0, 1, ...,N), let M = N. The above equations can be put into matrix form as :

$$(A + B)\vec{a} - C\vec{b} = \vec{\eta} \tag{2.21a}$$

$$C\vec{a} + (A + B)\vec{b} = \vec{\nu} \tag{2.21b}$$

where vectors $\vec{a} = [\, a_0 , a_1 , a_2 ,.....,a_N \,]^T$ and $\vec{b} = [\, b_0 , b_1 , b_2 ,....,b_N \,]^T$. Matrices A, B, C, and vectors $\vec{\eta}, \vec{\nu}$ can be found numerically once M and N are selected. Our problem is now to find positive integers M and N such that a_n and b_n converge to zero. As a first approximation, let M and N equal to 9. In evaluating a_n and b_n , we find out the values of a_n and b_n would converge to zero if M, N > 5. Thus, let M and N equal to 5. Substituting Eq. 2.18 into Eqs. 2.20a and 2.20b, we can express matrices A, B, C, and vectors $\vec{\eta}, \vec{\nu}$ as follows (Appendix B):

$$A = \begin{bmatrix} 2\cdot\pi\cdot L^2 & 0 & 0 & 0 & 0 & 0 \\ 0 & 4\cdot\pi\cdot L^2 & 0 & 0 & 0 & 0 \\ 0 & 0 & 6\cdot\pi\cdot L^2 & 0 & 0 & 0 \\ 0 & 0 & 0 & 8\cdot\pi\cdot L^2 & 0 & 0 \\ 0 & 0 & 0 & 0 & 10\cdot\pi\cdot L^2 & 0 \\ 0 & 0 & 0 & 0 & 0 & 12\cdot\pi\cdot L^2 \end{bmatrix} \tag{2.22}$$

$$B = \begin{bmatrix} B_{00} & 0 & B_{02} & 0 & B_{04} & 0 \\ 0 & B_{11} & 0 & B_{13} & 0 & B_{15} \\ B_{20} & 0 & B_{22} & 0 & B_{24} & 0 \\ 0 & B_{31} & 0 & B_{33} & 0 & B_{35} \\ B_{40} & 0 & B_{42} & 0 & B_{44} & 0 \\ 0 & B_{51} & 0 & B_{53} & 0 & B_{55} \end{bmatrix}, \quad C = \begin{bmatrix} C_{00} & 0 & C_{02} & 0 & C_{04} & 0 \\ 0 & C_{11} & 0 & C_{13} & 0 & C_{15} \\ C_{20} & 0 & C_{22} & 0 & C_{24} & 0 \\ 0 & C_{31} & 0 & C_{33} & 0 & C_{35} \\ C_{40} & 0 & C_{42} & 0 & C_{44} & 0 \\ 0 & C_{51} & 0 & C_{53} & 0 & C_{55} \end{bmatrix}$$

$$\vec{\eta} = \begin{bmatrix} 0 \\ \eta_{10} \\ 0 \\ \eta_{30} \\ 0 \\ \eta_{50} \end{bmatrix}, \quad \vec{\nu} = \begin{bmatrix} \nu_{00} \\ 0 \\ \nu_{20} \\ 0 \\ \nu_{40} \\ 0 \end{bmatrix}$$

where L = 1 and the elements of matrices A, B, C, and vectors $\vec{\eta}, \vec{\nu}$ are listed as following:

$$B_{00} = -1.481492\cdot\alpha^2\cdot L^4 - .0587599\cdot\alpha^4\cdot L^6 + .0119351\cdot\alpha^6\cdot L^8 - 5.9201\cdot 10^{-4}\cdot\alpha^8\cdot L^{10} + 2.3205\cdot 10^{-5}\cdot\alpha^{10}\cdot L^{12}$$

$$-.9675027\cdot\alpha^2\cdot L^4 + .1341\cdot\alpha^4\cdot L^6 - 9.1149\cdot 10^{-3}\cdot\alpha^6\cdot L^8 + 3.8671\cdot 10^{-4}\cdot\alpha^8\cdot L^{10} - 1.1252\cdot 10^{-5}\cdot\alpha^{10}\cdot L^{12}$$

$$+\frac{2\ln(\alpha L)}{\pi} C_{00}$$

$$B_{20} = .7853982\cdot\alpha^2\cdot L^4 + .0197076\cdot\alpha^4\cdot L^6 + .010776\cdot\alpha^6\cdot L^8 - 4.1084\cdot 10^{-4}\cdot\alpha^8\cdot L^{10} + 1.4488\cdot 10^{-5}\cdot\alpha^{10}\cdot L^{12}$$

$$+ .06705\cdot\alpha^4\cdot L^6 - 8.2034\cdot 10^{-3}\cdot\alpha^6\cdot L^8 + 4.6405\cdot 10^{-4}\cdot\alpha^8\cdot L^{10} - 1.6074\cdot 10^{-5}\cdot\alpha^{10}\cdot L^{12} + \frac{2\ln(\alpha L)}{\pi} C_{20}$$

$$B_{40} = -4.0906\cdot 10^{-3}\cdot\alpha^4\cdot L^6 + 1.3585\cdot 10^{-3}\cdot\alpha^6\cdot L^8 - 1.1743\cdot 10^{-4}\cdot\alpha^8\cdot L^{10} + 5.4453\cdot 10^{-6}\cdot\alpha^{10}\cdot L^{12}$$

$$-9.1149\cdot 10^{-4}\cdot\alpha^6\cdot L^8 + 1.1048\cdot 10^{-4}\cdot\alpha^8\cdot L^{10} - 5.741\cdot 10^{-6}\cdot\alpha^{10}\cdot L^{12} + \frac{2\ln(\alpha L)}{\pi} C_{40}$$

$$B_{11} = -1.8325958\cdot\alpha^2\cdot L^4 + .1242094\cdot\alpha^4\cdot L^6 - .0117654\cdot\alpha^6\cdot L^8 + 7.4239\cdot 10^{-4}\cdot\alpha^8\cdot L^{10} - 2.6978\cdot 10^{-5}\cdot\alpha^{10}\cdot L^{12}$$

$$-.1341\cdot\alpha^4\cdot L^6 + .145839\cdot\alpha^6\cdot L^8 - 7.7292\cdot 10^{-4}\cdot\alpha^8\cdot L^{10} + 2.5689\cdot 10^{-5}\cdot\alpha^{10}\cdot L^{12} + \frac{2\ln(\alpha L)}{\pi} C_{11}$$

$$B_{31} = 3.646\cdot 10^{-3}\cdot\alpha^6\cdot L^8 - 3.5356\cdot 10^{-4}\cdot\alpha^8\cdot L^{10} + 1.6068\cdot 10^{-5}\cdot\alpha^{10}\cdot L^{12} + \frac{2\ln(\alpha L)}{\pi} C_{31}$$

$$+ .5235988\cdot\alpha^2\cdot L^4 + .0253618\cdot\alpha^4\cdot L^6 - 3.5932\cdot 10^{-3}\cdot\alpha^6\cdot L^8 + 8.309\cdot 10^{-5}\cdot\alpha^8\cdot L^{10} - 7.7505\cdot 10^{-6}\cdot\alpha^{10}\cdot L^{12}$$

$$B_{51} = -1.6363\cdot10^{-3}\cdot\alpha^4\cdot L^6 - 1.7291\cdot10^{-3}\cdot\alpha^6\cdot L^8 + 2.9047\cdot10^{-5}\cdot\alpha^8\cdot L^{10} - 2.9449\cdot10^{-6}\cdot\alpha^{10}\cdot L^{12}$$

$$-3.3412\cdot10^{-5}\cdot\alpha^8\cdot L^{10} + 3.0715\cdot10^{-6}\cdot\alpha^{10}\cdot L^{12} + \frac{2\ln(\alpha L)}{\pi}C_{51}$$

$$B_{02} = .06705\cdot\alpha^4\cdot L^6 - 8.2034\cdot10^{-3}\cdot\alpha^6\cdot L^8 + 4.6405\cdot10^{-4}\cdot\alpha^8\cdot L^{10} - 1.6074\cdot10^{-5}\cdot\alpha^{10}\cdot L^{12} + \frac{2\ln(\alpha L)}{\pi}C_{20}$$

$$+.392699\cdot\alpha^2\cdot L^4 + 3.3451\cdot10^{-3}\cdot\alpha^4\cdot L^6 + 9.3506\cdot10^{-3}\cdot\alpha^6\cdot L^8 - 7.4002\cdot10^{-4}\cdot\alpha^8\cdot L^{10} + 3.1957\cdot10^{-5}\cdot\alpha^{10}\cdot L^{12}$$

$$B_{22} = -.9817478\cdot\alpha^2\cdot L^4 - .0404972\cdot\alpha^4\cdot L^6 + 6.2847\cdot10^{-3}\cdot\alpha^6\cdot L^8 - 4.5629\cdot10^{-4}\cdot\alpha^8\cdot L^{10} + 1.9495\cdot10^{-5}\cdot\alpha^{10}\cdot L^{12}$$

$$-5.4689\cdot10^{-3}\cdot\alpha^6\cdot L^8 + 4.972\cdot10^{-4}\cdot\alpha^8\cdot L^{10} - 2.1701\cdot10^{-5}\cdot\alpha^{10}\cdot L^{12}$$

$$B_{42} = 3.2868\cdot10^{-5}\cdot\alpha^8\cdot L^{10} - 6.6975\cdot10^{-6}\cdot\alpha^{10}\cdot L^{12} + \frac{2\ln(\alpha L)}{\pi}C_{42}$$

$$+.392699\cdot\alpha^2\cdot L^4 + .0323159\cdot\alpha^4\cdot L^6 - 2.3744\cdot10^{-4}\cdot\alpha^6\cdot L^8 - 8.4898\cdot10^{-5}\cdot\alpha^8\cdot L^{10} + 8.342\cdot10^{-6}\cdot\alpha^{10}\cdot L^{12}$$

$$B_{13} = .2617994\cdot\alpha^2\cdot L^4 + .0212712\cdot\alpha^4\cdot L^6 - 3.8489\cdot10^{-3}\cdot\alpha^6\cdot L^8 + 2.9795\cdot10^{-4}\cdot\alpha^8\cdot L^{10} - 1.5767\cdot10^{-5}\cdot\alpha^{10}\cdot L^{12}$$

$$+3.646\cdot10^{-3}\cdot\alpha^6\cdot L^8 - 3.5356\cdot10^{-4}\cdot\alpha^8\cdot L^{10} + 1.6068\cdot10^{-5}\cdot\alpha^{10}\cdot L^{12} + \frac{2\ln(\alpha L)}{\pi}C_{13}$$

$$B_{33} = -1.1048\cdot10^{-4}\cdot\alpha^8\cdot L^{10} + 8.5732\cdot10^{-6}\cdot\alpha^{10}\cdot L^{12} + \frac{2\ln(\alpha L)}{\pi}C_{33}$$

$$-.6806784\cdot\alpha^2\cdot L^4 - .0114537\cdot\alpha^4\cdot L^6 - 1.7532\cdot10^{-3}\cdot\alpha^6\cdot L^8 + 7.4518\cdot10^{-5}\cdot\alpha^8\cdot L^{10} - 1.8524\cdot10^{-6}\cdot\alpha^{10}\cdot L^{12}$$

$$B_{53} = .3141592\cdot\alpha^2\cdot L^4 + 3.5062\cdot10^{-3}\cdot\alpha^4\cdot L^6 + 8.1934\cdot10^{-4}\cdot\alpha^6\cdot L^8 - 4.7929\cdot10^{-5}\cdot\alpha^8\cdot L^{10} + 2.5555\cdot10^{-7}\cdot\alpha^{10}\cdot L^{12}$$

$$+1.0802\cdot10^{-6}\cdot\alpha^{10}\cdot L^{12} + \frac{2\ln(\alpha L)}{\pi}C_{53}$$

$$B_{04} = -9.1149\cdot10^{-4}\cdot\alpha^6\cdot L^8 + 1.1048\cdot10^{-4}\cdot\alpha^8\cdot L^{10} - 5.741\cdot10^{-6}\cdot\alpha^{10}\cdot L^{12} + \frac{2\ln(\alpha L)}{\pi}C_{04}$$

$$+.0224985\cdot\alpha^4\cdot L^6 + 4.7644\cdot10^{-4}\cdot\alpha^6\cdot L^8 - 1.6884\cdot10^{-4}\cdot\alpha^8\cdot L^{10} - 8.1124\cdot10^{-6}\cdot\alpha^{10}\cdot L^{12}$$

$$B_{24} = .1963496\cdot\alpha^2\cdot L^4 + 6.1359\cdot10^{-3}\cdot\alpha^4\cdot L^6 + 7.5332\cdot10^{-4}\cdot\alpha^6\cdot L^8 - 1.0109\cdot10^{-4}\cdot\alpha^8\cdot L^{10} + 6.7978\cdot10^{-6}\cdot\alpha^{10}\cdot L^{12}$$

$$+ 3.2868\cdot10^{-5}\cdot\alpha^8\cdot L^{10} - 6.6975\cdot10^{-6}\cdot\alpha^{10}\cdot L^{12} + \frac{2\ln(\alpha L)}{\pi} C_{24}$$

$$B_{44} = -1.3395\cdot10^{-6}\cdot\alpha^{10}\cdot L^{12} + \frac{2\ln(\alpha L)}{\pi} C_{44}$$

$$+ .3141592\cdot\alpha^2\cdot L^4 + 3.5062\cdot10^{-3}\cdot\alpha^4\cdot L^6 + 8.1934\cdot10^{-4}\cdot\alpha^6\cdot L^8 - 4.7929\cdot10^{-5}\cdot\alpha^8\cdot L^{10} + 2.5555\cdot10^{-7}\cdot\alpha^{10}\cdot L^{12}$$

$$B_{15} = -8.181\cdot10^{-4}\cdot\alpha^4\cdot L^6 - 1.3879\cdot10^{-4}\cdot\alpha^6\cdot L^8 + 1.0663\cdot10^{-5}\cdot\alpha^8\cdot L^{10} - 2.8634\cdot10^{-8}\cdot\alpha^{10}\cdot L^{12}$$

$$-3.3412\cdot10^{-5}\cdot\alpha^8\cdot L^{10} + 3.0715\cdot10^{-6}\cdot\alpha^{10}\cdot L^{12} + \frac{2\ln(\alpha L)}{\pi} C_{15}$$

$$B_{35} = 1.0802\cdot10^{-6}\cdot\alpha^{10}\cdot L^{12} + \frac{2\ln(\alpha L)}{\pi} C_{35}$$

$$+ .1570796\cdot\alpha^2\cdot L^4 + 2.6681\cdot10^{-3}\cdot\alpha^4\cdot L^6 + 9.135\cdot10^{-5}\cdot\alpha^6\cdot L^8 + 6.4375\cdot10^{-6}\cdot\alpha^8\cdot L^{10} - 1.7028\cdot10^{-8}\cdot\alpha^{10}\cdot L^{12}$$

$$B_{55} = \frac{2\ln(\alpha L)}{\pi} C_{55}$$

$$-.426359\cdot\alpha^2\cdot L^4 - 2.6297\cdot10^{-3}\cdot\alpha^4\cdot L^6 + 4.1019\cdot10^{-4}\cdot\alpha^6\cdot L^8 - 7.2087\cdot10^{-5}\cdot\alpha^8\cdot L^{10} + 4.3102\cdot10^{-7}\cdot\alpha^{10}\cdot L^{12}$$

$$C_{00} = .1542126\cdot\alpha^4\cdot L^6 + 8.0319\cdot10^{-3}\cdot\alpha^6\cdot L^8 - 2.9283\cdot10^{-4}\cdot\alpha^8\cdot L^{10} + 7.6868\cdot10^{-6}\cdot\alpha^{10}\cdot L^{12}$$

$$C_{20} = -.0771063\cdot\alpha^4\cdot L^6 + 7.2287\cdot10^{-3}\cdot\alpha^6\cdot L^8 - 3.514\cdot10^{-4}\cdot\alpha^8\cdot L^{10} + 1.0981\cdot10^{-5}\cdot\alpha^{10}\cdot L^{12}$$

$$C_{40} = 3.0319\cdot10^{-4}\cdot\alpha^6\cdot L^8 - 8.3666\cdot10^{-5}\cdot\alpha^8\cdot L^{10} + 3.9219\cdot10^{-6}\cdot\alpha^{10}\cdot L^{12}$$

$$C_{11} = .1542126\cdot\alpha^4\cdot L^6 - .012851\cdot\alpha^6\cdot L^8 + 5.8526\cdot10^{-4}\cdot\alpha^8\cdot L^{10} - 1.755\cdot10^{-5}\cdot\alpha^{10}\cdot L^{12}$$

$$C_{31} = -3.2128\cdot10^{-3}\cdot\alpha^6\cdot L^8 + 2.6773\cdot10^{-4}\cdot\alpha^8\cdot L^{10} - 1.0977\cdot10^{-5}\cdot\alpha^{10}\cdot L^{12}$$

$$C_{51} = 2.53\cdot10^{-5}\cdot\alpha^8\cdot L^{10} - 2.0984\cdot10^{-6}\cdot\alpha^{10}\cdot L^{12}$$

$$C_{02} = -.0771063\cdot\alpha^4\cdot L^6 + 7.2287\cdot 10^{-3}\cdot\alpha^6\cdot L^8 - 3.514\cdot 10^{-4}\cdot\alpha^8\cdot L^{10} + 1.0981\cdot 10^{-5}\cdot\alpha^{10}\cdot L^{12}$$

$$C_{22} = 4.8191\cdot 10^{-3}\cdot\alpha^6\cdot L^8 - 3.765\cdot 10^{-4}\cdot\alpha^8\cdot L^{10} + 1.4824\cdot 10^{-5}\cdot\alpha^{10}\cdot L^{12}$$

$$C_{42} = -6.275\cdot 10^{-5}\cdot\alpha^8\cdot L^{10} + 4.5755\cdot 10^{-6}\cdot\alpha^{10}\cdot L^{12}$$

$$C_{13} = -3.2128\cdot 10^{-3}\cdot\alpha^6\cdot L^8 + 2.6773\cdot 10^{-4}\cdot\alpha^8\cdot L^{10} - 1.0977\cdot 10^{-5}\cdot\alpha^{10}\cdot L^{12}$$

$$C_{33} = 3.3666\cdot 10^{-5}\cdot\alpha^8\cdot L^{10} - 5.8566\cdot 10^{-6}\cdot\alpha^{10}\cdot L^{12}$$

$$C_{53} = -7.3793\cdot 10^{-7}\cdot\alpha^{10}\cdot L^{12}$$

$$C_{04} = 3.0319\cdot 10^{-4}\cdot\alpha^6\cdot L^8 - 8.3666\cdot 10^{-5}\cdot\alpha^8\cdot L^{10} + 3.9219\cdot 10^{-6}\cdot\alpha^{10}\cdot L^{12}$$

$$C_{24} = -6.275\cdot 10^{-5}\cdot\alpha^8\cdot L^{10} + 4.5755\cdot 10^{-6}\cdot\alpha^{10}\cdot L^{12}$$

$$C_{44} = 9.1509\cdot 10^{-7}\cdot\alpha^{10}\cdot L^{12}$$

$$C_{15} = 2.53\cdot 10^{-5}\cdot\alpha^8\cdot L^{10} - 2.0984\cdot 10^{-6}\cdot\alpha^{10}\cdot L^{12}$$

$$C_{35} = -7.3793\cdot 10^{-7}\cdot\alpha^{10}\cdot L^{12}$$

$$C_{55} = 0$$

$$\eta_{10} = \sigma\cdot\alpha\cdot L^3\cdot\sin(\theta)\cdot\cos(\theta)*$$

$$\left[-.785398 + .0654498\cdot(L\cdot\alpha)^2\cdot\cos(\theta)^2 - 2.042\cdot 10^{-3}\cdot(L\cdot\alpha)^4\cdot\cos(\theta)^4 + 3.4127\cdot 10^{-5}\cdot(L\cdot\alpha)^6\cdot\cos(\theta)^6\right]$$

$$\eta_{30} = \sigma\cdot\alpha\cdot L^3\cdot\sin(\theta)\cdot\cos(\theta)$$

$$\left[.0327249\cdot(L\cdot\alpha)^2\cdot\cos(\theta)^2 - 1.6362\cdot 10^{-3}\cdot(L\cdot\alpha)^4\cdot\cos(\theta)^4 + 3.4127\cdot 10^{-5}\cdot(L\cdot\alpha)^6\cdot\cos(\theta)^6\right]$$

$$\eta_{50} = \sigma\cdot\alpha\cdot L^3\cdot\sin(\theta)\cdot\cos(\theta)*\left[4.1233\cdot 10^{-4}\cdot(L\cdot\alpha)^4\cdot\cos(\theta)^4 + 1.4492\cdot 10^{-5}\cdot(L\cdot\alpha)^6\cdot\cos(\theta)^6\right]$$

$$v_{00} = \sigma \cdot \alpha^2 \cdot L^4 \cdot \sin(\theta) \cdot \cos(\theta)^2 *$$

$$[.1963495 - .0081812 \cdot (L \cdot \alpha)^2 \cdot \cos(\theta)^2 + 1.7044 \cdot 10^{-4} \cdot (L \cdot \alpha)^4 \cdot \cos(\theta)^4 - 2.1305 \cdot 10^{-6} \cdot (L \cdot \alpha)^6 \cdot \cos(\theta)^6]$$

$$v_{20} = \sigma \cdot \alpha^2 \cdot L^4 \cdot \sin(\theta) \cdot \cos(\theta)^2 *$$

$$[.1963495 - .0122718 \cdot (L \cdot \alpha)^2 \cdot \cos(\theta)^2 + 3.068 \cdot 10^{-4} \cdot (L \cdot \alpha)^4 \cdot \cos(\theta)^4 - 4.2611 \cdot 10^{-6} \cdot (L \cdot \alpha)^6 \cdot \cos(\theta)^6]$$

$$v_{40} = \sigma \cdot \alpha^2 \cdot L^4 \cdot \sin(\theta) \cdot \cos(\theta)^2 *$$

$$[-4.0906 \cdot 10^{-3} \cdot (L \cdot \alpha)^2 \cdot \cos(\theta)^2 + 1.7044 \cdot 10^{-4} \cdot (L \cdot \alpha)^4 \cdot \cos(\theta)^4 - 3.0436 \cdot 10^{-6} \cdot (L \cdot \alpha)^6 \cdot \cos(\theta)^6]$$

where $\sigma = \sigma_0$.

2.4 Dynamic Stress Intensity Factor

It is important to note that while calculating the a_n and b_n , the stress intensity factor, K_{III} is not an independent constant, and it can be derived from Eq. 2.15a for given values α, θ. In order to perform the accurate K_{III} , it is noted to make sure the convergence of a_n and b_n . The results are listed in Table 2.1.

The values of the unknown functions in Eqs. 2.17a, 2.17b can now be solved. They are used to calculate the stress intensity factor from stress distribution along the dislocation. According to the definition of the stress intensity factor, one can define stress intensity factor at the crack tip from Eq. 2.15a as follows:

$$|K_{III}| = | \lim_{x \to 1} [2(x-1)]^{1/2} \sigma^* | \qquad (2.23)$$

where $|K_{III}|$ is the stress intensity factor at the crack tip.

Table 2.2 The values of a_n and b_n vs α, θ

$\alpha = 0.5$, $\theta = \pi/2$		$\alpha = 1$, $\theta = \pi/3$		$\alpha = 1$, $\theta = \pi/4$	
a_n	b_n	a_n	b_n	a_n	b_n
-0.032	-0.287	-0.149	-0.25	-0.118	-0.198
0	0	-0.031	$4.017\cdot10^{-4}$	-0.035	$4.543\cdot10^{-4}$
$4.259\cdot10^{-4}$	0.003	0.008	0.014	0.007	0.013
0	0	$8.323\cdot10^{-4}$	$-1.274\cdot10^{-4}$	0.001	$-1.44\cdot10^{-4}$
$-1.725\cdot10^{-6}$	$-1.236\cdot10^{-5}$	$-1.38\cdot10^{-4}$	$-2.259\cdot10^{-5}$	$-1.093\cdot10^{-4}$	$-2.225\cdot10^{-5}$
0	0	$-9.584\cdot10^{-6}$	$1.643\cdot10^{-7}$	$-1.118\cdot10^{-5}$	$1.858\cdot10^{-7}$

Knowing that $|K_{III}| = |\lim_{x\to1} [2(x-1)]^{1/2}\sigma^*|$, all factors with the regular parts can be neglected because of the limiting progress, except $\frac{1}{\pi}\sum_{j=0}^{1}\frac{(1-j)!}{j!}\left(\frac{2}{\alpha|x-s|}\right)^{2-2j}$ in Y. Thus at regular points, the stress intensity factor will be zero. For the singular points, the stress intensity factor is expressed as (Appendix C):

$$\lim_{x\to1} [2(x-1)]^{1/2}(-4/\pi)\int_{-1}^{1}\frac{1}{|x-s|^2}\,[A_1(s)\sin\omega t + A_2(s)\cos\omega t]ds \tag{2.24}$$

$$= \lim_{x\to1} [2(x-1)]^{1/2}(-4/\pi)\int_{-1}^{1}\sum_{n=0}^{5}[a_n U_n(s)\frac{(1-s^2)^{1/2}}{|x-s|^2}\sin\omega t + \sum_{n=0}^{5} b_n U_n(s)\frac{(1-s^2)^{1/2}}{|x-s|^2}\cos\omega t]\,ds$$

From Gradshteyn and Ryzhik (1965), we have:

$$\int_{-1}^{1}\frac{(1-s^2)^{1/2}}{(x-s)^2}ds = \frac{x\pi}{(x^2-1)^{1/2}}, \quad x \ge 1 \tag{2.25}$$

Substituting the Eq. 2.25 into above Eq. 2.24, the stress intensity factor can be expressed as follows:

$$K_{III} = 4\{[\sum_{n=0}^{N}\frac{a_n}{n+1}]^2 + [\sum_{n=0}^{N}\frac{b_n}{n+1}]^2\}^{1/2}\cos(\omega t-\theta_n) = |K_{III}|\cos(\omega t-\theta_n) \tag{2.26}$$

where $\theta_n = \tan^{-1} \frac{\sum_{n=0}^{N} a_n (n+1)^{-1}}{\sum_{n=0}^{N} b_n (n+1)^{-1}}$ and K_{III} is the stress intensity factor of mode III.

2.5 Results and Comparisons

The normalized stress intensity factor is plotted against the wave number α in Fig. 2.7 for several values of the incident angle θ. In Fig. 2.8, we compare the SIF curve for $\theta = \pi/2$ with that given in Mal (1969). He considered the jump discontinuity in the displacement vector that developed approximate techniques for the determination of the field on the crack surface. In that case, the approximate solutions are only valid at low frequency ($\alpha < 2$). He also showed the dynamic stress intensity factor exceeded the corresponding static value by about 28%. A comparison is made for $\theta = \pi/4$ with that of Stone (1980) in Fig. 2.9. It shows the dynamic stress intensity factors ($\alpha \neq 0$) will increase at low frequency when the α increases and reach the maximum value (when $\alpha \cong 0.9$) which is about 25% more than the static stress intensity factor ($\alpha = 0$). At relatively high frequencies, the stress intensity factor drops rapidly beyond the first maximum value and exhibits oscillations of approximately constant period as α increases which is shown in Fig. 2.10. In above cases, the values of the dynamic stress intensity factors are always bigger than the static stress intensity factors at low frequency and increase to maximum values when $\alpha \approx 1$. The normalized stress intensity factor is also plotted against the depth of surface crack in Fig. 2.11. As we mention in previous research, the surface crack of infinite length and finite width, lied in a homogeneous, isotropic, elastic, semi-infinite solid, is equivalent to the mirror image of the surface crack with respect to the free surface. It is a finite crack of length 2 in an infinite medium. Applying the dislocation model, the left side stress intensity factor K^L_{III} can be expressed as:

$$K^L_{III} = |\lim_{x \to -1} [2(x+1)^{1/2} \sigma^{*}|$$

$$= 4\{[\sum_{n=0}^{N} \frac{a_n(-1)^n}{n+1}]^2 + [\sum_{n=0}^{N} \frac{b_n(-1)^n}{n+1}]^2\}^{1/2} \cos(\omega t - \theta^L_n) = |K_{III}| \cos(\omega t - \theta^L_n) \qquad (2.27)$$

where $\theta^L_n = \tan^{-1} \dfrac{\sum_{n=0}^{N} a_n (-1)^n (n+1)^{-1}}{\sum_{n=0}^{N} b_n (-1)^n (n+1)^{-1}}$. The results for left side stress intensity factor are presented as K^L_{III} - α, K^L_{III} -θ, as shown in Fig. 2.12, which show that stress intensity factor will increase at low frequency when the α and θ increase. In Fig. 2.13, the curve shows the left side stress intensity factor drops rapidly at relatively high frequencies beyond the first maximum value and exhibits oscillations of approximately constant period as α increases. This result agrees with the right side stress intensity factor. At high frequency, the interference between the incident and reflected waves may reduce the dynamic stress intensity factor which can be clearly seen in the curves for incident angles different from zero. As a special interest, both sides of the stress intensity factors have been performed for different inclined angle to investigate and analyze the effect of θ. It shows both stress intensity factors will reach maximum value when the input shear waves are incident normally on the surface crack. At $0 < \theta < \pi/2$ or $3\pi/2 < \theta < 2\pi$, the right side stress intensity factor is always bigger than the left side (Fig. 2.14). A comparison between the left side and right side stress intensity factors has also been made showed in Fig. 2.15. It is note that the right side SIF are bigger than the left side at high frequencies.

The conclusions can be considered as fundamental concepts in practical cases. Furthermore, the comparisons of normalized stress intensity factor is made between the presented dislocation model and NISA program at very low frequency ($\alpha \approx 0$) shown in Fig. 2.16, 2.17. They show that the dislocation model is in a good agreement with NISA simulation.

2.6 Summary

In this chapter, an analytical dislocation model has been developed for a surface subjected to the inclined shear waves. The effects of dynamic loading on the distribution of stress around a surface crack and a finite crack are considered in this paper. When the input shear waves meet this dislocation, these waves are reflected due to the inhomogeneity of dislocation density. Previous works on this subject showed that if the input stress waves are SH waves, the reflected waves would also be SH waves. This result is equivalent to that produced from a crack. The surface crack can be represented by an continuous dislocation of Density. Unlike the static case, the stress intensity factor to the dynamic problem is more difficult to obtain. The object of the present paper is to discuss the stress intensity factor of a surface crack subjected to SH waves. The Chebyshev Polynomials, based on the stress boundary condition of the crack surface, are also presented for obtaining the stress intensity factor at the crack tip. The results are compared with those of Stone (1980) and Mal (1969) at low frequency ($\alpha \leq 2$). At high frequency the higher-order terms in a_n and b_n become very important in calculating the stress intensity factor. To overcome the limitation of the current model, the M and N must be considered as higher values. In other words, the choice of the M, N must be based on the wave numbers. Then the results of the present model will be valid at any frequency and would be useful for further investigations. The concepts of the current model have been used to developed an analytical dynamic model for interaction between a surface crack and a screw dislocation in chapter 3. Furthermore, the basic mathematical technique established in this chapter for solving elastodynamic problems of the surface crack, is extended to provide useful information to the internal crack interacted with the free surface in chapter 4.

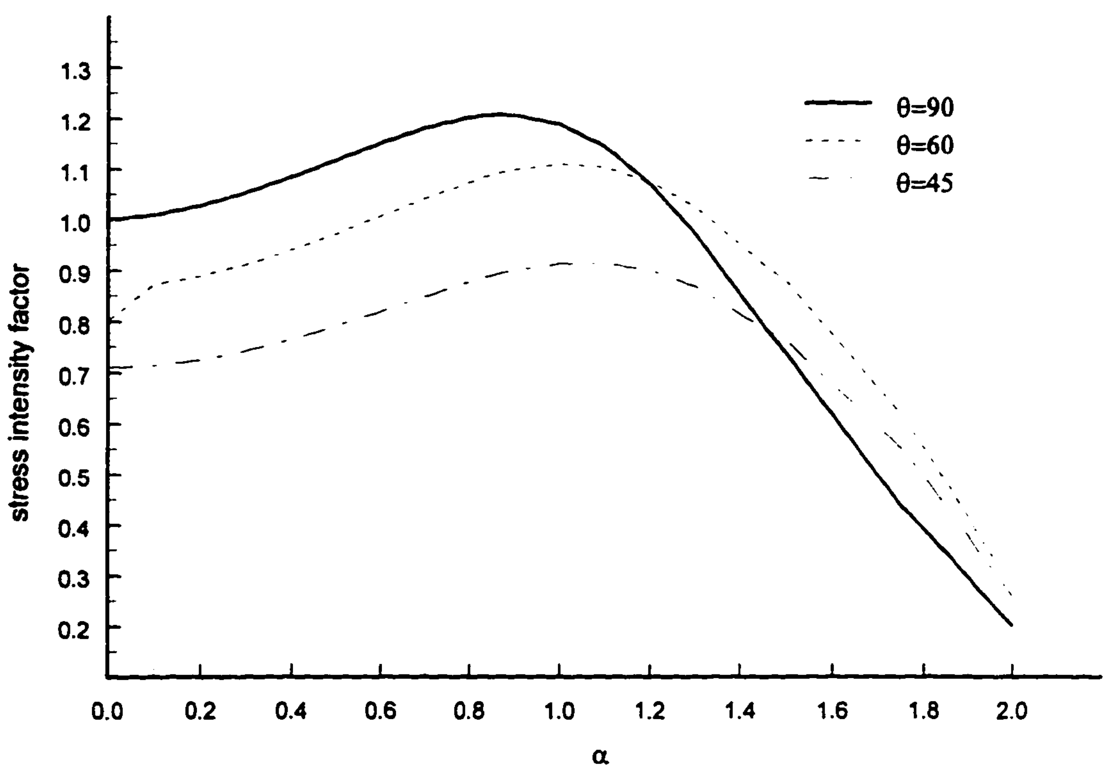

Figure 2.7 SIF $|K_{III}|$ vs α and θ

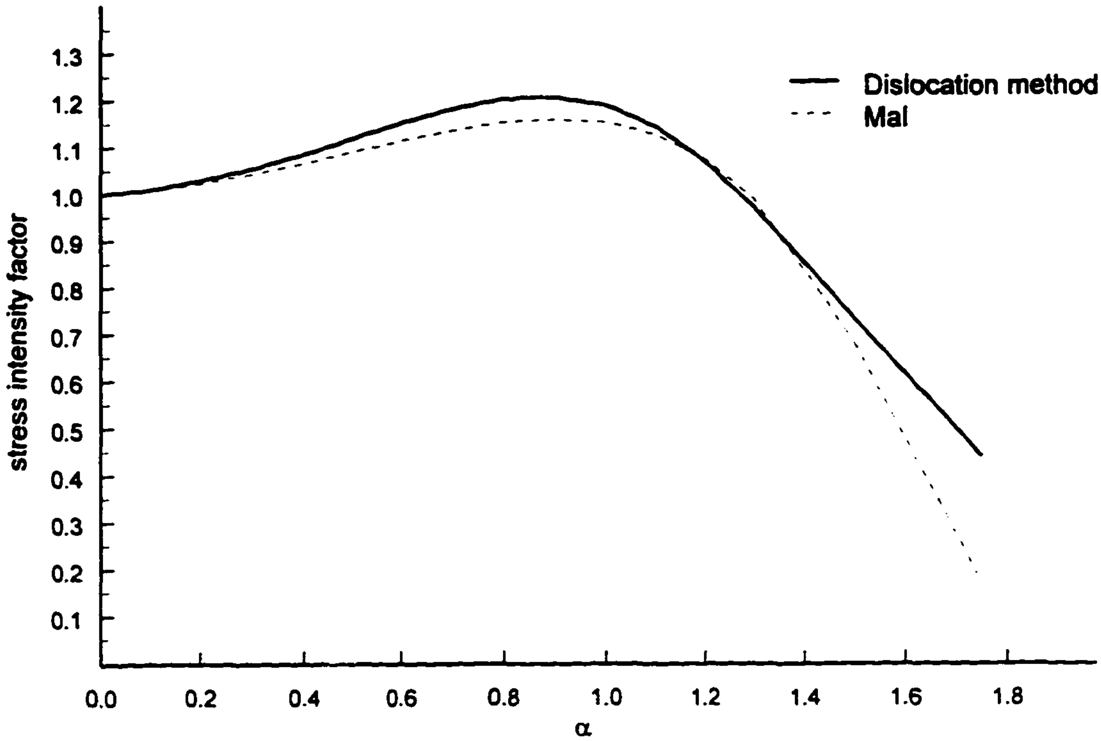

Figure 2.8 Comparison of dislocation and Mal model

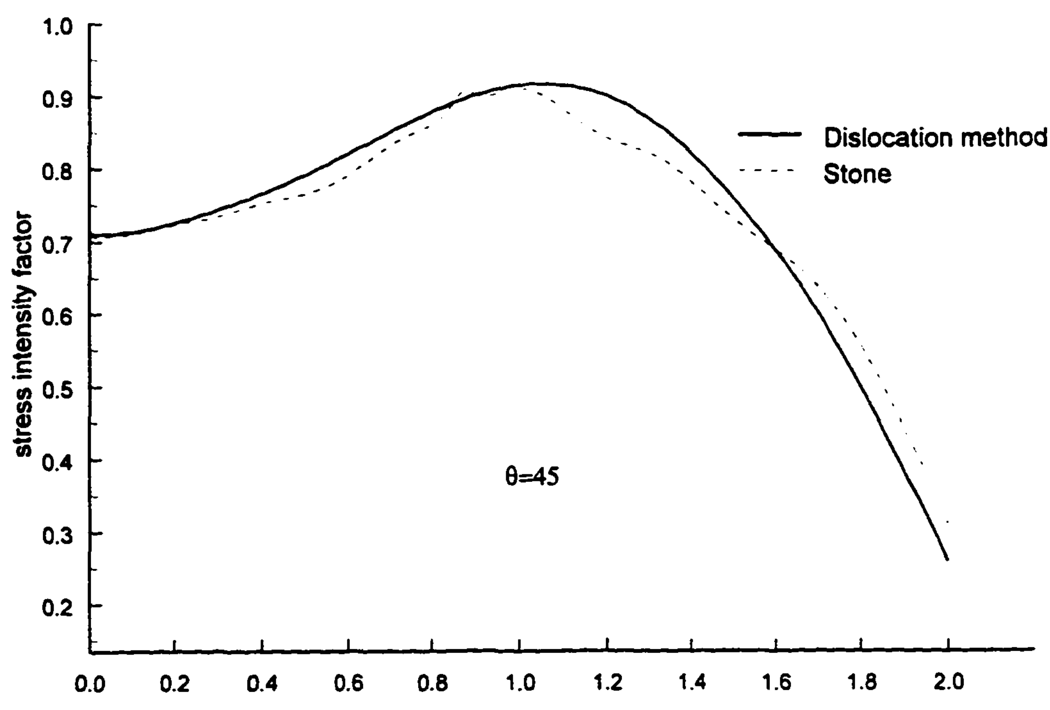

Figure 2.9 Comparison of dislocation and Stone model

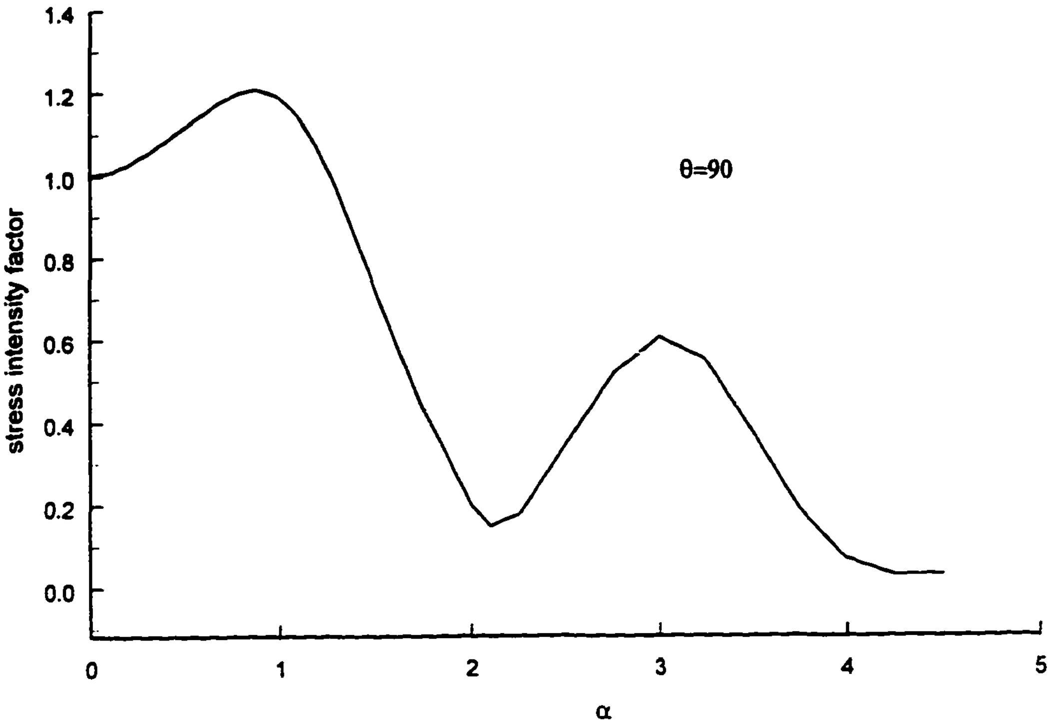

Figure 2.10 SIF $|K_{III}|$ vs α with inclined angle = $\pi/2$

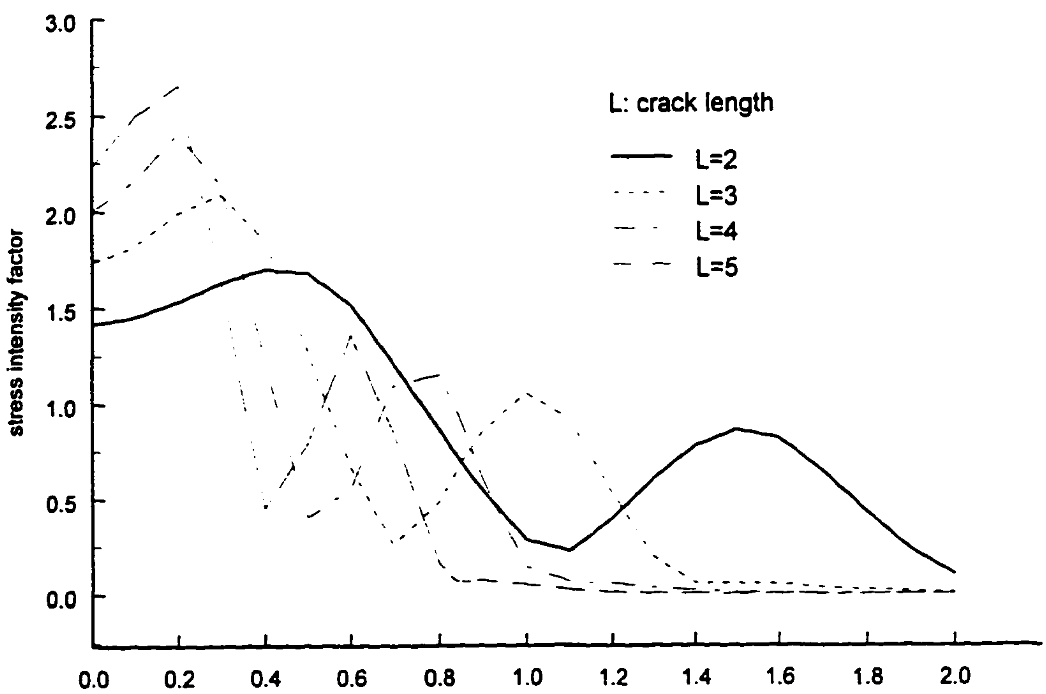

Figure 2.11 SIF $|K_{III}|$ vs α and L

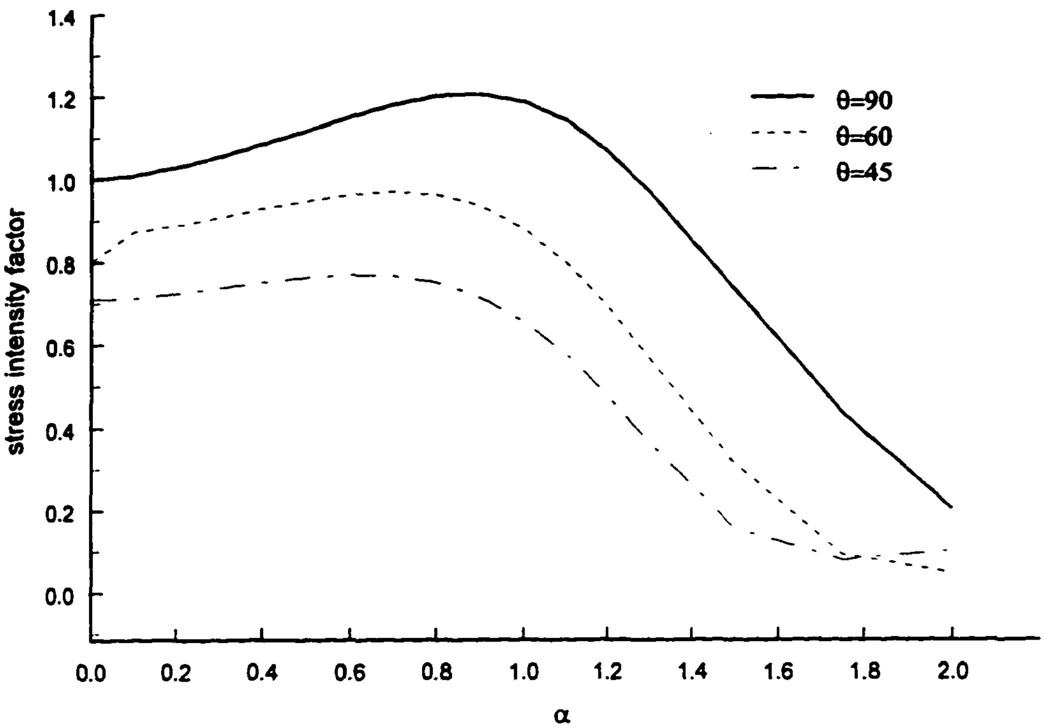

Figure 2.12 The left side SIF vs α and θ

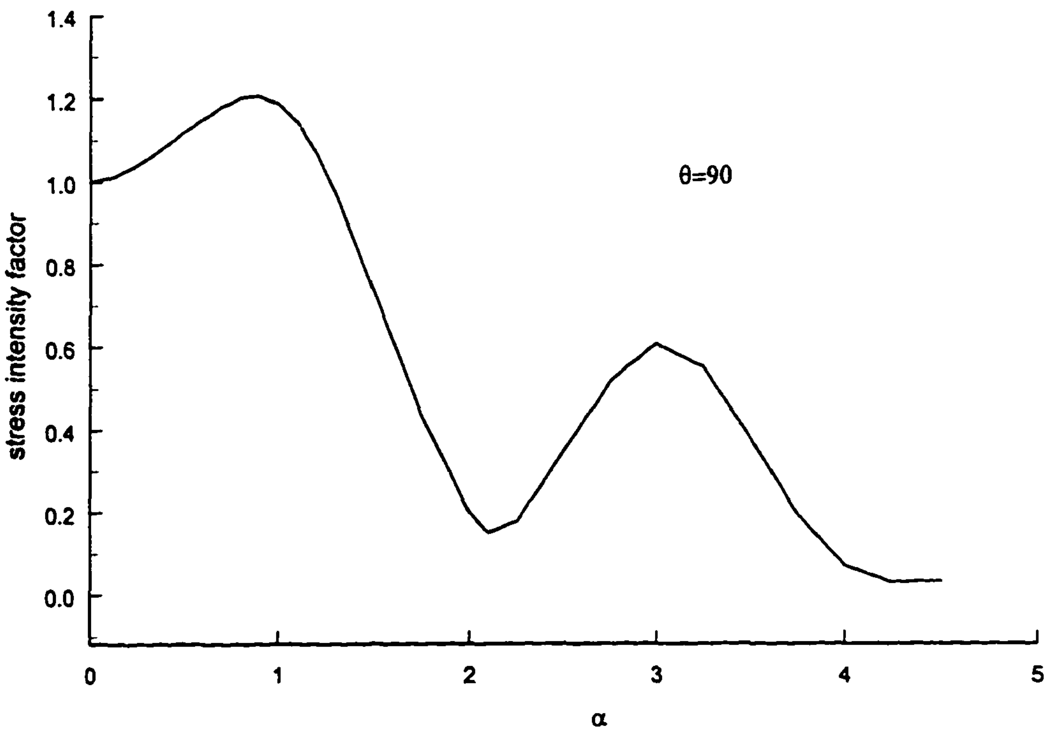

Figure 2.13 Left side SIF vs α with inclined angle = π/2

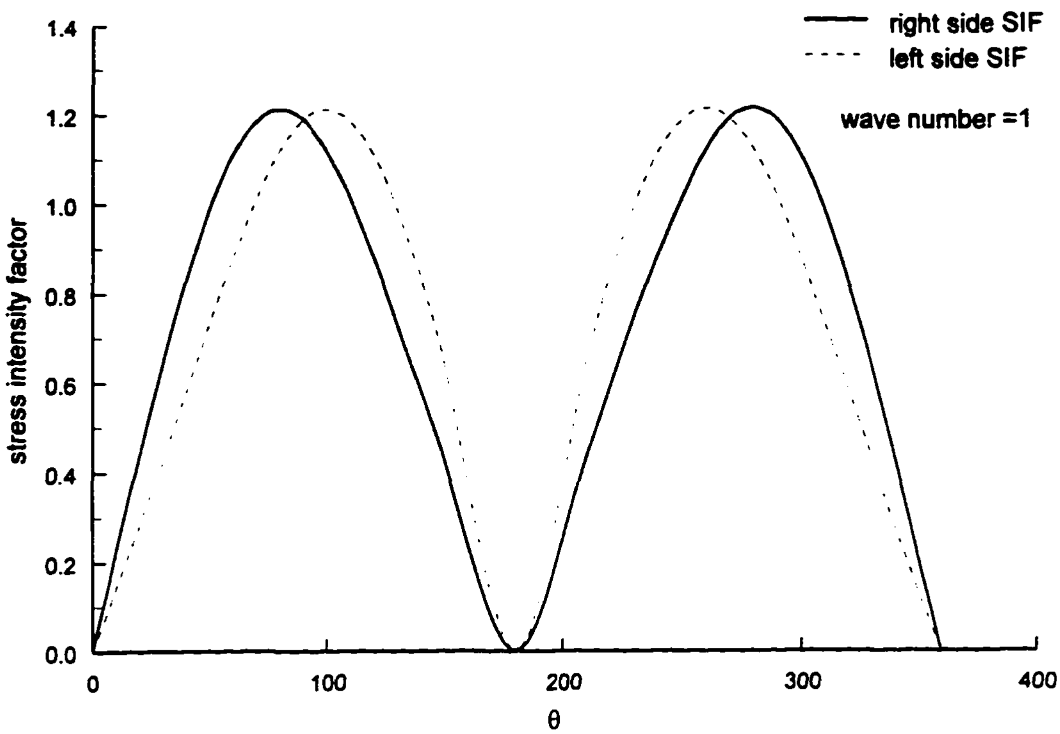

Figure 2.14 Both side SIF vs θ with wave number = 1

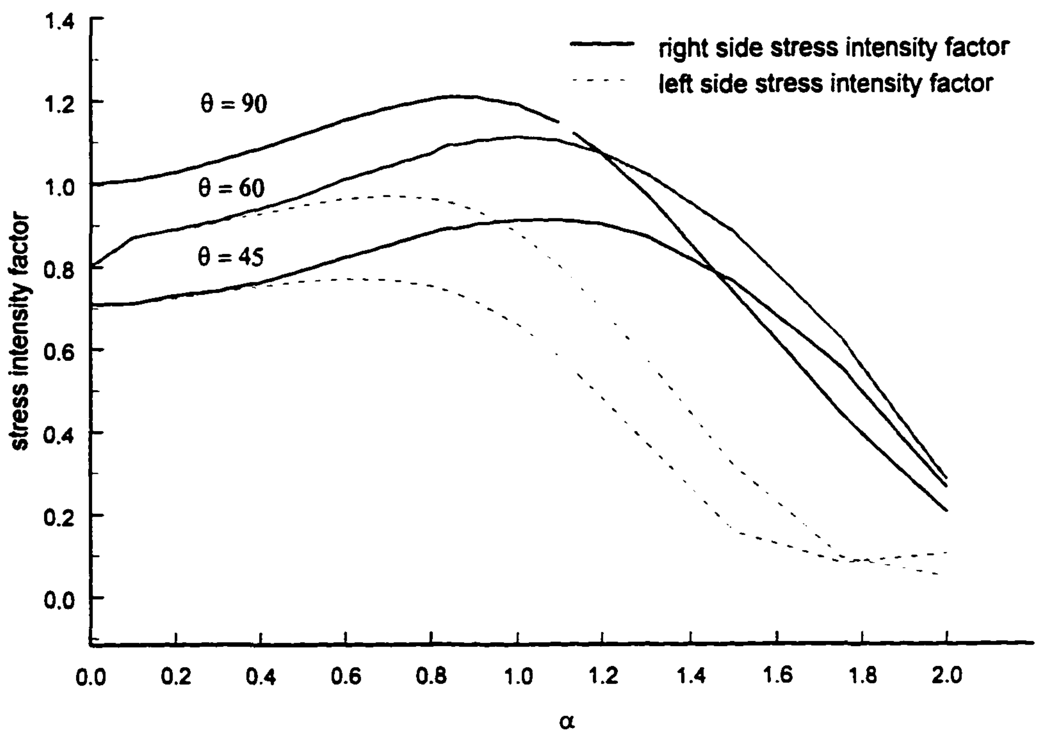

Figure 2.15 Comparison between left side and right side SIF

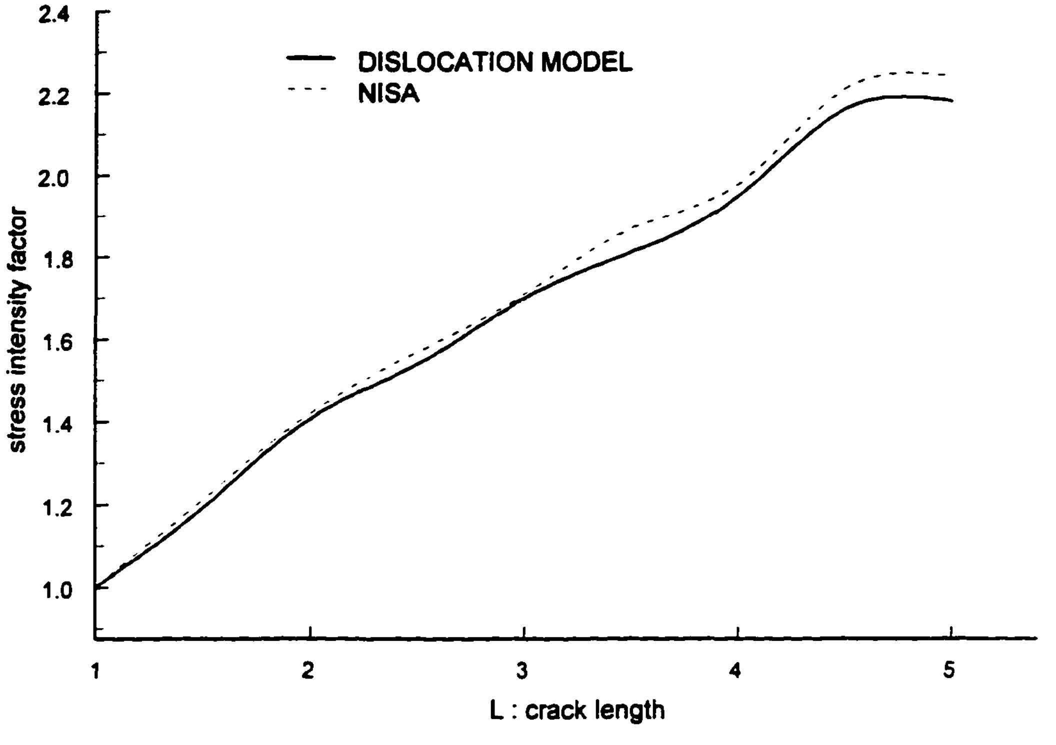

Figure 2.16 Comparison of dislocation model and NISA simulation at $\alpha \approx 0$

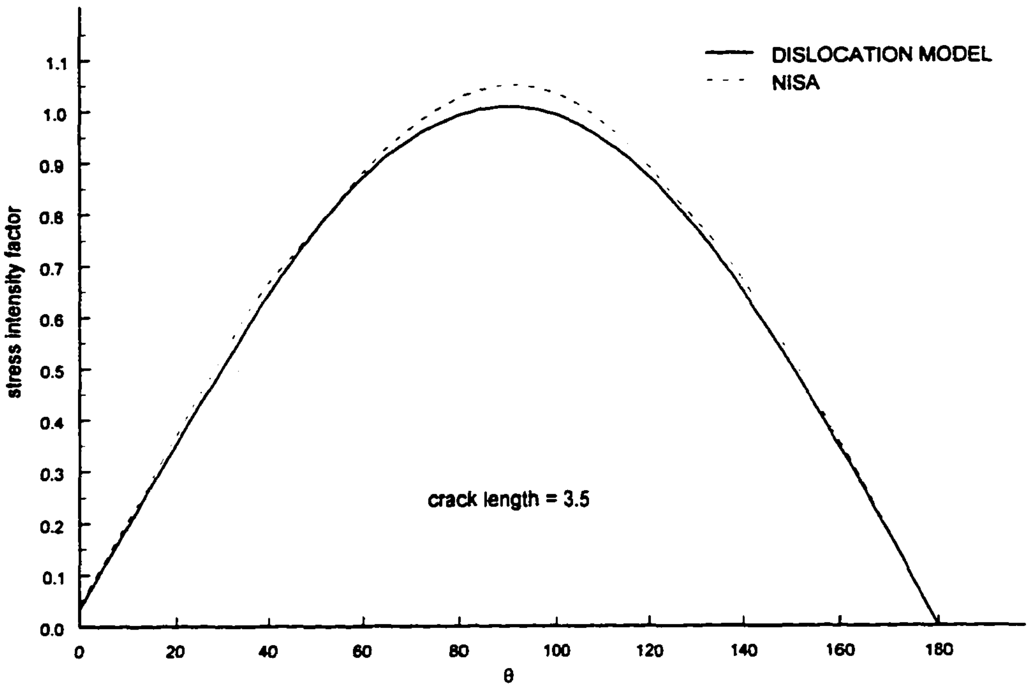

Figure 2.17 Comparison of dislocation model and NISA simulation at $\alpha \approx 0$

CHAPTER 3

DYNAMIC INTERACTION BETWEEN A SURFACE CRACK AND SCREW DISLOCATIONS

3.1 Introduction

The analytical model developed in the previous chapter is based on the mirrored dislocation model for investigating the stress intensity factor at crack tip. In this chapter, immediate objective of this study has been extended to the dynamic interaction between a surface crack and multi screw dislocations. It has been observed in silicon wafer that the dislocations near the free surface can be generated by introducing surface damage followed by a proper heat treatment. The surface damage, caused by grinding, scratching, etc., on brittle material usually introduce surface microcrack along with dislocations. It is believed that the dislocations are generated by surface microcracks during the heat treatment. It is therefore important to understand the interaction between a surface crack and a dislocation.

The general problem of the interaction of a dislocation with a surface notch has been studied by Warren (1970). However, due to the complexity of the potential he obtained, only an approximate solution for the force on the dislocation was reached. Chu (1982) solved the coplanar screw dislocation and sharp surface crack interaction. Li (1981) used dislocation modeling of the crack tip stress field to study the nucleation of dislocation near the tip of the crack. Lee (1985) also studied the same problem and compared the dislocation distributions in the crack, the total Burger vector, and the stress intensity factors with that of Li's models. However, until now the dynamic interaction between the general parallel screw dislocations and the surface crack has not been solved.

In this chapter, the method used in previous chapter (chapter 2) is extended to analyze the screw dislocation in the neighborhood of a surface crack. An analytical solution is presented and compared with those already obtained by other authors for $\alpha \approx 0$ case. Besides the stress intensity factors of the surface crack tip, the crack extension force is also discussed.

3.2 Problem Definition

The problem considered in this chapter is as follows: A surface crack of unit length lying in the xz plane with an infinite z dimension and a screw dislocation parallel to the z axis is situated at (x_0, 0) in the xz plane (Fig. 2.3). Both the crack and the dislocation are subjected to horizontal polarized shear waves (SH waves). The screw dislocation has a Burgers vector b. The problem is to calculate the stress intensity factor at the crack tip due to both the applied shear waves and the screw dislocation. Owing to the nature of geometry, the stress on the free surface is zero. According to the theories of dislocation-modeling technique and complex variable method proposed by Lee (1986), the problem is equivalent to the mirror image of the surface crack with respect to the free surface. The problem is now changed to simply a finite crack of length 2 interacting with two screw dislocations in an infinite medium as shown in Fig. 3.1.

3.3 Problem Formulation

Previous method is extended to express the stress distribution along the crack surface for the case of harmonic shear waves (SV, SH) impinging on a semi-infinite crack and a screw dislocation both lying along the x-axis. Since the total surface traction should be zero along the crack surface, we have:

$$\int_{-1}^{1} D(s)\, B\alpha^2\{[J_0(\alpha|x-s|) + J_2(\alpha|x-s|)]\cos[\omega t+p_1(s)] + [Y_0(\alpha|x-s|) + Y_2(\alpha|x-s|)]$$

$$\sin[\omega t+p_1(s)]\}ds + B\alpha^2\{[J_0(\alpha|x-x_0|) + J_2(\alpha|x-x_0|)]\cos[\omega t+p_2(x_0)] + [Y_0(\alpha|x-x_0|) + Y_2(\alpha|x-$$

$$x_0|)]\sin[\omega t+p_2(x_0)] - [J_0(\alpha|x+x_0|) + J_2(\alpha|x+x_0|)]\cos[\omega t+p_2(x_0)] - [Y_0(\alpha|x+x_0|) +$$

$$Y_2(\alpha|x+x_0|)]\sin[\omega t+p_2(x_0)]\} = -\sigma_0\sin\theta\cos(\alpha x\cos\theta-\omega t) \qquad (3.1)$$

where the $p_1(s)$ and $p_2(x_0)$ are phase lags of the surface crack modeled by a continuous distributed screw dislocation and the dislocation at $(x_0\,,\,0)$ respectively. It is noted that when x_0 equals to zero then the problem is reduced to the case of a surface crack.

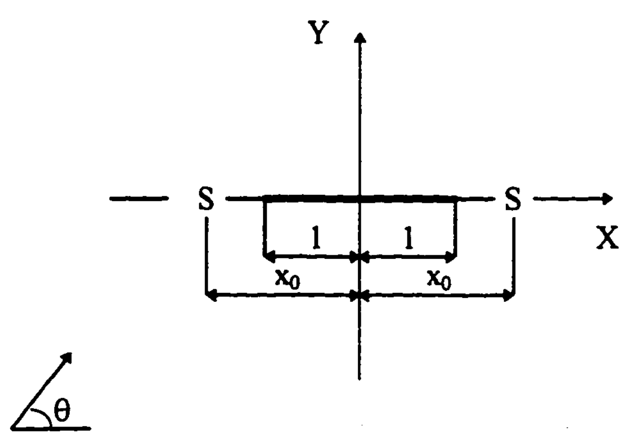

SH wave on xz plane plane

Figure 3.1 A positive screw dislocation, its image and a finite crack of length 2.

Expanding Eq. 3.1, we get the following two equations:

$$\int_{-1}^{1} D(s)\, B\alpha^2[Y\cos p_1(s) - J\sin p_1(s)]ds$$

$$= -\sigma_0 \sin\theta \sin(\alpha x \cos\theta) + B\alpha^2(\eta-\varepsilon)\cos p_2(x_0) + B\alpha^2(\chi-\xi)\sin p_2(x_0) \tag{3.2a}$$

$$\int_{-1}^{1} D(s)\, B\alpha^2[J\cos p_1(s) + Y\sin p_1(s)]ds$$

$$= -\sigma_0 \sin\theta \cos(\alpha x \cos\theta) + B\alpha^2(\eta-\varepsilon)\sin p_2(x_0) + B\alpha^2(\xi-\chi)\cos p_2(x_0) \tag{3.2b}$$

where $J = J_0(\alpha|x\text{-}s|) + J_2(\alpha|x\text{-}s|)$, $Y = Y_0(\alpha|x\text{-}s|) + Y_2(\alpha|x\text{-}s|)$

$\chi = J_0(\alpha|x\text{-}x_0|) + J_2(\alpha|x\text{-}x_0|)$, $\varepsilon = Y_0(\alpha|x\text{-}x_0|) + Y_2(\alpha|x\text{-}x_0|)$

$\xi = J_0(\alpha|x+x_0|) + J_2(\alpha|x+x_0|)$, $\eta = Y_0(\alpha|x+x_0|) + Y_2(\alpha|x+x_0|)$

Each of right sides of Eqs. 3.2a, 3.2b includes three terms: first term is due to the applied SH waves, the second and third are due to the screw dislocation at (x_0 , 0) and its image respectively. There are two unknown functions D(s) and $p_1(s)$ on the left side of Eqs. 3.2a, 3.2b. We replace them with another two functions, $A_1(s) = D(s)B\cos p_1(s)$ and $A_2(s) = D(s)B\sin p_1(s)$. Since there is singularity in Y when the value of x approaches to s, we must separate Y into singular and regular parts. Eqs. 3.2a, 3.2b can be expressed in the following forms :

$$-4/\pi \int_{-1}^{1} A_1(s)/(x\text{-}s)^2 ds + 2\alpha^2/\pi \int_{-1}^{1} A_1(s) J \ln(\alpha|x\text{-}s|)ds + \int_{-1}^{1} \alpha^2 [A_1(s) f(x, s) - A_2(s) J]ds$$

$$= -\sigma_0 \sin\theta \sin(\alpha x \cos\theta) + B\alpha^2(\eta-\varepsilon)\cos p_2(x_0) + B\alpha^2(\chi-\xi)\sin p_2(x_0) \tag{3.3a}$$

$$-4/\pi \int_{-1}^{1} A_2(s)/(x\text{-}s)^2 ds + 2\alpha^2/\pi \int_{-1}^{1} A_2(s) J \ln(\alpha|x\text{-}s|)ds + \int_{-1}^{1} \alpha^2 [A_2(s) f(x, s) + A_1(s) J]ds$$

$$= -\sigma_0 \sin\theta \cos(\alpha x \cos\theta) + B\alpha^2(\eta-\varepsilon)\sin p_2(x_0) + B\alpha^2(\xi-\chi)\cos p_2(x_0) \tag{3.3b}$$

From previous chapter, we know the stress intensity factors at the tip of the crack rely on the existence of the $r^{1/2}$ stress singularity. We therefore expect that $A_1(s)$ and $A_2(s)$ contain the term $(1-s^2)^{1/2}$. We choose to express $A_1(s)$ and $A_2(s)$ as $A_1(s) = (1-s^2)^{1/2}\sum_{n=0}^{\infty} a_n U_n(s)$ and $A_2(s) = (1-s^2)^{1/2}\sum_{n=0}^{\infty} b_n U_n(s)$. Substituting $A_1(s)$ and $A_2(s)$ into Eqs. 3.3a, 3.3b, we have:

$$\sum_{n=0}^{\infty} a_n \{-4/\pi \int_{-1}^{1} U_m(x)(1-x^2)^{1/2} \int_{-1}^{1} \frac{U_n(s)}{(x-s)^2}(1-s^2)^{1/2}\, dsdx + \alpha^2 \int_{-1}^{1} U_m(x)(1-s^2)^{1/2}$$

$$\int_{-1}^{1}[\frac{2}{\pi}J\ln(\alpha|x-s|) + f(x,s)]U_n(s)(1-s^2)^{1/2}\, dsdx\} - \sum_{n=0}^{\infty} b_n \alpha^2 \int_{-1}^{1} U_m(x)(1-x^2)^{1/2} \int_{-1}^{1} JU_n(s)(1-s^2)^{1/2} dsdx$$

$$= -\int_{-1}^{1} U_m(x)(1-x^2)^{1/2}[\sigma_0 \sin\theta \sin(\alpha x\cos\theta)]dx + \int_{-1}^{1} U_m(1-x^2)^{1/2} B\alpha^2(\eta-\varepsilon)\cos p_2(x_0)dx$$

$$+ \int_{-1}^{1} U_m(1-x^2)^{1/2} B\alpha^2(\chi-\xi)\sin p_2(x_0)dx \tag{3.4a}$$

$$\sum_{n=0}^{\infty} b_n \{-4/\pi \int_{-1}^{1} U_m(x)(1-x^2)^{1/2} \int_{-1}^{1} \frac{U_n(s)}{(x-s)^2}(1-s^2)^{1/2}\, dsdx + \alpha^2 \int_{-1}^{1} U_m(x)(1-s^2)^{1/2}$$

$$\int_{-1}^{1}[\frac{2}{\pi}J\ln(\alpha|x-s|)\} + f(x,s)]U_n(s)(1-s^2)^{1/2}\, dsdx + \sum_{n=0}^{\infty} a_n \alpha^2 \int_{-1}^{1} U_m(x)(1-x^2)^{1/2} \int_{-1}^{1} JU_n(s)(1-s^2)^{1/2} dsdx$$

$$= -\int_{-1}^{1} U_m(x)(1-x^2)^{1/2}[\sigma_0 \sin\theta \cos(\alpha x\cos\theta)]dx + \int_{-1}^{1} U_m(1-x^2)^{1/2} B\alpha^2(\eta-\varepsilon)\sin p_2(x_0)dx$$

$$+ \int_{-1}^{1} U_m(1-x^2)^{1/2} B\alpha^2(\xi-\chi)\cos p_2(x_0)dx \tag{3.4b}$$

where m = 0, 1, 2, 3, ..., M, ...∞ and n = 0, 1, 2, 3, ..., N, ..., ∞. The integrals in Eqs. 3.4a, 3.4b are evaluated with the help of Chebyshev Polynomials (see Appendix 2). Since U_n

does not vanish when n approaches ∞, a_n and b_n should converge to zero as n approaches ∞. Therefore we assume that the problem can be approximated with the following series:

$$\sum_{n=0}^{N}[(A_{mn}+B_{mn})a_n - C_{mn}b_n]=\eta_m + f_m\cos p_2(x_0) + g_m\sin p_2(x_0) \quad (m=0, 1, ..M) \quad (3.5a)$$

$$\sum_{n=0}^{N}[C_{mn}a_n + (A_{mn}+B_{mn})b_n] = \nu_m + f_m\sin p_2(x_0) - g_m\cos p_2(x_0) \quad (m=0, 1, ..M) \quad (3.5b)$$

where

$$A_{mn} = -4/\pi \int_{-1}^{1} U_m(x)(1-x^2)^{1/2} \int_{-1}^{1} \frac{U_n(s)}{(x-s)^2}(1-s^2)^{1/2}\,dsdx = \begin{cases} 0 & m\neq n \\ 2(n+1)\pi & m=n \end{cases}$$

$$B_{mn} = \alpha^2 \int_{-1}^{1} U_m(x)(1-s^2)^{1/2} \int_{-1}^{1} [\frac{2}{\pi} J\ln(\alpha|x-s|) + f(x,s)]U_n(s)(1-s^2)^{1/2}\,dsdx$$

$$C_{mn} = \alpha^2 \int_{-1}^{1} U_m(x)(1-x^2)^{1/2} \int_{-1}^{1} JU_n(s)(1-s^2)^{1/2}\,dsdx$$

$$\eta_m = -\int_{-1}^{1} U_m(x)(1-x^2)^{1/2}[\sigma_0 \sin\theta \sin(\alpha x\cos\theta)]dx$$

$$\nu_m = -\int_{-1}^{1} U_m(x)(1-x^2)^{1/2}[\sigma_0 \sin\theta \cos(\alpha x\cos\theta)]dx$$

$$f_m = \int_{-1}^{1} U_m(1-x^2)^{1/2} B\alpha^2(\eta-\varepsilon)dx, \quad g_m = \int_{-1}^{1} U_m(1-x^2)^{1/2} B\alpha^2(\chi-\xi)dx$$

Eqs. 3.5a, 3.5b contain 2(N+1) unknown coefficients a_n and b_n with 2(M+1) equations. The above equations can be put into matrix form as:

$$(A+B)\vec{a} - C\vec{b} = \vec{\eta} + \vec{f}\cos p_2(x_0) + \vec{g}\sin p_2(x_0) \quad (3.6a)$$

$$C\vec{a} + (A+B)\vec{b} = \vec{\nu} + \vec{f}\sin p_2(x_0) - \vec{g}\cos p_2(x_0) \quad (3.6b)$$

where $\vec{a} = [\, a_0 , a_1 , a_2 ,..., a_N \,]^T$ and $\vec{b} = [\, b_0 , b_1 , b_2 ,..., b_N \,]^T$. Matrices A, B, C, and vectors $\vec{\eta}, \vec{\nu}$ and $\vec{f}, \vec{g}$ can be found once M and N are selected. Since all quantities in Eqs. 3.5a, 3.5b are constants except a_n and b_n, we deal with them as linear equations. Separating them by superposition method, Eqs. 3.6a, 3.6b become:

$$(A + B)\vec{a}' - C\vec{b}' = \vec{\eta} \tag{3.7a}$$

$$C\vec{a}' + (A + B)\vec{b}' = \vec{\nu} \tag{3.7b}$$

and

$$(A + B)\vec{a}'' - C\vec{b}'' = \vec{f}\cos p_2(x_0) + \vec{g}\sin p_2(x_0) \tag{3.8a}$$

$$C\vec{a}'' + (A + B)\vec{b}'' = \vec{f}\sin p_2(x_0) - \vec{g}\cos p_2(x_0) \tag{3.8b}$$

where $\vec{a} = \vec{a}' + \vec{a}''$ and $\vec{b} = \vec{b}' + \vec{b}''$. To solve for a_n and b_n ($n = 0, 1, ..., N$), let $M = N$. Our problem is now to find positive integers M and N such that a_n and b_n converge to zero. As a first approximation, let M and N equal to 9. Evaluating a'_n and b'_n in Eqs. 3.7a, 3.7b, we find out the values of a'_n and b'_n would converge to zero if $M, N > 5$. The results are listed in Table 3.1. Let

$$\vec{f}\cos p_2(x_0) + \vec{g}\sin p_2(x_0) = \vec{R}\cos\varphi \tag{3.9a}$$

$$\vec{f}\sin p_2(x_0) - \vec{g}\cos p_2(x_0) = \vec{R}\sin\varphi \tag{3.9b}$$

where $0 \le \varphi \le 2\pi$. We now have

$$\vec{R} = (\vec{f}^2 + \vec{g}^2)^{1/2} \tag{3.10}$$

where matrices A, B and C can be derived from Eq. 2.22 in Chapter 2. The corresponding a''_n and b''_n defines the maximum value of the stress intensity factor at the crack tip. In general, only the maximum value of the stress intensity factor is of interest. It means that φ can be defined when K_{III} reaches the maximum value. With the same method used to solve Eqs. 3.7a, 3.7b, we find the solutions as listed in Table 3.2. The solutions can now be used to get $A_1(s)$, $A_2(s)$ and $p_2(x_0)$. The results may be used to calculate the stress intensity factor from stress distribution along the dislocation.

3.3.1 Stress Intensity Factor

The stress intensity factor at the crack tip from Eq. 2.15a may now be defined as follows:

$$|K_{III}| = |\lim_{x\to 1} [2(x-1)]^{1/2}\sigma^*| \tag{3.11}$$

where $|K_{III}|$ is the stress intensity factor at the crack tip. The stress intensity factor K_{III} at the crack tip for a mode III surface crack is defined as follows:

$$K_{III} = K_S + K_C \tag{3.12}$$

where the first term, K_S, is due to stress field of the dislocation and the second term, K_C, is due to the applied SH waves. Both of them derive from Eq. 2.26. Eq. 3.12 is plotted in Fig. 3.2 for some arbitrary values of α and x_0. It is seen that the net stress intensity factor K_{III} can be drastically reduced by a screw dislocation generated in the vicinity of the crack tip. It also can be shown that $K_{III} \approx 0$ when $x_0 \geq 20$.

3.3.2 Crack Extension Force

From Eqs. 3.12, we know the stress intensity factor can also be increased by the presence of the dislocation depending upon the relative sign of the applied SH waves and the

Burgers vector of the dislocation. By holding the screw dislocation stationary, the strain energy release rate corresponding to the virtual displacement of the crack tip gives the crack extension force G_{III} under the stress fields of the screw dislocation and the applied SH waves. The G_{III} is defined as:

$$G_{III} = \frac{K_{III}^2}{2\mu} \tag{3.13}$$

The change of G_{III} as the surface crack propagating towards the screw dislocation is illustrated in Figs. 3.2a, 3.2b. Without the applied SH waves, the dislocation stress fields tends to drag the surface crack to the dislocation where the strain energy can be relaxed. Under the applied SH waves, the surface crack can be repelled by the dislocation depending upon the direction of the applied SH waves and the Burgers vector the screw dislocation. There is a stable position x_0 where the crack extension force G_{III} is zero. In Fig. 3.3, the SIF curve for $\alpha = 0$ (static) is compared with that given in Chu (1982). In Fig. 3.4, it shows the dynamic stress intensity factors will increase at low frequency when the α increases and reach the maximum value. At relatively high frequencies, the stress intensity factor drops rapidly beyond the first maximum value and exhibits oscillations as α increases. To extend the study further to include the relation between the input angle θ and stress intensity factor shown in Fig. 3.5. It shows that the stress intensity factor increases with increasing the input angle θ at low frequencies. It is noted that the stable position x_0 will decrease when the input angle θ increases as shown in Figs. 3.6a, 3.6b.

3.4 Two Dislocations on the Crack Plane

As this model is an extension of the dislocation model developed for dynamic interactions between a screw dislocation and a surface crack in previous sections, the concepts developed in Eq. 3.1 is valid for the present analysis, with a minor modification in screw dislocations. In this model, derivation of the stress distribution is similar to the Eq. 3.1, but it includes an extra part from the second screw dislocation. To extend the study a step further to include the dynamic interactions between the dislocations and the surface crack. The case of two screw dislocations of Burgers vector b_1 and b_2 of the same sign is situated at (x_1, 0) and (x_2, 0) respectively. By using the dislocation model for the surface crack and images for the free surface, The problem is now changed to simply a finite crack of length 2 interacting with four screw dislocations in an infinite medium as shown in Fig. 3.7.

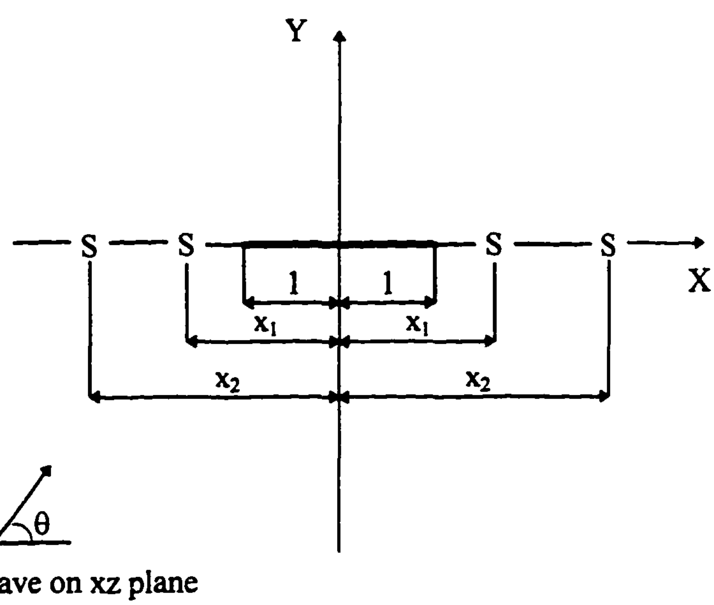

Figure 3.7 Two positive screw dislocations, their images and a finite crack of length 2.

For applying Eq. 3.1, we have:

$$\int_{-1}^{1} D(s)\,B\alpha^2\{[J_0(\alpha|x-s|) + J_2(\alpha|x-s|)]\cos[\omega t+p_1(s)] + [Y_0(\alpha|x-s|) + Y_2(\alpha|x-s|)]\sin[\omega t+p_1(s)]\}ds$$

$$+B_1\alpha^2\{[J_0(\alpha|x-x_1|) + J_2(\alpha|x-x_1|)]\cos[\omega t+p_2(x_1)]+[Y_0(\alpha|x-x_1|) + Y_2(\alpha|x-x_1|)]\sin[\omega t+p_2(x_1)]$$

$$- [J_0(\alpha|x+x_1|) + J_2(\alpha|x+x_1|)]\cos[\omega t+p_2(x_1)]- [Y_0(\alpha|x+x_1|) + Y_2(\alpha|x+x_1|)]\sin[\omega t+p_2(x_1)]\}$$

$$+ B_2\alpha^2\{[J_0(\alpha|x-x_2|) + J_2(\alpha|x-x_2|)]\cos[\omega t+p_2(x_2)]+[Y_0(\alpha|x-x_2|) + Y_2(\alpha|x-x_2|)]\sin[\omega t+p_2(x_2)]$$

$$- [J_0(\alpha|x+x_2|) + J_2(\alpha|x+x_2|)]\cos[\omega t+p_2(x_2)]- [Y_0(\alpha|x+x_2|) + Y_2(\alpha|x+x_2|)]\sin[\omega t+p_2(x_2)]\}$$

$$= -\sigma_0\sin\theta\cos(\alpha x\cos\theta-\omega t) \qquad (3.14)$$

where $B_1 = -b_1u\mu/8$, $B_2 = -b_2u\mu/8$. The $p_1(s)$, $p_2(x_1)$ and $p_2(x_2)$ are phase lags of the surface crack modeled by a continuous distribution of screw dislocation and the screw dislocation at $(x_1, 0)$ and $(x_2, 0)$ respectively. Expanding Eq. 3.14, we get the following two equations:

$$\int_{-1}^{1} D(s)\,B\alpha^2[Y\cos p_1(s) - J\sin p_1(s)]ds$$
$$= -\sigma_0\sin\theta\sin(\alpha x\cos\theta) + B_1\alpha^2(\eta_1-\varepsilon_1)\cos p_2(x_1) + B_1\alpha^2(\chi_1-\xi_1)\sin p_2(x_1)$$
$$+B_2\alpha^2(\eta_2-\varepsilon_2)\cos p_2(x_2) + B_2\alpha^2(\chi_2-\xi_2)\sin p_2(x_2) \qquad (3.15a)$$

$$\int_{-1}^{1} D(s)\,B\alpha^2[J\cos p_1(s) + Y\sin p_1(s)]ds$$
$$= -\sigma_0\sin\theta\cos(\alpha x\cos\theta) + B_1\alpha^2(\eta_1-\varepsilon_1)\sin p_2(x_1) + B_1\alpha^2(\xi_1-\chi_1)\cos p_2(x_1)$$
$$+ B_2\alpha^2(\eta_2-\varepsilon_2)\sin p_2(x_2) + B_2\alpha^2(\xi_2-\chi_2)\cos p_2(x_2) \qquad (3.15b)$$

where $J = J_0(\alpha|x-s|) + J_2(\alpha|x-s|)$, $Y = Y_0(\alpha|x-s|) + Y_2(\alpha|x-s|)$

$\chi_1 = J_0(\alpha|x-x_1|) + J_2(\alpha|x-x_1|)$, $\varepsilon_1 = Y_0(\alpha|x-x_1|) + Y_2(\alpha|x-x_1|)$

$\xi_1 = J_0(\alpha|x+x_1|) + J_2(\alpha|x+x_1|)$, $\eta_1 = Y_0(\alpha|x+x_1|) + Y_2(\alpha|x+x_1|)$

$\chi_2 = J_0(\alpha|x-x_2|) + J_2(\alpha|x-x_2|)$, $\varepsilon_2 = Y_0(\alpha|x-x_2|) + Y_2(\alpha|x-x_2|)$

$\xi_2 = J_0(\alpha|x+x_2|) + J_2(\alpha|x+x_2|)$, $\eta_2 = Y_0(\alpha|x+x_2|) + Y_2(\alpha|x+x_2|)$

Each of right sides of Eqs. 3.15a, 3.15b includes five terms: first part is due to the applied SH waves, others are due to the screw dislocation at $(x_1, 0)$ and $(x_2, 0)$ and their images respectively. Following the proceedings in previous sections, we separate them by superposition method, Eqs. 3.15a, 3.15b become:

$$(A+B)\vec{a}' - C\vec{b}' = \vec{\eta} \tag{3.16a}$$

$$C\vec{a}' + (A+B)\vec{b}' = \vec{\nu} \tag{3.16b}$$

and

$$(A+B)\vec{a}'' - C\vec{b}'' = \vec{f}_1 \cos p_2(x_1) + \vec{g}_1 \sin p_2(x_1) \tag{3.17a}$$

$$C\vec{a}'' + (A+B)\vec{b}'' = \vec{f}_1 \sin p_2(x_1) - \vec{g}_1 \cos p_2(x_1) \tag{3.17b}$$

$$(A+B)\vec{a}''' - C\vec{b}''' = \vec{f}_2 \cos p_2(x_2) + \vec{g}_2 \sin p_2(x_2) \tag{3.18a}$$

$$C\vec{a}''' + (A+B)\vec{b}''' = \vec{f}_2 \sin p_2(x_2) - \vec{g}_2 \cos p_2(x_2) \tag{3.18b}$$

$$\vec{f}_1 = \int_{-1}^{1} U_m (1-x^2)^{1/2} B_1 \alpha^2 (\eta_1 - \varepsilon_1) dx \qquad \vec{g}_1 = \int_{-1}^{1} U_m (1-x^2)^{1/2} B_1 \alpha^2 (\chi_1 - \xi_1) dx$$

$$\vec{f}_2 = \int_{-1}^{1} U_m (1-x^2)^{1/2} B_2 \alpha^2 (\eta_2 - \varepsilon_2) dx \qquad \vec{g}_2 = \int_{-1}^{1} U_m (1-x^2)^{1/2} B_2 \alpha^2 (\chi_2 - \xi_2) dx$$

where $\vec{a} = \vec{a}' + \vec{a}'' + \vec{a}'''$ and $\vec{b} = \vec{b}' + \vec{b}'' + \vec{b}'''$.

Let

$$\vec{f}_1 \cos p_2(x_1) + \vec{g}_1 \sin p_2(x_1) = \vec{R}_1 \cos\varphi_1 \tag{3.19a}$$

$$\vec{f_1}\sin p_2(x_1)-\vec{g_1}\cos p_2(x_1)=\vec{R_1}\sin\varphi_1 \tag{3.19b}$$

and

$$\vec{f_2}\cos p_2(x_2)+\vec{g_2}\sin p_2(x_2)=\vec{R_2}\cos\varphi_2 \tag{3.20a}$$

$$\vec{f_2}\sin p_2(x_2)-\vec{g_2}\cos p_2(x_2)=\vec{R_2}\sin\varphi_2 \tag{3.20b}$$

where $0 \le \varphi_1 \le 2\pi$ and $0 \le \varphi_2 \le 2\pi$. We now have

$$\vec{R_1}=(\vec{f_1}^2+\vec{g_1}^2)^{1/2} \tag{3.21a}$$

$$\vec{R_2}=(\vec{f_2}^2+\vec{g_2}^2)^{1/2} \tag{3.21b}$$

where matrices A, B and C can be derived from Eq. 2.22 in Chapter 2. The corresponding a_n'' b_n'' and a_n'', b_n'' define the maximum value of the stress intensity factor at the crack tip. In general, only the maximum value of the stress intensity factor is of interest. It means that φ_1, φ_2 can be defined when K_{III} reaches the maximum value. The Fig. 3.8a, b have been presented as stress intensity factor versus x_1, x_2 for given shear modulus, wave number and Burgers vectors b_1 and b_2.

3.5 Summary

By using the dislocation model for the surface crack and images for the free surface, an analytical solution for interaction between a screw dislocation near a mode III surface crack, subjected to the dynamic antiplane stress, has been derived. The change of the crack extension force as the surface crack propagation towards the dislocation is also presented in present chapter.

Without the applied stress, the dislocation stress field tends to drag the surface crack to the dislocation where the strain energy can be relaxed. Under the periodic dynamic stress, the surface crack can be repelled by the dislocation depending upon the direction of the applied stress and the Burgers vector of the dislocation. The effects of the wave number, the input incident angle and the dislocation on the stress intensity factor are also discussed in 3.3.2.

In absence of the applied SH waves, dislocations are always attracted towards the crack. When the SH waves are in the direction of driving the dislocation into the medium, a stable position is created at some distance from the crack tip beyond which the dislocations will be repelled by the crack. The stable position decreases with increasing input angle θ. At low frequencies, the stress intensity factor increases with increasing the input angle θ. The stress intensity factor can also be increased by the presence of the screw dislocation depending upon the relative sign of the Burgers vector of the dislocation.

Theses solutions obtained in this chapter are valid for the time interval from initial loading until first wave scattered at surface crack tip to the same crack tip after being diffracted by the screw dislocation. Ma and Tsai (1991) showed that the stress intensity factors due to the diffracted waves emitted at another crack are much less influential than the incident waves. In this study, we neglect the effects of diffracted waves.

The advantage of the present model is demonstrated when dealing with two or more screw dislocations because the dislocation distribution inside the crack is additive. A numerical example with multi dislocation is used to illustrate our method.

Table 3.1 The values of a'_n and b'_n vs α, θ

$\alpha = 0.5$, $\theta = \pi/2$		$\alpha = 1$, $\theta = \pi/3$		$\alpha = 1$, $\theta = \pi/4$	
a_n	b_n	a_n	b_n	a_n	b_n
-0.032	-0.287	-0.149	-0.25	-0.118	-0.198
0	0	-0.031	$4.017 \cdot 10^{-4}$	-0.035	$4.543 \cdot 10^{-4}$
$4.259 \cdot 10^{-4}$	0.003	0.008	0.014	0.007	0.013
0	0	$8.323 \cdot 10^{-4}$	$-1.274 \cdot 10^{-4}$	0.001	$-1.44 \cdot 10^{-4}$
$-1.725 \cdot 10^{-6}$	$-1.236 \cdot 10^{-5}$	$-1.38 \cdot 10^{-4}$	$-2.259 \cdot 10^{-5}$	$-1.093 \cdot 10^{-4}$	$-2.225 \cdot 10^{-5}$
0	0	$-9.584 \cdot 10^{-6}$	$1.643 \cdot 10^{-7}$	$-1.118 \cdot 10^{-5}$	$1.858 \cdot 10^{-7}$

Table 3.2 The values of a''_n and b''_n vs α, θ, x_0

$\alpha = 1$, $x_0 = 2$, $\theta = \pi/2$		$\alpha = 1$, $x_0 = 2.5$, $\theta = \pi/3$		$\alpha = 1$, $x_0 = 3$, $\theta = \pi/4$	
a_n	b_n	a_n	b_n	a_n	b_n
0.027	0.026	0.023	0.021	0.017	0.022
0.001	0.003	0.002	0.001	0/001	0.003
$-6.015 \cdot 10^{-4}$	$9.986 \cdot 10^{-4}$	$-4.011 \cdot 10^{-4}$	$7.686 \cdot 10^{-4}$	$-3.341 \cdot 10^{-3}$	$5.346 \cdot 10^{-4}$
$1.578 \cdot 10^{-3}$	$5.946 \cdot 10^{-4}$	$3.478 \cdot 10^{-4}$	$2.556 \cdot 10^{-4}$	$1.238 \cdot 10^{-3}$	$1.998 \cdot 10^{-4}$
$4.003 \cdot 10^{-5}$	$3.768 \cdot 10^{-5}$	$7.24 \cdot 10^{-5}$	$5.763 \cdot 10^{-5}$	$6.254 \cdot 10^{-5}$	$5.433 \cdot 10^{-5}$
0	$1.493 \cdot 10^{-4}$	$2.003 \cdot 10^{-5}$	$2.462 \cdot 10^{-5}$	$1.034 \cdot 10^{-5}$	$2.462 \cdot 10^{-5}$

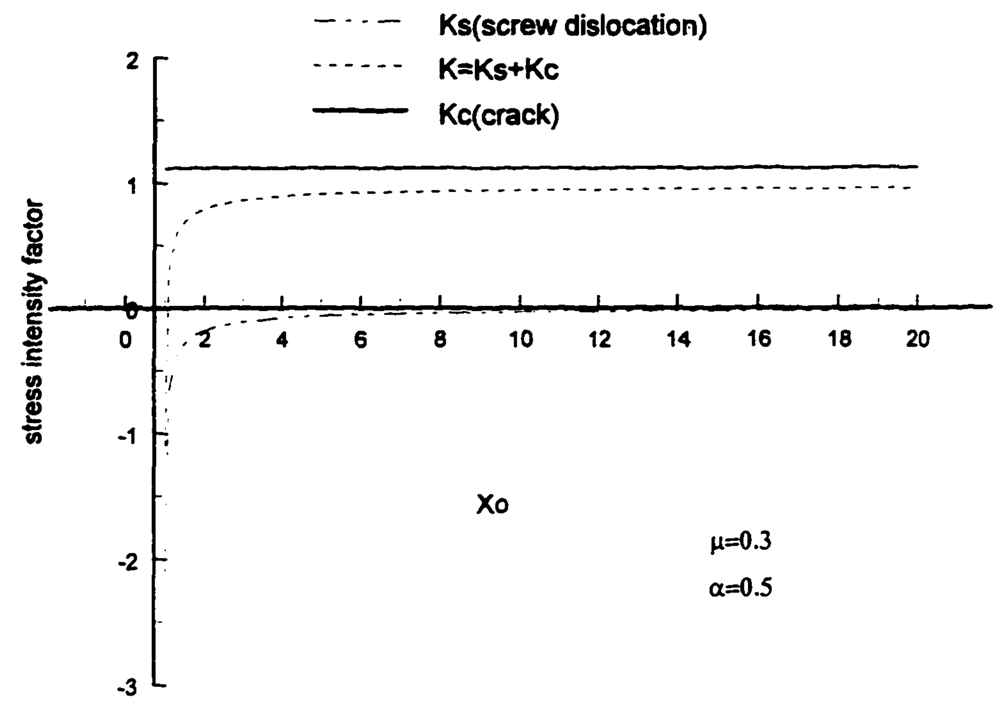

Figure 3.2a Effect of a screw dislocation on the SIF for α

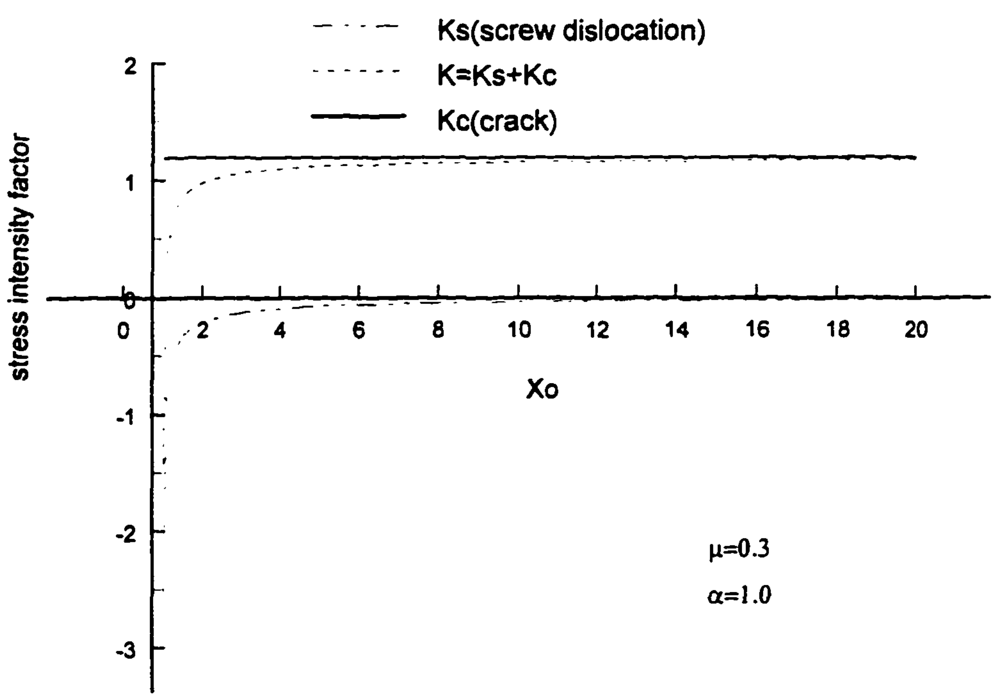

Figure 3.2b Effect of a screw dislocation on the SIF for $\alpha = 1.0$

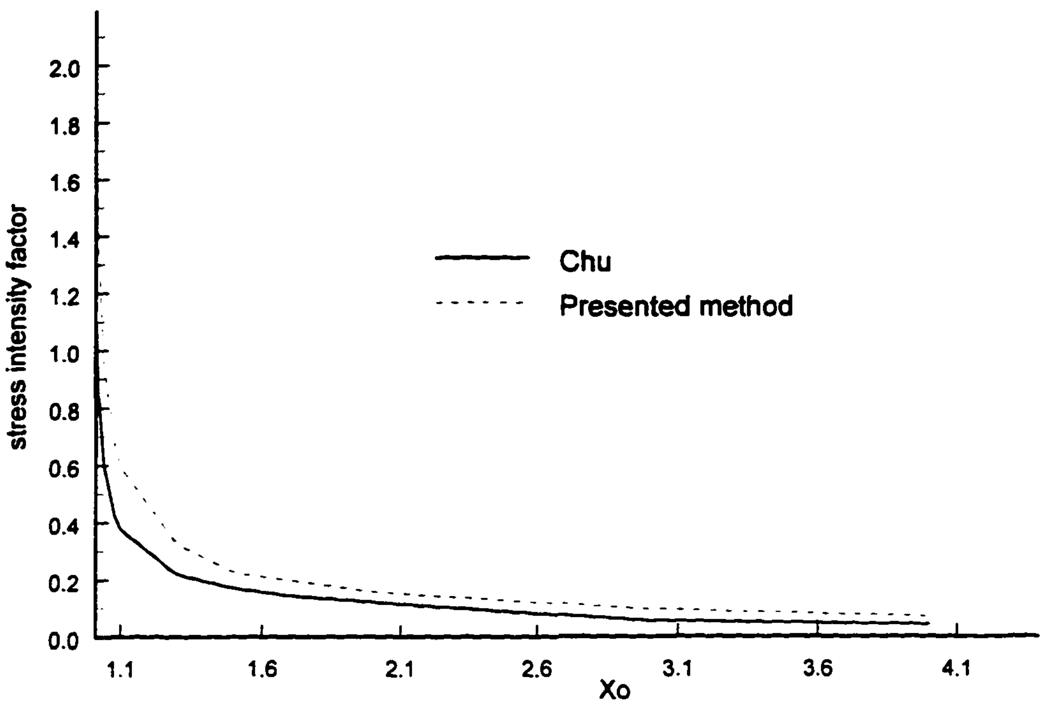

Figure 3.3 Comparison of dislocation and Chu model

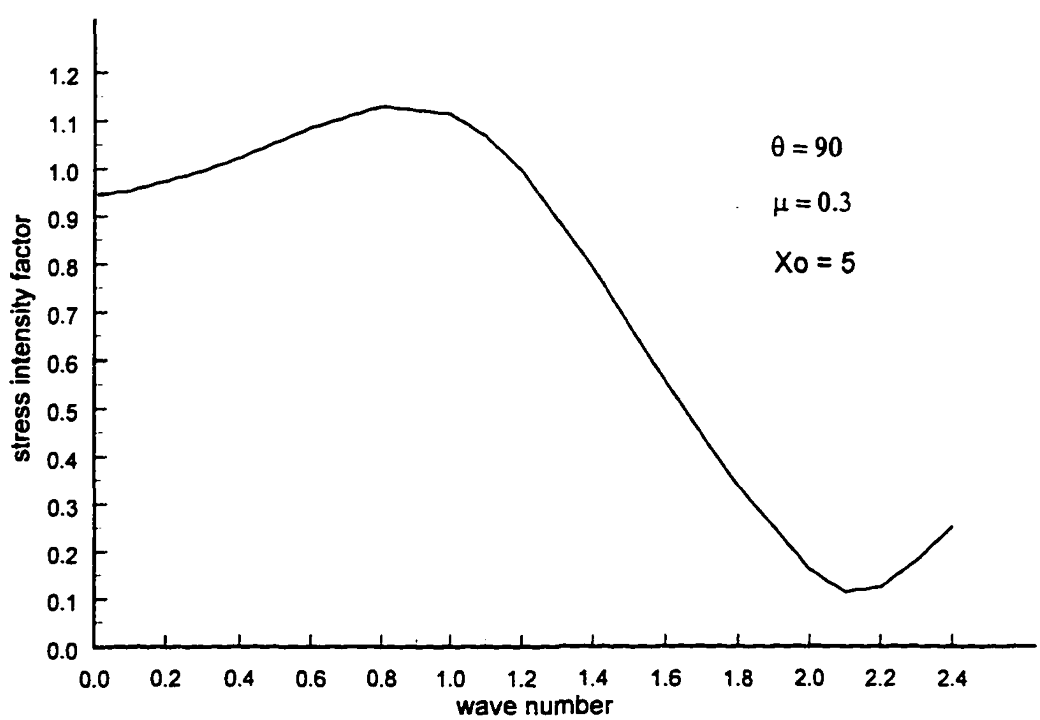

Figure 3.4 Effect of wave number on the SIF

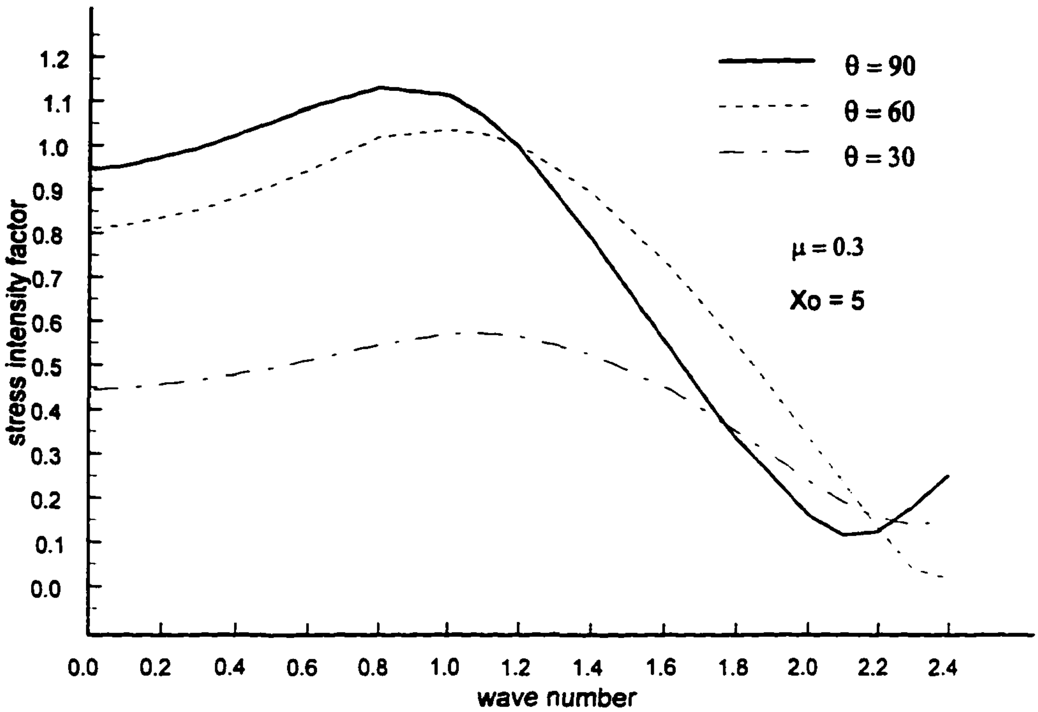

Figure 3.5 SIF vs wave number and incident angle

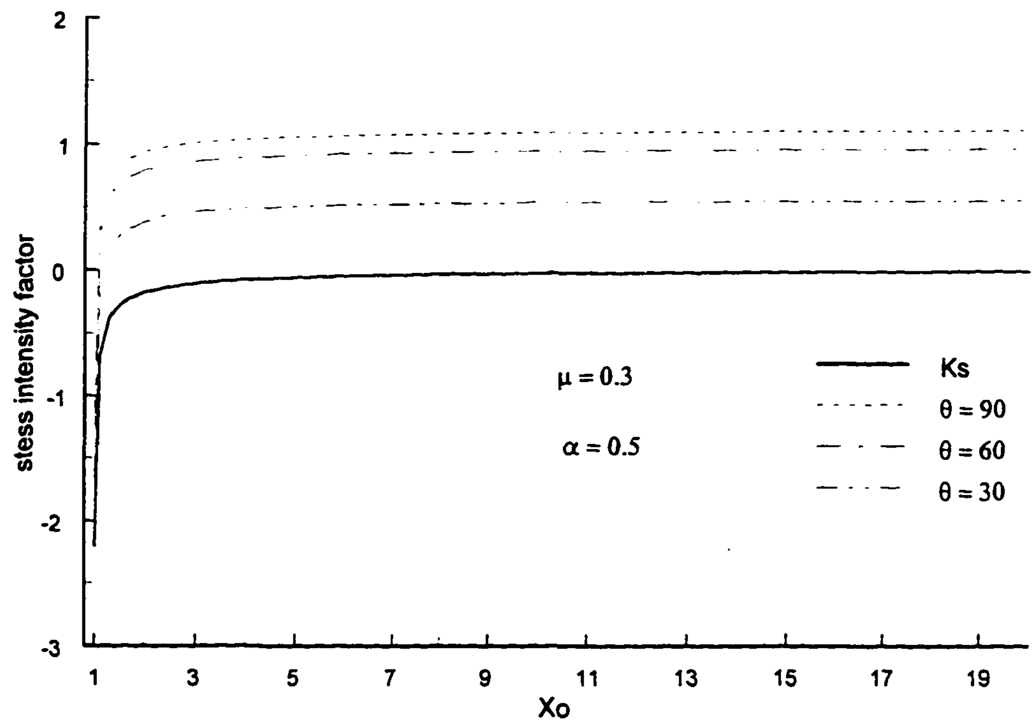

Figure 3.6a SIF vs x_0 and incident angle

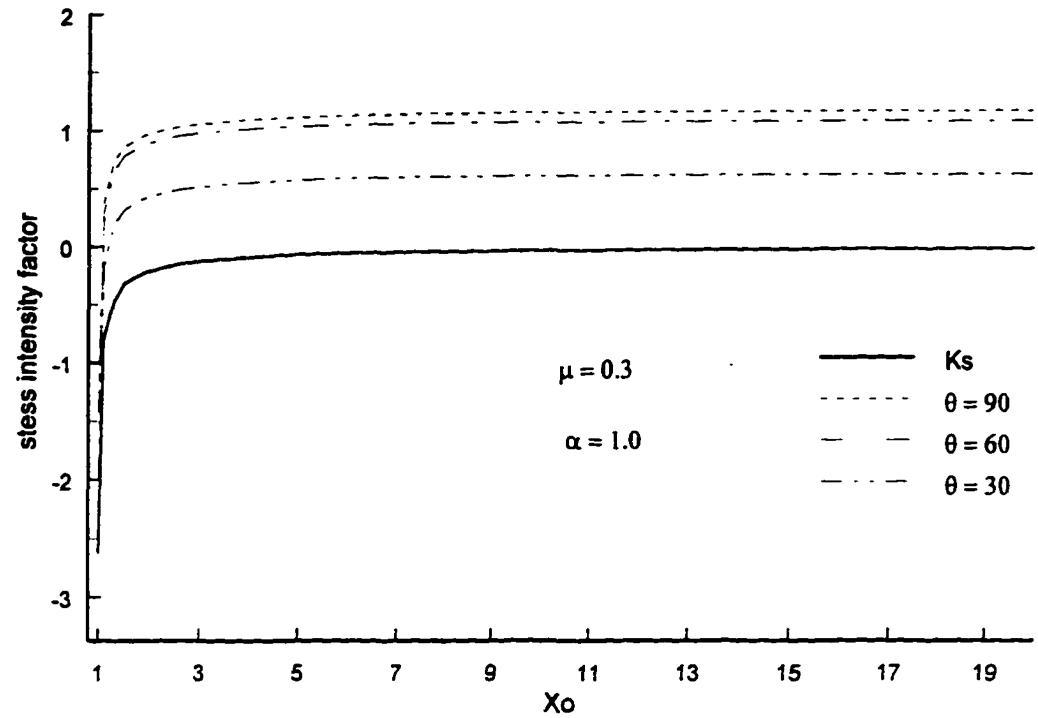

Figure 3.6b SIF vs x_0 and incident angle

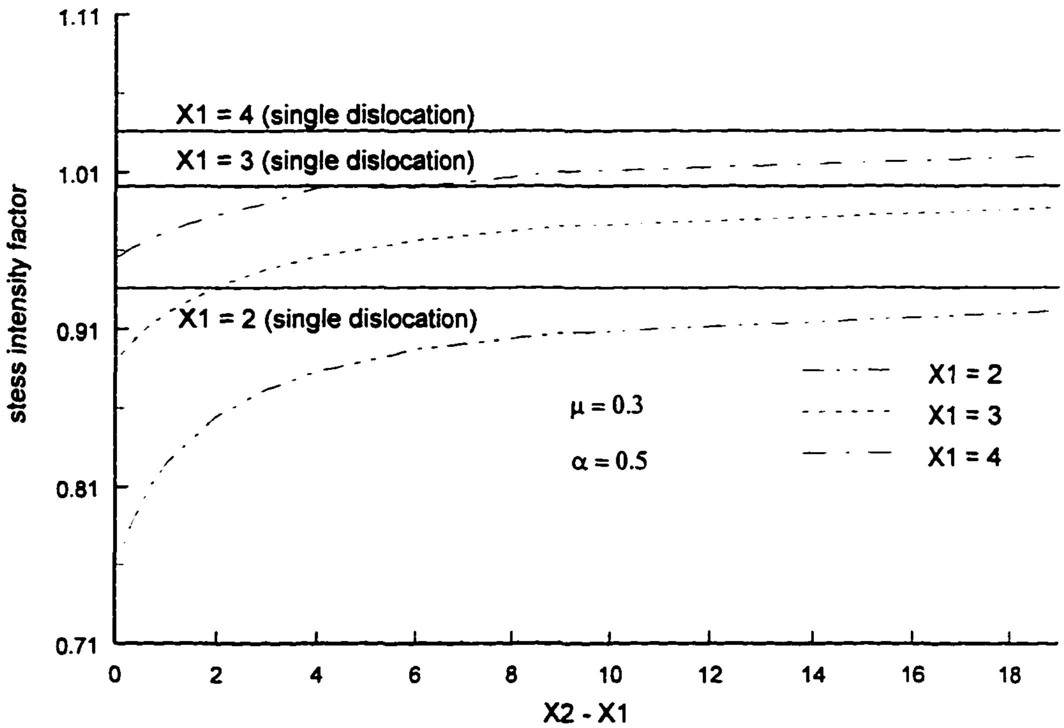

Figure 3.8a SIF vs x_2 - x_1 for interaction between two screw dislocations ($b_1 = b_2$) and a surface crack

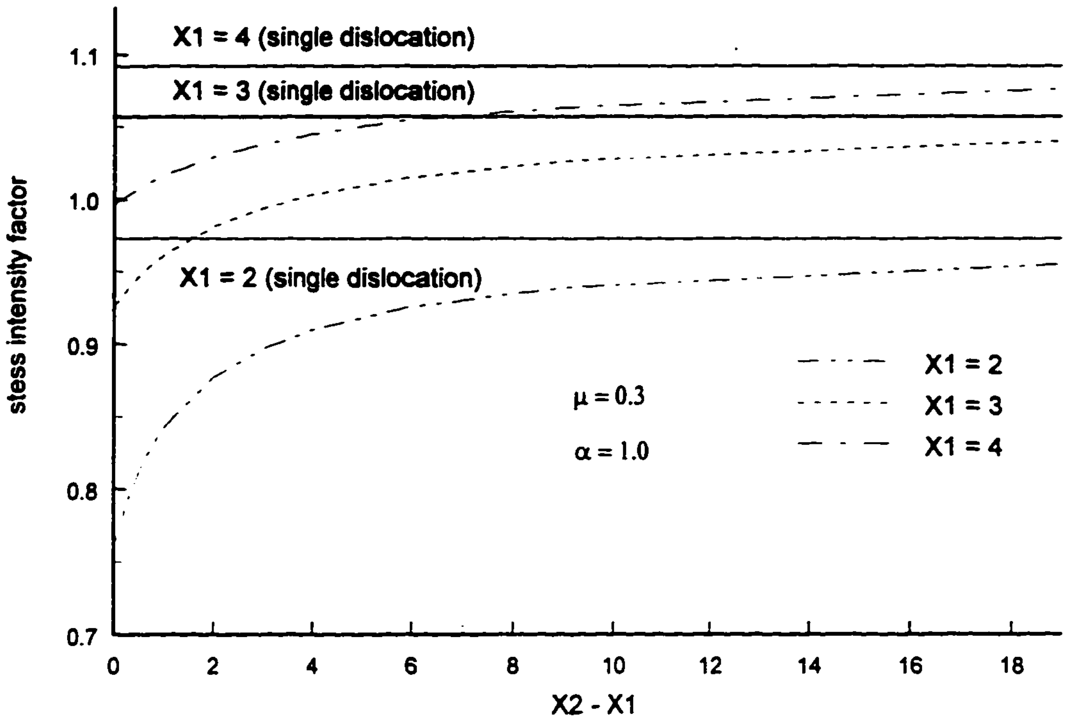

Figure 3.8b SIF vs $x_2 - x_1$ for interaction between two screw dislocations ($b_1 = b_2$) and a surface crack

CHAPTER 4

DYNAMIC STRESS INTENSITY FACTORS FOR A CRACK NEAR FREE SURFACE

4.1 Introduction

A dislocation model based on the mirror image with respect to the free surface of a surface crack has been developed in Chapter 2 to determine the stress intensity factor at the crack tip in a semi-infinite isotropic elastic solid which is subjected to period cyclic loadings. The investigations stated above treated a surface crack in a semi-infinite medium and a finite crack in an infinite medium respectively. In fact, the internal crack also played an important role in fracture mechanics because of its practical applications. Among all the available methods, the Fourier Transform and Laplace Transform methods are mostly used to solve the integral equations derived form the wave equations and boundary conditions. But, in order to consider the necessary boundary conditions, they must convert the integral equations to Fredholm's equations which are not convenient for numerical solutions because of the associated improper integrals.

In an earlier paper, Achenbach (1981) has considered the two dimensional scattering of Rayleigh waves by a subsurface crack. The boundary value problem for the scattered field was stated in mathematical terms and an integral representation for its solution derived. The problem was reduced by standard methods to the solution of an uncoupled system of strongly singular integral equations which were solved numerically using a method due to Erdogan and Cupta (1976). Formulas were given for the far field amplitudes of the waves in the scattered field and for the near field quantities of the crack tip. The data in the integral equations were the values taken at the location of the crack by the stress components of the incident field. Applying previous research, Achenbach also considered the elastodynamic Mode I and Mode II stress intensity factors for a crack near a free surface. He derived the equations of stress components of the incident field along with boundary conditions (stress on the surface of the half space) and side conditions (displacements along the crack surface) then the elastodynamic field generated by the integral equations satisfied all the required conditions. Although the integral equations and together with the side conditions can be solved by standard methods, but they preserved the incorrect form of the singularities of the solution at the crack tip.

The objected of the present study is to developed a dynamic model based on the previous surface crack model for an internal crack subjected to SH dynamic loadings. The model, with proper integration, can be expected to get the stress intensity factors at both sides of crack tips at any frequencies. In fact, the model shows that the cases of the surface crack and the finite crack in an infinite medium are special cases of the internal crack. With the known coefficients of the model, the model can be applied for static problems. This can be achieved by setting the wave number to zero. Research shows that there is an interesting relation between the internal crack and surface crack model, in the sense that the internal crack is affected by the free surface within certain region. In fact, an internal crack will be easily extended to a surface crack when the internal crack is very close to the surface crack. In the other hand, an internal crack can be considered as a finite crack in infinite medium if the internal crack is out of the certain region. The present model not only can offer a better insight into the dynamic behavior of the internal crack but present new areas of the effects of the inclined angle. A set of integral equations relating singularities of the crack tip have been developed. The results have been presented in the form of stress intensity factors versus wave number, crack position and inclined angle. The proposed model shows the dynamic stress intensity factors will increase at low frequency when wave number increases and reach the maximum value. At relatively high frequencies, the stress intensity factor drops rapidly beyond the first maximum value and exhibits oscillations of approximately constant period as wave number increases. However, this study shows, that the effect of free surface is significant for the stress intensity factors at the crack tips.

4.2 Derivation of Equations

The dislocation model developed in Chapter 2 can be extended for the internal crack near a free surface subjected to dynamic SH loadings. Consider the configuration in Fig. 4.1, the crack of Fig. 2.3 is now moved in the x direction by b + 1. The stress released from the crack is equal to the anti-plane shear waves at $b \le x \le a$, which satisfies $\sigma_T + \sigma^* = 0$ along the crack surface.

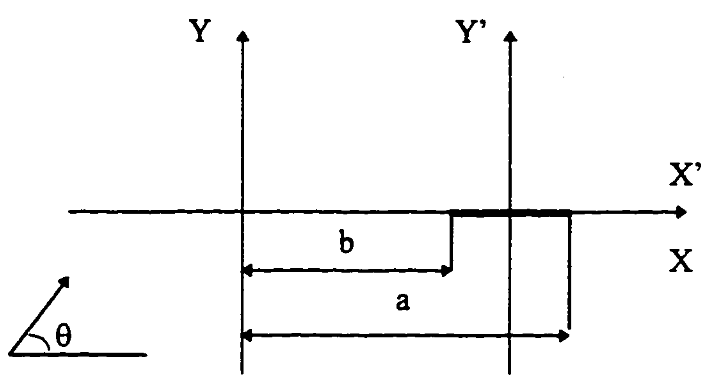

Figure 4.1 Internal crack

Again, the internal crack can be simulated by a distribution of continuous screw dislocation and the method is same as that derived in previous chapter. Now, consider a surface crack subjected to applied stress σ_a is modeled by a continuous distribution of a screw dislocation all parallel to the z axis. The stress field in the medium is induced by the screw dislocation. Using the method of Juang and Lee (1986), we obtain the stress field S(x) of normalized length of a surface crack :

$$S(x) = \sigma_a x/(x^2-1)^{1/2} \qquad (4.1)$$

Where σ_a is applied stress. In order to satisfy the boundary condition along the crack surface, the S(x) must equal to the stress released from the screw dislocation (crack). The stress released from the surface crack can be expressed as:

$$\sigma_T = \int_{-1}^{1} D(s)\,\sigma_d(x-s)ds = \int_{-1}^{1} D(s)\,B\alpha^2\{[Jo(\alpha|x-s|) + J_2(\alpha|x-s|)]\cos[\omega t+p(s)] + [Y_0(\alpha|x-s|) + Y_2(\alpha|x-s|)]\sin[\omega t+p(s)]\}ds$$

$$= \int_{-1}^{1} \alpha^2 \{[Jo(\alpha|x-s|) + J_2(\alpha|x-s|)][A_1\cos\omega t - A_2\sin\omega t] + [Y_0(\alpha|x-s|) + Y_2(\alpha|x-s|)][A_1\sin\omega t + A_2\cos\omega t]\}ds = 4\{[\sum_{n=0}^{N}\frac{a_n}{n+1}]^2 + [\sum_{n=0}^{N}\frac{b_n}{n+1}]^2\}^{1/2}\cos(\omega t-\theta_n)\, x/(x^2-1) \qquad (4.2)$$

In order to satisfy the boundary condition along the crack surface, we can express the equation $\sigma_T + \sigma^* = 0$ as $S(x) + \sigma^* = 0$. Thus

$$S(x) = -\sigma_T = -\int_{-1}^{1} D(s)\,\sigma_d(x-s)ds = -\int_{-1}^{1} D(s)\,B\alpha^2\{[Jo(\alpha|x-s|)+J_2(\alpha|x-s|)]\cos[\omega t+p(s)] + [Y_0(\alpha|x-s|)+Y_2(\alpha|x-s|)]\sin[\omega t+p(s)]\}ds$$

$$= -4\{[\sum_{n=0}^{N}\frac{a_n}{n+1}]^2 + [\sum_{n=0}^{N}\frac{b_n}{n+1}]^2\}^{1/2}\cos(\omega t-\theta_n)\, x/(x^2-1)^{1/2} \qquad (4.3)$$

Comparing Eqs. 4.1 and 4.3, the σ_a can be expressed in the following form:

$$\sigma_a = -4\{[\sum_{n=0}^{N}\frac{a_n}{n+1}]^2 + [\sum_{n=0}^{N}\frac{b_n}{n+1}]^2\}^{1/2}\cos(\omega t-\theta_n) \tag{4.4}$$

It is noted that the Eq 4.4 is applied to analyze the surface crack. Based on the same method used by Juang and Lee (1986), Shiue and Lee (1991) have investigated the elastic interaction between screw dislocation and the internal crack near a free surface also the stress intensity factor at the crack tip, crack extension force, the image force on the dislocation. They found out the stress field S'(x) arised from the dislocation distribution inside the crack, the screw dislocation and its image, and the applied stress. Using the method of Juang and Lee, we express the stress field S'(x) derived from the applied stress of normalized length of internal crack as:

$$S'(x) = \sigma_a\,[x^2-a^2E(\kappa)/G(\kappa)]/(x^2-a^2)^{1/2}(x^2-b^2)^{1/2} \tag{4.5}$$

where κ^2 equals to $(a^2-b^2)/a^2$. $G(\kappa)$ and $E(\kappa)$ are the first and second kinds of complete elliptic integrals as defined as:

$$E(\kappa) = \int_0^{\pi/2}\frac{d\beta}{\sqrt{1-\kappa^2\sin^2\beta}} \tag{4.6a}$$

$$G(\kappa) = \int_0^{\pi/2}\sqrt{1-\kappa^2\sin^2\beta}\,d\beta \tag{4.6b}$$

where $0 \le \beta \le 2\pi$. These equations together with Eq. 4.4 constitute the dynamic stress intensity factors being sought for the dynamic interaction between an internal crack and a screw dislocation. In order to derive the dynamic stress intensity factors of the internal crack, the equations presented in Chapter 2 are listed below:

$$|K_{III}| = |\lim_{x\to a}[2(x-a)]^{1/2}\sigma^{*}| \tag{4.7}$$

From above equation, all factors with the regular parts can be neglected because of the limiting progress, except $\frac{1}{\pi}\sum_{j=0}^{1}\frac{(1-j)!}{j!}\left(\frac{2}{\alpha|x-s|}\right)^{2-2j}$ in Y. Substituting Eqs. 4.4 , 4.5 into Eq. 4.7, the stress intensity factors at the right-hand and left-hand side crack tips are obtained as:

$$|H_{III}|^R = |\lim_{x\to a+}[2(x-a)]^{1/2}\tau_{yz}| = |\lim_{x\to a+}[2(x-a)]\,[x^2-a^2E(\kappa)/G(\kappa)]/(x^2-a^2)^{1/2}(x^2-b^2)^{1/2} -$$

$$4\{[\sum_{n=0}^{N}\frac{a_n}{n+1}]^2+[\sum_{n=0}^{N}\frac{b_n}{n+1}]^2\}^{1/2}\cos(\omega t-\theta_n)| = \left(\frac{a^2}{a^2-b^2}\right)^{1/2}[1-E(\kappa)/G(\kappa)]a^{1/2}|K_{III}| \quad (4.8a)$$

$$|H_{III}|^L = |\lim_{x\to b-}[2(x-b)]^{1/2}\tau_{yz}| = |\lim_{x\to b-}[2(x-a)]\,[x^2-a^2E(\kappa)/G(\kappa)]/(x^2-a^2)^{1/2}(x^2-b^2)^{1/2} -$$

$$4\{[\sum_{n=0}^{N}\frac{a_n}{n+1}]^2+[\sum_{n=0}^{N}\frac{b_n}{n+1}]^2\}^{1/2}\cos(\omega t-\theta_n)| = \left(\frac{b^2}{a^2-b^2}\right)^{1/2}[a^2E(\kappa)/b^2\,G(\kappa)-1]b^{1/2}|K_{III}| \quad (4.9b)$$

where $|K_{III}|$ is derived from Eq. 2.26.

In order to understand the effect of free surface on the stress intensity factor, the Fig. 4.2, 4.3 are plotted ($\theta = \pi/2$) to analyze the relation between the distance b and the stress intensity factors. In Fig. 4.2, the $|H_{III}|^R$ decreases with increasing b. When b approaches infinity, the $|H_{III}|^R$ will approach to $|K_{III}|$. Then crack near a free surface can be known as a crack embedded in an infinite solid. When we increase b, the $|H_{III}|^L$ will decrease and approaches $|K_{III}|$ while b approaches infinity. In Eq. 4.9b, the $|H_{III}|^L$ will become infinity when b close to zero (but not zero). It means an internal crack which is very close to a free surface will be easily extended to a surface crack. Therefore, there are two special cases worthy of mention. First, when b is equal to zero, the problem becomes that of a surface crack. Secondly, when b approaches infinity, then the problem is reduced to the case of an internal crack. The effect of interference between the input incident angle θ and the stress intensity factors also can be clearly seen in Fig. 4.4, 4.5. Figure 4.6, 4.7 4.8, 4.9, 4.10, 4.11 display the interference between the input incident angle θ and the stress intensity factors with various values of a. The proposed model reveals that there is an interesting relation between the stress intensity factors and the distance from the left side of crack tip to free surface. At $b > 2$, the left side stress intensity factor can be considered as same as a finite crack in an infinite medium. The dynamic stress intensity factor curve in Fig. 4.6, 4.7, 4.8, and 4.9 exhibit the above conclusions. From the left side stress intensity factor curve, it appears that the condition, $b/a > 0.5$ in the case of an internal crack, is sufficient to insure that results do not depend greatly on the distance from the free surface to the nearest crack tip. It should be noted that the intensity factors derived from Eqs. 4.9a and 4.9b are in good agreement with the results of Murakami (1987). It means that Eqs. 4.9a and 4.9b not only satisfy the dynamic problems also agree with static's.

4.3 Free Surface Effect

In this chapter we examine the dynamic results of a surface crack, dynamic interaction between a surface crack and a screw dislocation to the application at the surface of a uniform traction that varies harmonically with time. Attention is directed toward the quantities that are of interest in fracture mechanics, namely stress intensity factors at the crack tips. In particular, in a mechanical structure, an internal crack may induce undesirable crack propagation, failure. The negative effect of an internal crack is more significant when this internal crack is very close to free surface. The precision of stress intensity factors of the internal crack can improve the engineer's abilities to prevent the failure occurs.

Eqs. 4.9a and 4.9b show that stress intensity factor at the left side of an internal crack, that is eventually propagating towards a suffice under the influence of SH waves, suffers a sharp increases when the crack almost broken the surface. It means an internal crack which is very close to a free surface will be easily extended to a surface crack. It may be expected that the effect of the free surface diminishes as the crack moves away from it. The stress intensity factor should then approach the values for a crack in an infinite medium. In other words, the $|H_{III}|^R$ decreases with increasing b. When b approaches infinity, the $|H_{III}|^R$ will approach to $|K_{III}|$. To determine more precisely in what circumstances the effect of the free surface is negligible, the graphs of the stress intensity factors of a finite crack in an infinite medium are compared to those for an internal crack with various values of a and b. The finite crack in an infinite medium is the limit of an internal crack as $\alpha a \to \infty$ but $\alpha(b - a)$ remains constant, or equivalently $a/b \to 1$ with $\alpha(b - a)$ fixed. We expect that the internal crack curves will lie close to the finite crack curve. From the left side stress intensity factor curve, it appears that the condition, $b/a < 0.5$ in the case of an internal crack, is sufficient to insure that results do not depend greatly on the distance from the free surface to the nearest crack tip. This result can be used to test each of the parameters (wave number, incident angle) affecting stress intensity factors so that the role of each can be defined separately to insure the effects of free surface is negligible. Therefore, there are two special cases worthy of mention. First, when b is equal to zero, the problem becomes that of a surface crack. Secondly, when b approaches infinity, then the problem is reduced to the case of an finite crack in an infinite medium.

4.4 Summary

A dislocation model for an internal crack, based on the dislocation model for the surface crack and the applications of previous studies on the internal crack has been developed. The model considers the stress intensity factor both sides of an internal crack as well as the effects of free surface. Simulation results of the model show that free surface effect plays a very important role in crack propagation. Also, the results determine more precisely in what circumstances the effect of the free surface is negligible. The graphs show that the stress intensity factors at crack tip which is nearest to the free surface suffer a sharp increase. It means an internal crack which is very close to a free surface will be easily extended to a surface crack. It may be expected that the effect of the free surface diminishes as the crack moves away from it and larger when a/b approaches unity. In fact, the right side stress intensity factor will also increase with decreasing b. When b approaches infinity, the internal crack curve will lie very close to the finite crack curve. The effect of interference between the input incident angle and stress intensity factors also presented.

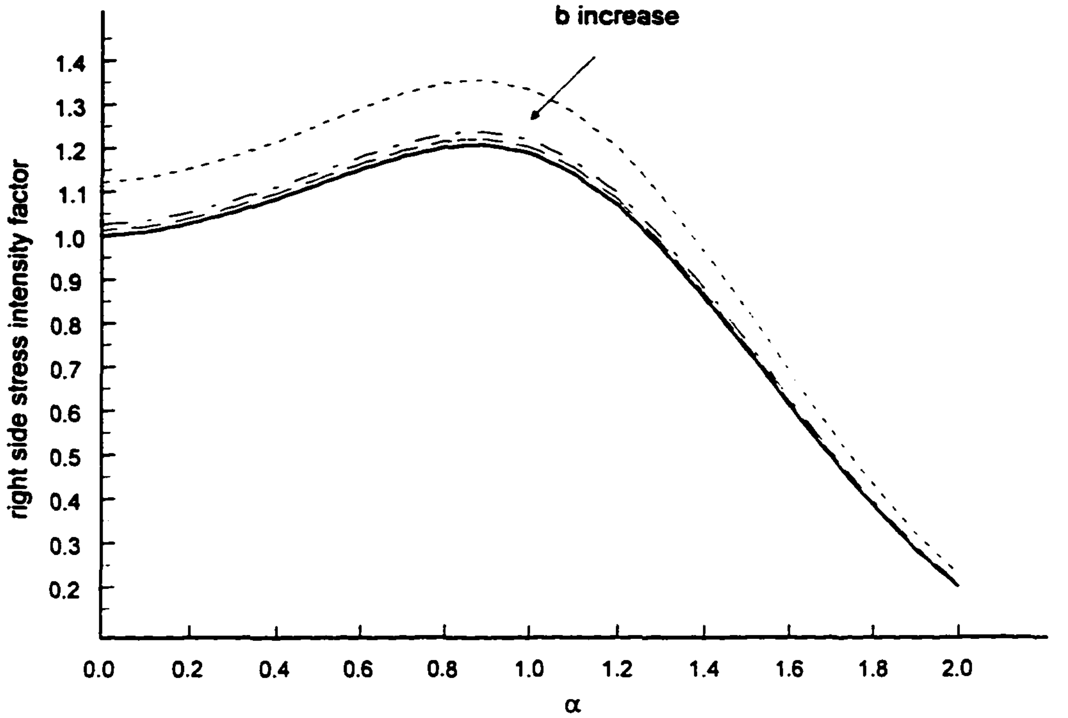

Figure 4.2 Effect of b on $|H_{III}|^R$ for $\theta = \pi/2$

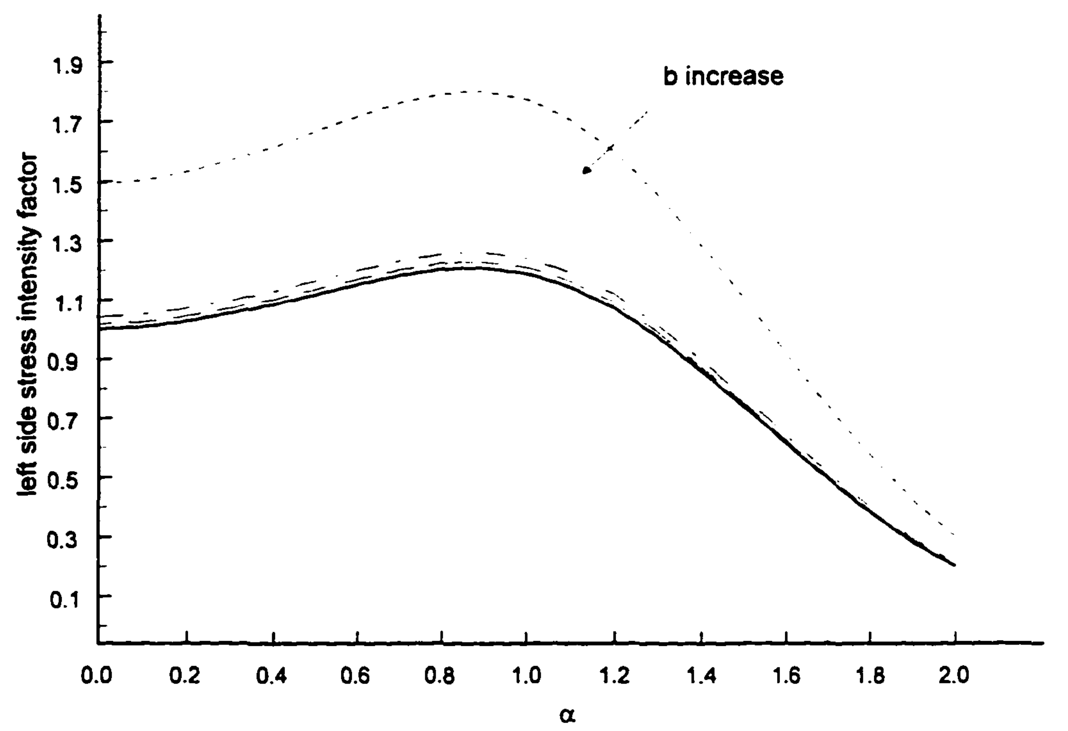

Figure 4.3 Effect of b on $|H_{III}|^L$ for $\theta = \pi/2$

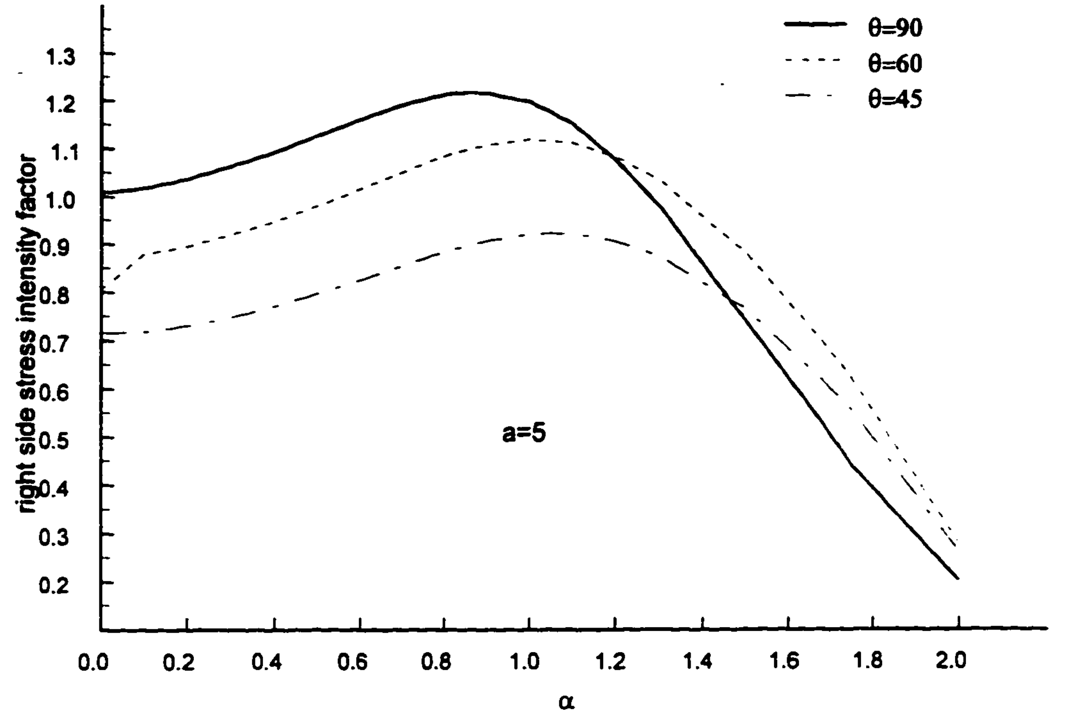

Figure 4.4 $|H_{III}|^R$ vs α and θ for $a = 5$

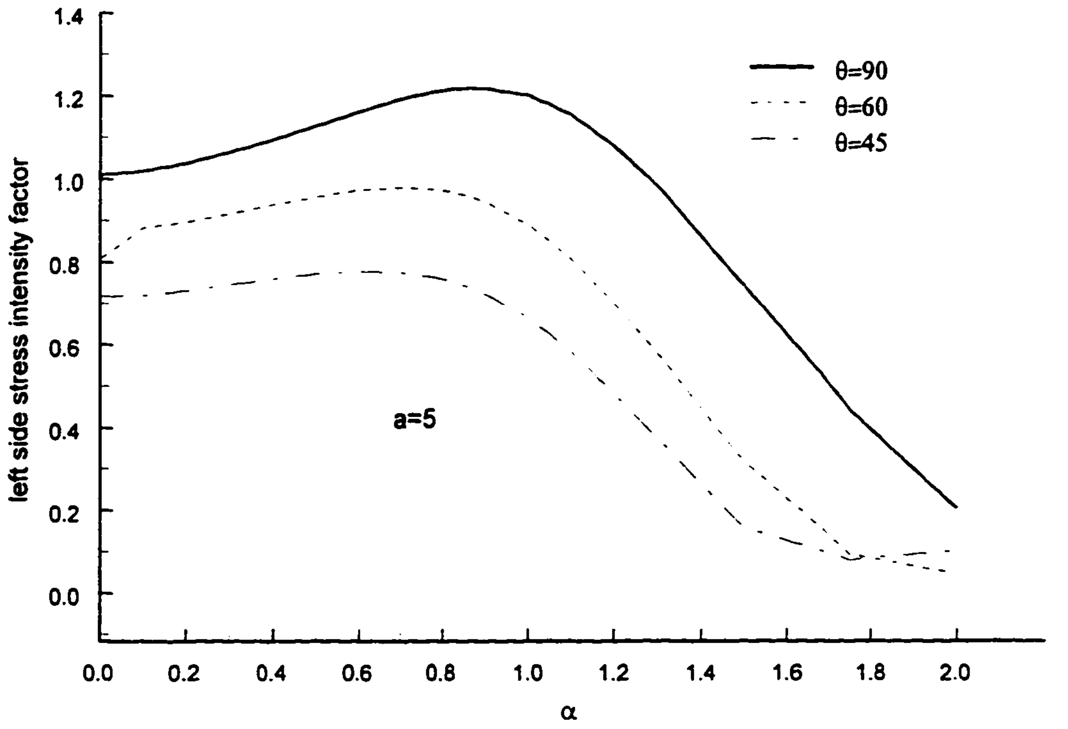

Figure 4.5 $|H_{III}|^L$ vs α and θ for $a = 5$

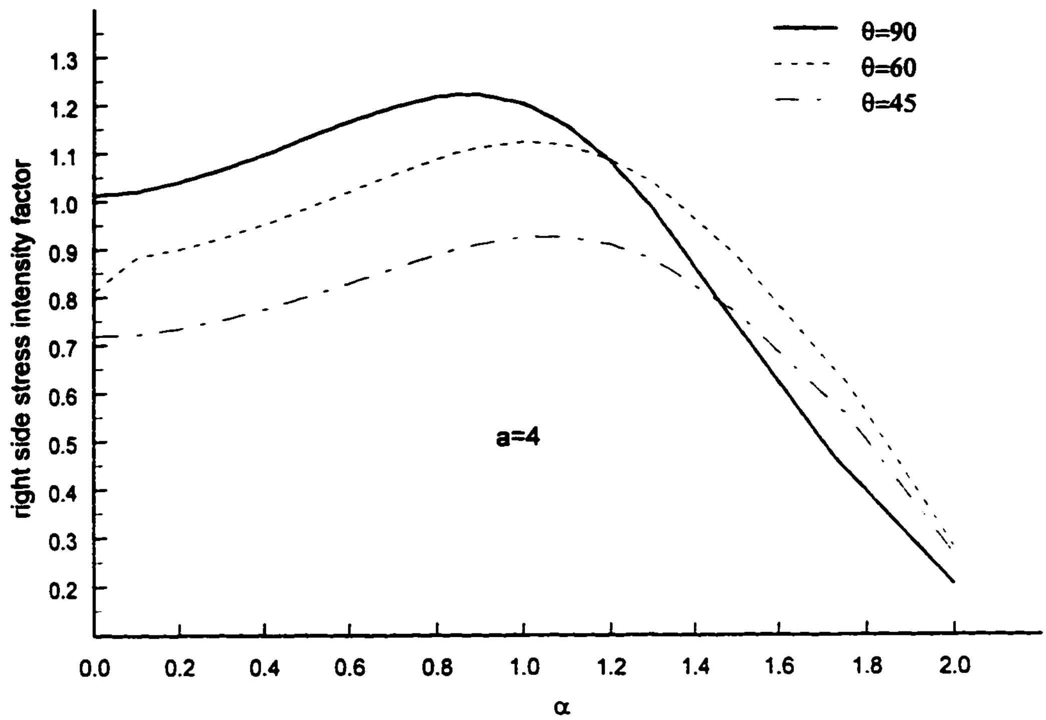

Figure 4.6 $|H_{III}|^R$ vs α and θ for $a = 4$

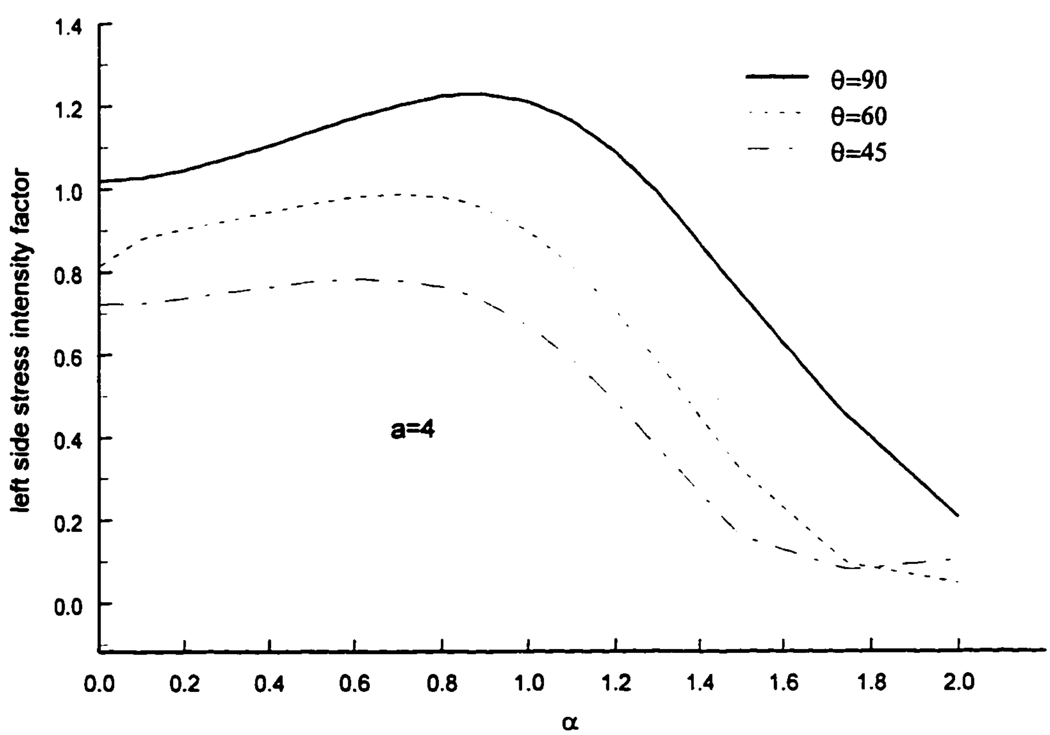

Figure 4.7 $|H_{III}|^L$ vs α and θ for $a = 4$

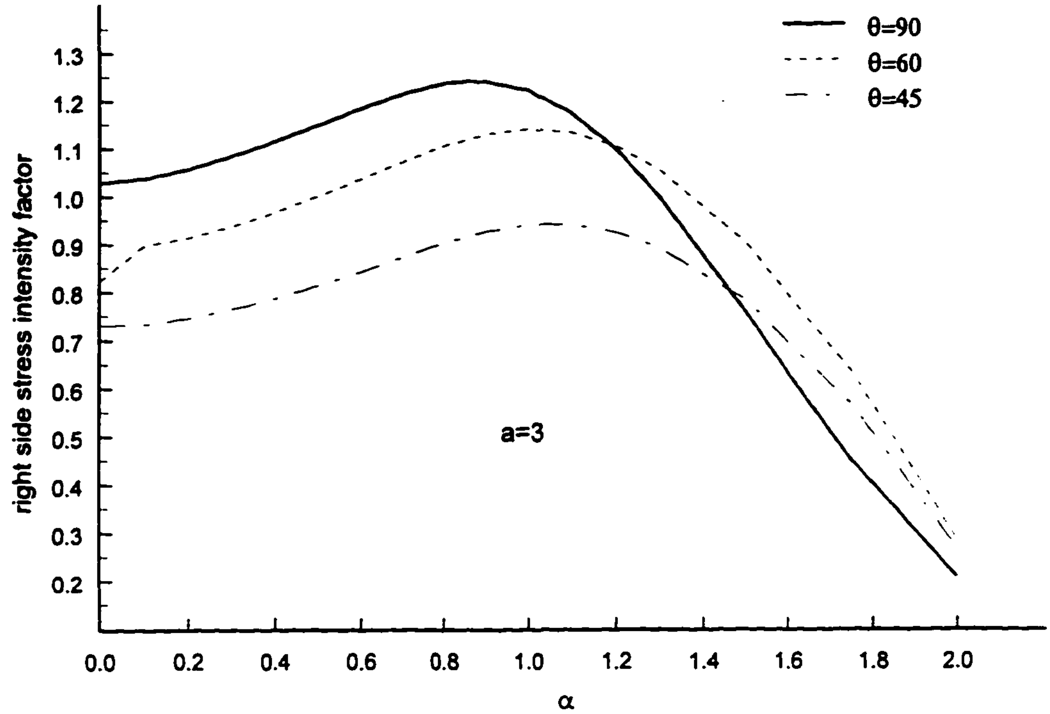

Figure 4.8 $|H_{III}|^R$ vs α and θ for $a = 3$

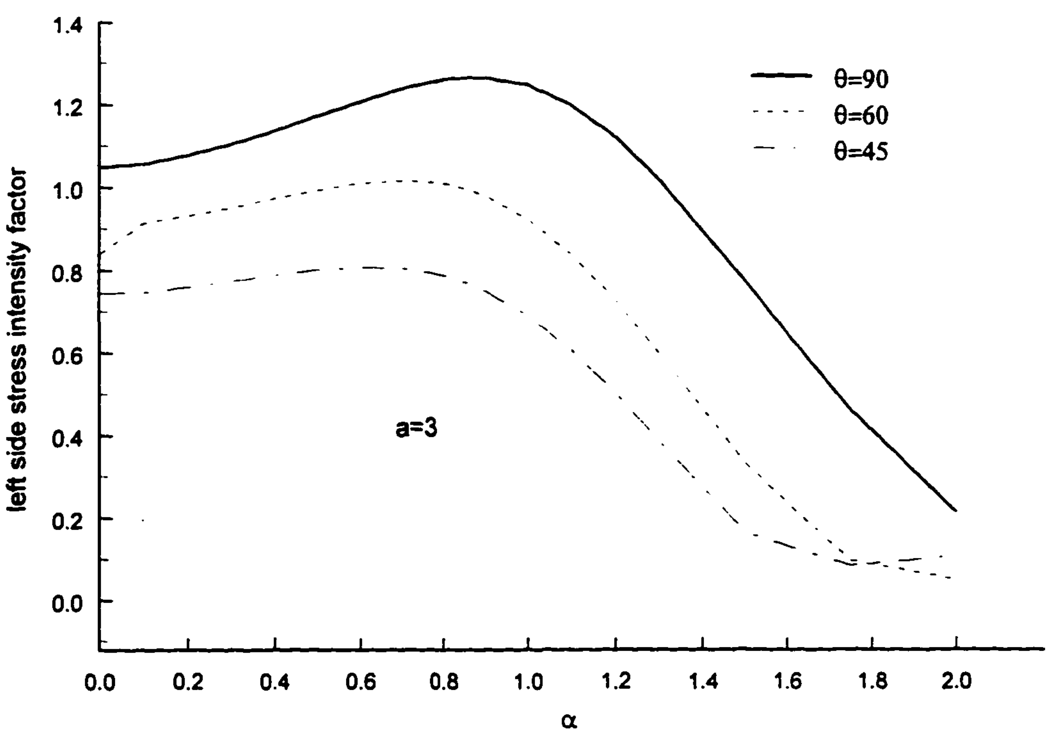

Figure 4.9 $|H_{III}|^L$ vs α and θ for $a = 3$

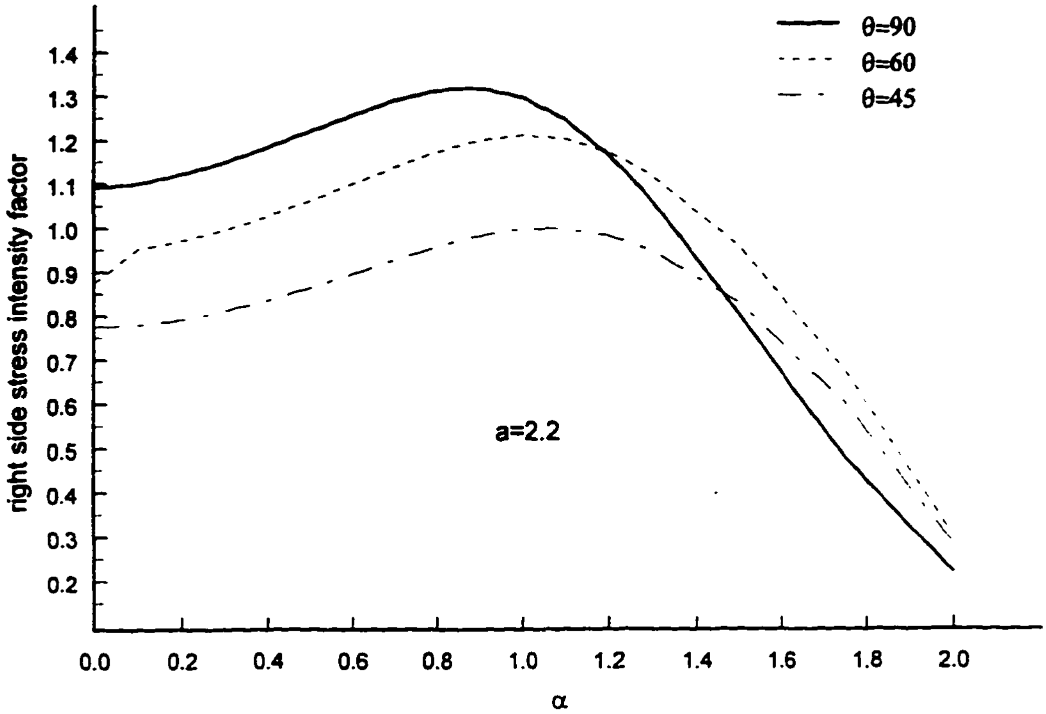

Figure 4.10 $|H_{III}|^R$ vs α and θ for $a = 2.2$

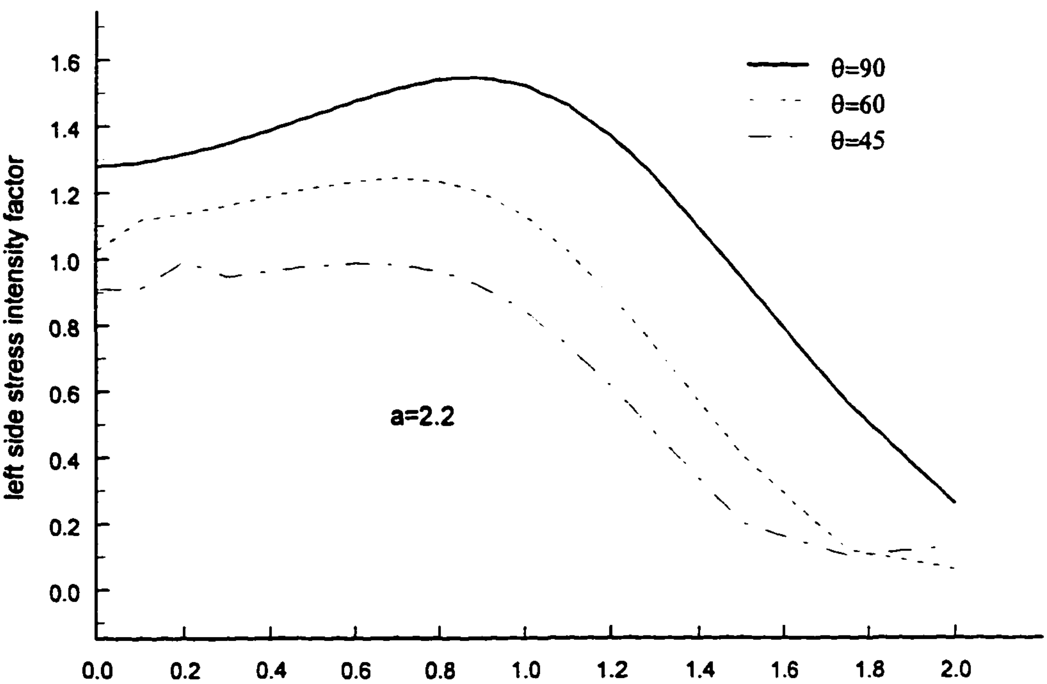

Figure 4.11 $|H_{III}|^L$ vs α and θ for $a = 2.2$

CHAPTER 5

DYNAMICS STRESS INTENSITY FACTOR OF A MOVING CRACK

5.1 Introduction

The assessment of crack initiation and propagation has been the subject of many past discussions on fracture mechanics. Depending on how the chosen failure criterion is combined with the solution of a particular theory of continuum mechanics, the outcome could vary over a wide range. As in all crack problems, the detailed stress field near crack tip must be known before any fracture analyses could be made. Once the crack is in motion, it is important to know the conditions under which it can be arrested. To avoid such phenomena, the wave numbers, inclined angle of input shear waves and velocity of the crack have to be calculated, which can be done by proper modeling of the moving crack.

Earlier works on moving crack shows that the velocity of a moving crack has a significant effect on the propagation at the crack tip. In particular, high velocity may induce undesirable failure occurs. The negative effect of the crack propagation is more significant at high velocity, where the moving crack will tend to bifurcate. Therefore, it is important to develop a suitable model to show the upper limit of the crack velocity to prevent failure occurs. The present study applies the dislocation model developed in the previous chapters as well as the works by Sih and Loeber (1970) to derive the stress intensity factor which serves as a useful parameter in studying the dynamics of crack propagation. It is noted that the dislocation model can be applied to moving coordinate system not just for stationary case. Therefore, a relatively simple dislocation model has been developed in the present study, in which the model can be derived by suitable modeling the moving crack as a moving screw dislocation.

By using the dislocation model for a moving crack subjected to the dynamic antiplane stress, the dynamic stress intensity factors at the crack tips have been derived. A brief description of this model is given for the case of an infinite elastic solid contained a finite crack of length 2 which is moving at a constant velocity c_2. This paper derives the exact analytical solutions of the crack-tip stress intensity factor of mode III. Based on the dislocation concept applied to a stationary crack subjected to dynamic SH loadings (1997) and the works of Sih and Loeber (1970), we represent a moving crack subjected to SH (horizontal polarized shear waves) with an array of continuous distribution of screw dislocations, all parallel to z axis. The effects of the wave number, the input incident angle and Mesh number on the stress intensity factors are presented.

5.2 Development of Moving Crack Model

Limited by the available mathematical techniques, solutions to problems of cracks traveling at constant velocity are usually based on the assumption that the load is independent of time. The problem of a constant length crack moving at a uniform velocity was first considered by Yoffé (1951). She assumed that the crack is self sealing at the trailing end by an amount equal to the extended portion at the leading edge of the crack and investigated the dynamic stress field near the crack branching on basis of the maximum circumferential stress criterion. This model was improved by Broberg (1960) who considers the crack tips to move in opposite directions with constant velocities. The simpler problem of a semi-infinite crack extended by tractions applied to a finite segment of the crack surfaces was solved by Craggs (1960). The problem later extended by Sih (1968) to include general loading conditions and various crack geometries. He derived a path independent integral for calculating the energy release rate of cracks moving at a constant velocity. Instead of solving directly for the potential functions, Sih (1969) has reduced the dynamic crack problem to a Riemann-Hilbert problem as in static plane elasticity. He derived two wave equations of anti-plane deformation problems using the Riemann-Hibert formulation together with Schwartz-Christoffel transformation. Although Sih has solved a pair of wave equations involving two potential functions, it is still very difficult to derive the exact solutions due to mathematical complexity. This paper presents an effective solution with less complexity for the stress intensity factor of a moving crack located in an elastic infinite isotropic solid which is subjected to harmonic shear waves.

5.3 Deriving Equations of a Moving Crack

Consider a moving coordinate system (X, Y, Z) located at middle of a crack moving at a uniform velocity c_2 along the X axis and normalize all lengths with respect to the width of the crack such that the moving crack occupies the region $-1 \leq X \leq 1$, $Y = 0$, $-\infty < Z < \infty$ as shown in Fig. 5.1. It is assumed that the crack reseals itself spontaneously, i.e., the crack length remains constant at all times. This is justified by the fact that the stress distribution close to one end of the crack is not influenced by its distance from the other end, as is shown by Yoffé [1951]

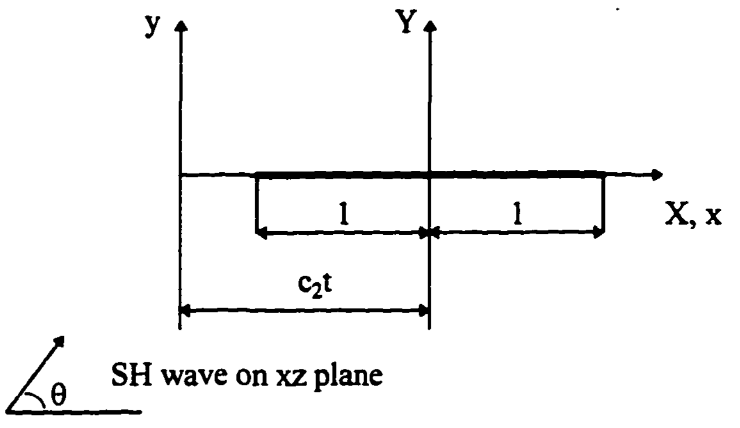

Figure 5.1 Moving crack in an infinite elastic medium

The position of the moving crack at a given time t is refereed to the stationary coordinate system (x, y, z) which are related to the moving axes attached to the crack as:

$$x = X + c_2\,t,\ \ y = Y,\ \ z = Z \tag{5.1}$$

The ratio $M^* = c_2/c$ is referred to as the Mach number, which is always smaller than 1 since the crack cannot run any faster than its limiting speed beyond which the crack will tend to bifurcate. Sih and Han (1974) explained bifurcate based on the strain energy theory in which the crack is assumed to run along the path where energy density due to volume change exceeds that of shape change. The apparent circular frequency ω^*, apparent wave number λ and apparent incidence angle φ , as the results of crack movement, are related to ω, θ, α and M^* as:

$$\omega^* = \varepsilon\,\omega,\ \tan\varphi = \frac{\beta\sin\theta}{M^*+\cos\theta},\ \lambda = \varepsilon\,\alpha/\beta^2 \tag{5.2}$$

where $\varepsilon = 1 + M^*\cos\theta$ and $\beta = (1 - M^{*2})^{1/2}$. Our previous study shows that the total stress wave released from the stationary dislocation from $-1 \leq x \leq 1$ is the convolution of the density function and the released stress wave:

$$\sigma_T = \int_{-1}^{1} D(s)\,\sigma_d(x-s)ds = \int_{-1}^{1} D(s)B\alpha^2\{[J_0(\alpha|x-s|)+J_2(\alpha|x-s|)]\cos[\omega t+p(s)]+[Y_0(\alpha|x-s|)$$

$$+Y_2(\alpha|x-s|)]\sin[\omega t+p(s)]\}ds \tag{5.3}$$

Since the total surface traction should be zero along the crack surface, we have $\sigma_T + \sigma^* = 0$ along the y = 0 plane. Therefore,

$$\int_{-1}^{1} D(s)\,B\alpha^2\{[J_0(\alpha|x-s|) + J_2(\alpha|x-s|)]\cos[\omega t+p(s)]+ [Y_0(\alpha|x-s|) + Y_2(\alpha|x-s|)]\sin[\omega t+p(s)]\}ds$$

$$= -\sigma_0\sin\theta\cos(\alpha x\cos\theta-\omega t) \tag{5.4}$$

It is expected that Eq. 5.4 is solved with reference to the moving coordinate system X, Y, Z. We assume the total stress wave released from the moving dislocation can be expressed in the form of stationary's in Eq. 5.3. Inserting Eq. 5.2 into Eq. 5.4 in terms of the translating coordinates and apparent parameters, Eq. 5.4 is expressed as:

$$\int_{-1}^{1} D(S)\,B\lambda^2\{[J_0(\lambda|X-S|) + J_2(\lambda|X-S|)]\cos[\omega^* t+p(S)]+ [Y_0(\lambda|X-S|) + Y_2(\lambda|X-S|)]$$

$$\sin[\omega^* t+p(S)]\}dS= -\sigma_1 \sin\varphi\cos[\lambda(\cos\varphi - M^*)X - \omega^* t] \tag{5.5}$$

where $S = s - c_2t$ and $\sigma_1 = w_0\mu\lambda$.. After expanding $\cos[\omega^* t+p(S)]$, $\sin[\omega^* t+p(S)]$, and $\cos[\lambda(\cos\varphi-M^*)X-\omega^* t]$, Eq. 5.5 may be expressed:

$$\int_{-1}^{1} D(S)B\lambda^2\,[\,J\cos\omega^* t\cos p(S) + Y\sin\omega^* t\cos p(S) - J\sin\omega^* t\sin p(S)+ Y\cos\omega^* t\sin p(S)\,]dS$$

$$= -\sigma_1\sin\varphi\cos[\lambda(\cos\varphi - M^*)X]\cos\omega^* t- \sigma_1\sin\varphi\sin[\lambda(\cos\varphi - M^*)X]\sin\omega^* t \tag{5.6}$$

From the coefficients of $\sin\omega^* t$ and $\cos\omega^* t$, we have:

$$\int_{-1}^{1} D(S)\, B\lambda^2[Y\cos p(S) - J\sin p(S)]dS = -\sigma_1 \sin\varphi \sin[\lambda(\cos\varphi - M^*)X] \quad (5.7a)$$

$$\int_{-1}^{1} D(S)\, B\lambda^2[J\cos p(S) + Y\sin p(S)]dS = -\sigma_1 \sin\varphi \cos[\lambda(\cos\varphi - M^*)X] \quad (5.7b)$$

where $J = J_0(\lambda|X\text{-}S|)+J_2(\lambda|X\text{-}S|)$ and $Y = Y_0(\lambda|X\text{-}S|)+Y_2(\lambda|X\text{-}S|)$. We replace D(S) and p(S) with another two functions $A_1(S) = D(S)B\cos p(S)$ and $A_2(S) = D(S)B\sin p(S)$. Since there is singularity in Y when the value of X approaches to S, we must separate Y into singular and regular parts. Eqs. 5.7a, 5.7b can be expressed in the following forms:

$$-4/\pi \int_{-1}^{1} A_1(S)/(X\text{-}S)^2 dS + 2\lambda^2/\pi \int_{-1}^{1} A_1(S) J \ln(\lambda|X\text{-}S|)dS + \int_{-1}^{1} \lambda^2 [A_1(S)f(X,S) - A_2(S)J]dS$$

$$= -\sigma_1 \sin\varphi \sin[\lambda(\cos\varphi - M^*)X] \quad (5.8a)$$

$$-4/\pi \int_{-1}^{1} A_2(S)(/(X\text{-}S)^2 dS + 2\lambda^2/\pi \int_{-1}^{1} A_2(S) J \ln(\lambda|X\text{-}S|)dS + \int_{-1}^{1} \lambda^2 [A_2(S)f(X,S) + A_1(S)J]dS$$

$$= -\sigma_1 \sin\varphi \cos[\lambda(\cos\varphi - M^*)X] \quad (5.8b)$$

where $f(X,S) = -1/\pi + 2/\pi[(\gamma\text{-}\ln 2)J_0(\lambda|X\text{-}S|) - \ln 2 J_2(\lambda|X\text{-}S|)] - 2/\pi \sum_{j=0}^{\infty}(-1)^j (\lambda/2)^{2j+2}(X\text{-}S)^{2j+2}$

$\left[\frac{\Psi(j+1)+\Psi(j+3)}{2\,j!(2+j)!} - \frac{\Psi(j+2)+\gamma}{[(j+1)!]^2}\right]$. From previous chapter, we know the stress intensity factors at the tip of the crack rely on the existence of the $r^{1/2}$ stress singularity. We therefore expect that $A_1(S)$ and $A_2(S)$ contain the term $(1\text{-}S^2)^{1/2}$. We choose to express $A_1(S)$ and $A_2(S)$ as $A_1(S) = (1-S^2)^{1/2} \sum_{n=0}^{\infty} a_n U_n(S)$ and $A_2(S) = (1-S^2)^{1/2} \sum_{n=0}^{\infty} b_n U_n(S)$.

Substituting $A_1(S)$ and $A_2(S)$ into Eqs. 5.8a, 5.8b, we have:

$$\sum_{n=0}^{\infty} a_n \{-4/\pi \int_{-1}^{1} U_m(X)(1-X^2)^{1/2} \int_{-1}^{1} \frac{U_n(S)}{(X-S)^2}(1-S^2)^{1/2}\, dSdX + \lambda^2 \int_{-1}^{1} U_m(X)(1-S^2)^{1/2}$$

$$\int_{-1}^{1} [\frac{2}{\pi} J \ln(\lambda|X-S|) + f(X,S)] U_n(S)(1-S^2)^{1/2} dSdX\} - \sum_{n=0}^{\infty} b_n \lambda^2 \int_{-1}^{1} U_m(X)(1-X^2)^{1/2} \int_{-1}^{1} J U_n(S(1-S^2)^{1/2} dSdX$$

$$= -\int_{-1}^{1} U_m(X)(1-X^2)^{1/2} \sigma_1 \sin\varphi \sin[\lambda(\cos\varphi - M^*)X] dX \tag{5.9a}$$

$$\sum_{n=0}^{\infty} b_n \{-4/\pi \int_{-1}^{1} U_m(X)(1-X^2)^{1/2} \int_{-1}^{1} \frac{U_n(S)}{(X-S)^2}(1-S^2)^{1/2}\, dSdX + \lambda^2 \int_{-1}^{1} U_m(X)(1-S^2)^{1/2}$$

$$\int_{-1}^{1} [\frac{2}{\pi} J \ln(\lambda|X-S| + f(X,S)] U_n(S)(1-S^2)^{1/2} dSdX + \sum_{n=0}^{\infty} a_n \lambda^2 \int_{-1}^{1} U_m(X)(1-X^2)^{1/2} \int_{-1}^{1} J U_n(S)(1-S^2)^{1/2} dSdX$$

$$= -\int_{-1}^{1} U_m(X)(1-X^2)^{1/2} \sigma_1 \sin\varphi \cos[\lambda(\cos\varphi - M^*)X] dX \tag{5.9b}$$

where $m = 0, 1, 2, 3, ..., M, ...\infty$ and $n = 0, 1, 2\ 3, ..., N, ..., \infty$. Following previous method, we simplify above equations as follows:

$$\sum_{n=0}^{N} [(A_{mn} + B_{mn})a_n - C_{mn} b_n] = \eta_m \quad (m = 0, 1, ..M) \tag{5.10a}$$

$$\sum_{n=0}^{N} [C_{mn} a_n + (A_{mn} + B_{mn}) b_n] = \nu_m \quad (m = 0, 1, ..M) \tag{5.10b}$$

where

$$A_{mn} = -4/\pi \int_{-1}^{1} U_m(X)(1-X^2)^{1/2} \int_{-1}^{1} \frac{U_n(S)}{(X-S)^2}(1-S^2)^{1/2}\, dSdX = \begin{cases} 0 & m \neq n \\ 2(n+1)\pi & m = n \end{cases}$$

$$B_{mn} = \lambda^2 \int_{-1}^{1} U_m(X)(1-S^2)^{1/2} \int_{-1}^{1} [\frac{2}{\pi} J \ln(\lambda|X-S|) + f(X,S)] U_n(s)(1-S^2)^{1/2} dSdX$$

$$C_{mn} = \lambda^2 \int_{-1}^{1} U_m(X)(1-X^2)^{1/2} \int_{-1}^{1} J U_n(S)(1-S^2)^{1/2}\, dSDdX$$

$$\eta_m = -\int_{-1}^{1} U_m(X)(1-X^2)^{1/2}\sigma_1 \sin\varphi \sin[\lambda(\cos\varphi - M^*)X]dX$$

$$v_m = -\int_{-1}^{1} U_m(X)(1-X^2)^{1/2}\sigma_1 \sin\varphi \cos[\lambda(\cos\varphi - M^*)X]dX$$

Eqs. 5.10a, 5.10b contain 2(N+1) unknown coefficients a_n and b_n with 2(M+1) equations. To solve for a_n and b_n (n = 0, 1, ...,N), let M = N. The above equations can be put into matrix form as :

$$(A+B)\vec{a} - C\vec{b} = \vec{\eta} \tag{5.11a}$$

$$C\vec{a} + (A+B)\vec{b} = \vec{v} \tag{5.11b}$$

Our problem is to find positive integers M and N such that a_n and b_n converge to zero.

5.3.1 Dynamic Stress Intensity Factor

The stress intensity factor at the crack tip from Eq. 2.15a may now be defined as follows:

$$|K_{III}| = |\lim_{x\to 1}[2(x-1)]^{1/2}\sigma^*| \tag{5.12}$$

At regular points, the stress intensity factor will be zero. For the singular points, the stress intensity factor is expressed as :

$$|K_{III}| = \lim_{X\to 1}[2(X-1)]^{1/2}(-4/\pi)\{\sum_{n=0}^{N}[a_n \sin\omega^* t\} + b_n \cos\omega^* t]\int_{-1}^{1} U_n(S)\frac{(1-S^2)^{1/2}}{|X-S|^2}dS\}$$

$$= 4\{[\sum_{n=0}^{N}\frac{a_n}{n+1}]^2 + [\sum_{n=0}^{N}\frac{b_n}{n+1}]^2\}^{1/2}\cos(\omega^* t-\theta_n) = |K_{III}|\cos(\omega^* t-\theta_n) \tag{5.13}$$

In order to explain the effects of the wave number, the input incident angle and Mach number on the stress intensity factor, we focused in a small region about the left side of crack tip.

5.3.2 Crack Bifurcation

The phenomenon of crack bifurcation is one of the most intriguing features of crack propagation at high speed. Here, the crack, when traveling at a high velocity, suddenly, and for no obvious reason, divided into two branches. In glass or hard plastic, this process may continue until a pattern of multiple crack divisions is obtained. The instability that occurs in crack bifurcation is undoubtedly associated with the empirical fact that a high speed crack tends to change its path abruptly when encountering an obstacle in the material. The excess energy in the vicinity where the original crack turned initiates a new crack. This event occurs so quickly that the crack appears to have been split in two or bifurcated.

Many attempts have been mode to explain the crack bifurcation phenomenon. As mentioned earlier, Yoffé (1951) assumed the prospective sites of crack branching to coincide with the maximum of the local circumferential stresses ahead of the moving crack.

5.3.3 The Critical Mach Number

The stress distribution along the crack surface can be derived from Eqs. 2.15a, 2.15b and Sih (1970). This gives:

$$\tau_{xz} = -\frac{K_{III}}{\sqrt{2r_2}}\sin(\phi_2/2) = -\frac{K_{III}}{\sqrt{2\rho}}\left[\frac{\sqrt{1-M^{*2}\sin^2\vartheta}-\cos\vartheta}{2(1-M^{*2})\sqrt{1-M^{*2}\sin^2\vartheta}}\right]^{1/2} \tag{5.14a}$$

$$\tau_{yz} = \frac{K_{III}}{\sqrt{2r_2}}\cos(\phi_2/2) = \frac{K_{III}}{\sqrt{2\rho}}\left[\frac{\sqrt{1-M^{*2}\sin^2\vartheta}+\cos\vartheta}{2\sqrt{1-M^{*2}\sin^2\vartheta}}\right]^{1/2} \tag{5.14b}$$

where $r_2 = \rho[1 - M^{*2}\sin^2\vartheta]^{1/2}$, $\rho = [(X-1)^2 + Y^2]^{1/2}$, $\vartheta = \tan^{-1}[Y/(X-1)]$ and

$$\sin(\phi_2/2) = \frac{\sqrt{1-M^{*2}\sin^2\vartheta}-\cos\vartheta}{2\sqrt{1-M^{*2}\sin^2\vartheta}}, \quad \cos(\phi_2/2) = \frac{\sqrt{1-M^{*2}\sin^2\vartheta}+\cos\vartheta}{2\sqrt{1-M^{*2}\sin^2\vartheta}} \tag{5.15}$$

Note that the crack cannot run any faster than its limiting speed beyond which the crack will tend to bifurcate It is important to know the critical Mach number at which the crack may start to branch. This limit can be found by calculating the maximum circumferential shear stress τ_φ, from

$$\tau_\varphi = -\tau_{xz}\sin\vartheta + \tau_{yz}\cos\vartheta = \frac{K_{III}}{\sqrt{2\rho}\sqrt{1-M^{*2}}}\frac{(\sqrt{1-M^{*2}\sin^2\vartheta}-M^{*2}\cos\vartheta)\sin\vartheta}{\sqrt{2(1-M^{*2}\sin^2\vartheta)}\sqrt{1-M^{*2}\sin^2\vartheta-\cos\vartheta}} \tag{5.16}$$

By differentiating τ_φ with respect to ϑ and setting the result equal to zero, the critical Mach number M is obtain ≈ 0.6. Loeber and Sih (1970) derived the critical Mach number from two complex functions which were determined from the system of Fredholm integral equations. Although they have overcame the mathematical difficulty in the application of the Wiener-Hopf technique, it is still not clear and easy to solve the kernal in Fredholm integral equations. The present method has led to effective solutions in this dynamic problem.

5.4 Comparison of Normalized SIF Curves for Various Parameters

The stress intensity factor K_{III} is a useful parameter in studying the moving crack problem. Numerical results have been obtained for the dimensionless quantity of the stress intensity factor as a function of α, θ and M^*. In Figs. 5.2-5.4, graphs for $\theta = 0, 90,$ 180, deg and various values of M^* are given. Fig. 5.2 shows that all the peaks are almost the same magnitude and their locations move into the higher frequency range as M^* is increased. At normal incident angle $\theta = 90$ deg, Fig. 5.3 gives the variation of normalized stress intensity factor with the wave number for different values of the crack velocity. As M^* increases, the peaks of the curves decrease in magnitude and occur at lower frequencies. The curve corresponding to $M^* = 0.8$ in Fig. 5.3 is physically implausible since the crack cannot run any faster than its limiting speed. The curves in Fig. 5.4 display that all peaks are almost same magnitude and their locations move into the lower frequency range as M^* is increased. A set of parametric curves for $\alpha = 0.5$ is given in Fig. 5.5 to illustrate the variation of the normalized stress intensity factor with the incident angle θ of the input SH waves. It is noted that the peaks in Fig 5.5 are moved toward larger values of incident angle when M^* is increased.

5.5 Summary

An analysis of the scattering of horizontally shear waves by a finite extending uniformly crack subjected to anti-plane shear waves has been carried out by using the dislocation method. It is based on dislocation model used by in chapter 2 in wave diffraction problems dealing with stationary surface crack. The Chebyshev Polynomials, based on the stress boundary condition of the crack surface, are also presented for obtaining the stress intensity factor at the crack tip. It is found that the dynamic stress intensity factor of the singular stresses depends upon the speed of crack propagation, the frequency of the incoming shear waves, and the angle of incidence. As the crack speed is increased at normal incidence, the peaks of the dynamic stress intensity factor curves tend to decrease and occur at lower wave numbers. The significant result is that the dynamic stress intensity factors can be higher than the static ones depending upon the frequency of the incoming shear waves and speed of crack propagation. At high frequency, the higher-order terms in a_n and b_n become very important in calculating the stress intensity factor. The choice of the M, N must be based on the wave number. Although the present paper deals only with the diffraction of SH waves by a running crack, the same method may be used to treat the scattering of plane harmonic compressional waves (P-waves) and vertically polarized shear waves (SV-waves).

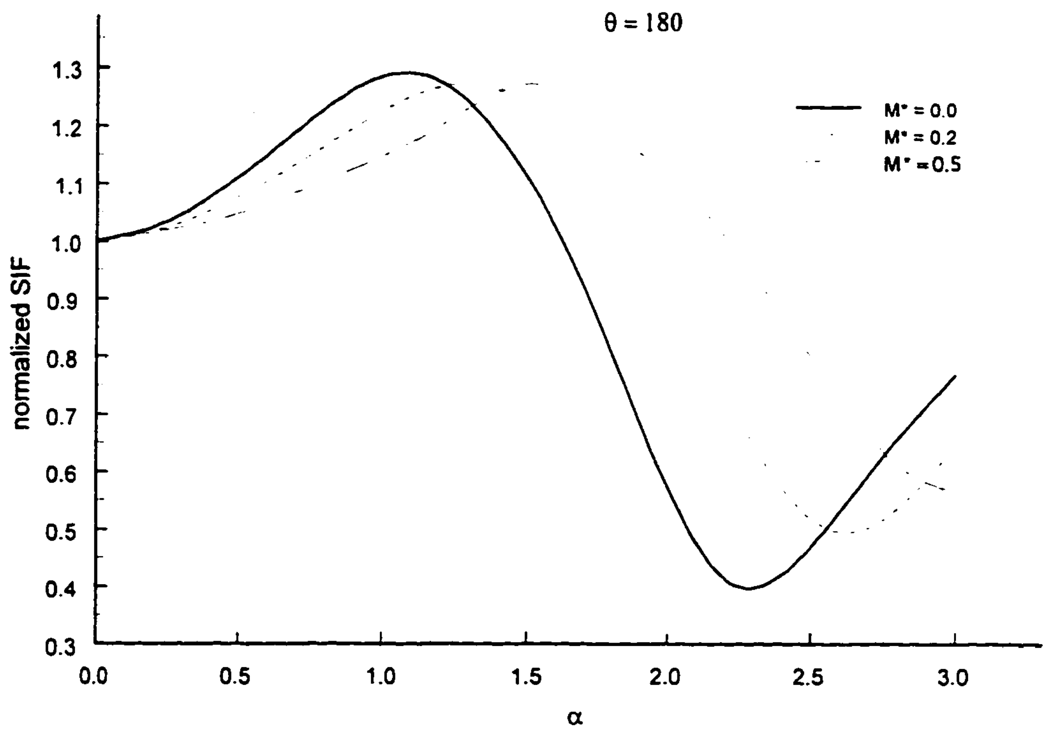

Figure 5.2 Stress intensity factor as a function of actual wave number for incident angle of 180 deg

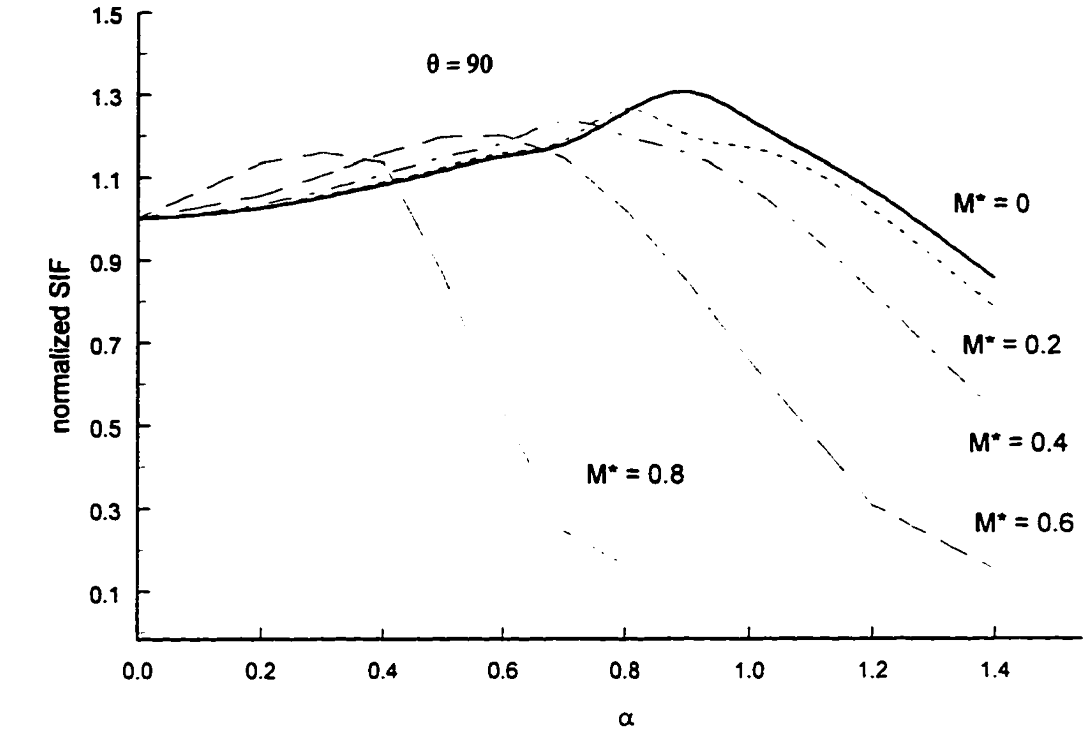

Figure 5.3 Stress intensity factor as a function of actual wave number at normal incidence

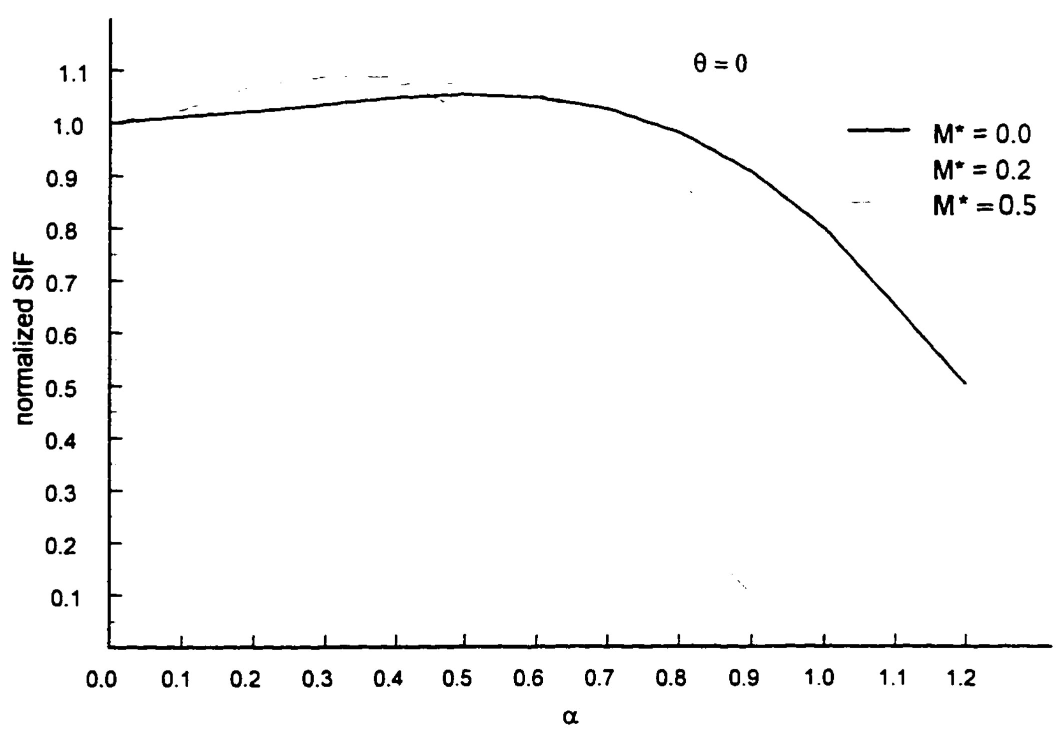

Figure 5.4 Stress intensity factor as a function of actual wave number for incident angle of 0 deg

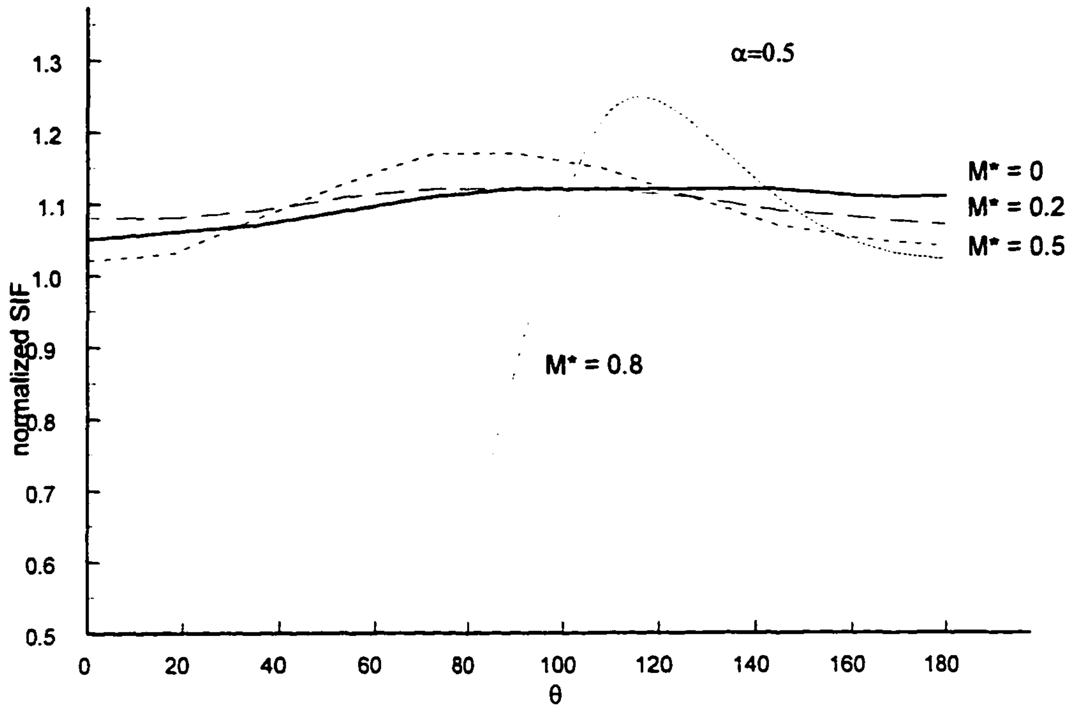

Figure 5.5 Stress intensity factor against actual incident angle for $\alpha = 0.5$

CHAPTER 6

CONCLUSIONS AND RECOMMENDATIONS

6.1 Conclusions

The dynamic dislocation models for a surface crack and finite crack have been developed for both the stationary and moving types. The normalized stress intensity factor serves as a useful parameter in studying the characteristics of a stationary crack or a moving crack since it can be associated with the strain energy release rate corresponding to crack extension force. The following are the results of this research:

1. A dislocation model based on the mirror image with respect to the free surface of a surface crack has been developed to determine the stress intensity factors at the crack tip in a semi-infinite isotropic elastic solid which is subjected to periodic cyclic loadings. This model represents a crack by a continuous distribution of dislocation singularities. A brief description of this model is given for the case of a surface crack lying in the xz plane with an infinite z dimension extended to the yz free surface. This paper derives the exact analytical solutions of the crack-tip stress intensity factor of mode III. Based on the dislocation concept applied to static crack problem, we represent a mirrored surface crack subjected to SH (horizontal polarized shear waves) with an array of screw dislocations. Similarly, we model the cracks subjected to P (primary waves) or SV (vertical polarized shear waves) with two arrays of edge dislocations: one vibrates on its glide plane and the other along its climbing direction. By using the conformal mapping technique and the

numerical solution for edge crack subjected to anti-plane shear and inplane waves, the distribution densities of the dislocations as well as the phase lags are expressed as a system of singular integral equations, which contains Bessel functions. Galerkin method is applied to find out the dynamic stress intensity factor of an internal crack near a free surface under SH loadings. The results show the dynamic stress intensity factors ($\alpha \neq 0$) will increase at low frequency when the α increases and reach the maximum value (when $\alpha \cong 0.9$) which is about 25% more than the static stress intensity factor ($\alpha = 0$). At relatively high frequencies, the stress intensity factor drops rapidly beyond the first maximum value and exhibits oscillations of approximately constant period as α increases. The values of the dynamic stress intensity factors are always bigger than the static stress intensity factors at low frequency and increase to maximum values when $\alpha \approx 0.9$. The simulation results have been compared and verified with works of Mal (1969) and Stone (1980). The comparison shows a qualitative agreement in the dynamic behavior.

2. By using the dislocation model for the surface crack and images for the free surface, an analytical solution for interaction between a screw dislocation near a mode III surface crack subjected to the dynamic antiplane stress has been derived. The change of the crack extension force as the surface crack propagation towards the dislocation is presented. Without the applied stress, the dislocation stress field tends to drag the surface crack to the dislocation where the strain energy can be relaxed. Under the periodic dynamic stress, the surface crack can be repelled by the dislocation depending upon the direction of the applied stress and wave number and the Burgers vector of the dislocation. The effects of the wave number, the input incident angle and the dislocation on the stress intensity

factor are also presented. The results showed this problem can be reduced to a crack embedded in an infinite solid when the distance between the dislocation and the free surface is ≥ 20. It is noted that the stress intensity factor increases with increasing the input angle θ at low frequencies and the stable position x_0 will decrease when the input angle θ increases. The SIF curve for $\alpha = 0$ is in a good agreement with that given in Chu (1982).

3. A dislocation model for an internal crack ($b \leq x \leq a$), based on the dislocation model for the surface crack and the applications of previous studies on the internal crack has been developed. The model considers the stress intensity factor on both sides of an internal crack as well as the effects of free surface. Simulation results of the model that free surface effect plays a very important role in crack propagation. Also, the results determine more precisely in what circumstances the effect of the free surface is negligible. The contours near the free surface for both left and right side stress intensity factors are almost parallel to the y-axis due to the effect of free surface. The results show that the stress intensity factors at crack tip which is nearest to the free surface suffer a sharp increase. It means an internal crack which is very close to a free surface will be easily extended to a surface crack. It may be expected that the effect of the free surface diminishes as the crack moves away from it and larger when a/b approaches unity. In fact, the right side stress intensity factor will also increase with decreasing b. When b approaches infinity, the internal crack curve will lie very close to the finite crack curve. The effect of interference between the input incident angle and stress intensity factors also presented in this research. It is noted that the stress intensity factor increases with

increasing the input angle θ at low frequencies. At relatively high frequencies, the stress intensity factor drops rapidly beyond the first maximum value and exhibits oscillations of approximately constant period as α increases. values of the dynamic stress intensity factors are always bigger than the static stress intensity factors at low frequency.

4. An analysis of the scattering of horizontally shear waves by a finite extending uniformly crack subjected to anti-plane shear waves has been carried out by using the dislocation method. It is found that the dynamic stress intensity factor of the singular stresses depends upon the speed of crack propagation, the frequency of the incoming shear waves, and the angle of incidence. As the crack speed is increased at normal incidence, the peaks of the dynamic stress intensity factor curves tend to decrease and occur at lower wave numbers. The significant result is that the dynamic stress intensity factors can be higher than the static ones depending upon the frequency of the incoming shear waves and speed of crack propagation. Numerical results have been obtained for the dimensionless quantity of the stress intensity factor as a function of α, θ and M^*. At incident angle θ = 180 deg, the figure shows that all the peaks are almost the same magnitude and their locations shift into the lower frequency range as M^* is increased. At normal incident angle θ = 90 deg, the peaks of the curves decrease in magnitude and occur at lower frequencies as M^* increases. A set of normalized stress intensity factor curves for α = 0.5 is given to illustrate the variation of the normalized stress intensity factor with the incident angle θ of the input SH waves. The results show the peaks are moved toward larger values of incident angle when M^* is increased. The simulation results are in good agreement with that of Sih and Mal (1970).

6.2 Application

Recent cases of catastrophic failure of primary structure in aircraft due in part to the presence of undetected cracks has emphasized the need for fracture control procedures to augment traditional static and fatigue design. Such procedures, when effectively implemented, would insure the safe operation of the air vehicle within the prescribed service period. With regard to aircraft structure design, fracture control implies the intelligent selection, usage and control of structure materials, the design and usage of highly accessible, inspectable and damage tolerant structure configurations, and the control of safe operating stresses.

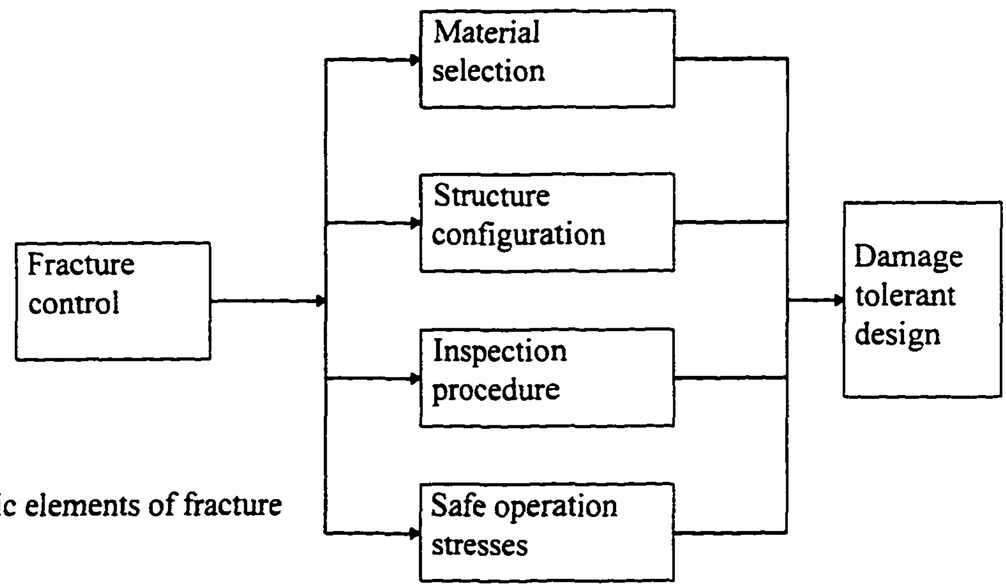

The basic elements of fracture control

6.2.1 Example

The following document prescribed a technical plan of implement rational fracture mechanics theory into design criteria, material selection, analysis, qualification and utilization of aircraft structure system.

I. ***Criteria***

(a) Chemical and thermal environment (b) Review of past experience, structural review (c) Establish fracture criteria for material selection (d) Mission definition and analysis

II. ***Data Requirements and Applications***

(a) Establishment of measurable parameters K, K_c (b) Fatigue crack growth data (c) Effect of loading sequence (d) Effect of stress state on fracture (e) mixed mode fracture study.

III. ***Fracture analysis methodology***

(a) Development of K for complex cases (b) Analytical crack model under dynamic loadings (c) Plasticity and free surface effects (d) Residual strength

IV. ***Qualification for fracture resistance***

(a) Real-time flaw growth testing (b) Crack growth resistance and crack arrest testing (c) Proof testing

V. ***Utilization - structural concept***

(a) Concepts for flaw and crack arrest (b) Performance and weight trade off studies (c) Fabrication of structural concept and full scale testing (d) Inspection

6.3 Recommendations for Future Works

All the above models have been focused on a mode III crack subjected to the dynamic antiplane stress. Further investigation is required to determine the stress distribution of a mode I, II crack when it is subjected to plane harmonic compressional waves (P- waves) or vertically polarized shear waves (SV-waves). As we mentioned earlier, the cracks subjected to P or SV waves can be simulated by two arrays of edge dislocates: one vibrates on its glide plane and the other along its climbing direction. When the input P or SV waves meet the edge dislocation, these waves are reflected due to the imhomogeneity of dislocation density and will generate mixed mode I and II deformation fields. In order to determine the stress intensity factors of a mode I or II crack, the reflected waves emitted from two array of edge dislocations are recommended. The analysis will be very useful for improving an understanding of the behavior of material failure under dynamic loadings.

Further, the stress along the crack is expressed as a system of singular integral equations containing Bessel functions and the distribution densities D(s) and the phase lags p(s) of the dislocations. From the Simpson integration method, we expressed the unknowns D(s) and p(s) in the form of the Chebyshev Polynomials. In evaluating a_n and b_n , we find out the values of a_n and b_n would converge to zero if M, N > 5 at low frequency. At high frequency, the higher-order terms in a_n and b_n become very important in calculating the stress intensity factor. In order to determine the precise solutions, the choice of the M, N must be based on the wave number α. The relationship between α and the convergency of M, N needs to be established.

APPENDIX A

DERIVATION of EQUATIONS 2.14a and 2.14b

From Eqs. 2.13a and 2.13b

$$J_n(x) = \sum_{j=0}^{\infty}\frac{(-1)^j}{j!(n+j)!}\left(\frac{x}{2}\right)^{n+j},\; Y_0(x) = \frac{2}{\pi}\left[\ln\left(\frac{x}{2}\right)+\gamma\right]-\frac{2}{\pi}\sum_{j=1}^{\infty}(-1)^j\frac{\left(\frac{x}{2}\right)^{2j}}{(j!)^2}\left\{1+\frac{1}{2}+\ldots+\frac{1}{j}\right)$$

$$Y_n(x) = \frac{2}{\pi}\ln\left(\frac{x}{2}\right)J_n(x)-\frac{1}{\pi}\sum_{j=0}^{n-1}\frac{(n-j-1)!}{j!}\left(\frac{2}{x}\right)^{n-2j}-\frac{1}{\pi}\sum_{j=0}^{\infty}\frac{(-1)^j\left(\frac{x}{2}\right)^{n+2j}[\psi(n+j+1)+\psi(j+1)]}{j!(n+j)!}$$

In $Y_0(x)$, $1+\frac{1}{2}+\frac{1}{3}\ldots+\frac{1}{j} = \psi(j+1)+\gamma$, then Eq. 2.13b gives:

$$\int_{-1}^{1}\alpha^2 [A_1(s)J + A_2(s)Y]ds = \int_{-1}^{1}\alpha^2 A_1(s)Jds + 2/\pi \int_{-1}^{1}\alpha^2 A_2(s)\ln(\alpha|x-s|)J_0(\alpha|x-s|)ds +$$

$$2/\pi \int_{-1}^{1}\alpha^2 A_2(s)(\gamma-\ln 2)J_0(\alpha|x-s|)ds + \pi/2 \int_{-1}^{1}\alpha^2 A_2(s)\ln(\alpha|x-s|)J_2(\alpha|x-s|)ds- 1/\pi \int_{-1}^{1}\alpha^2 A_2(s)\, ds$$

$$+\pi/2 \int_{-1}^{1}\alpha^2 A_2(s) \sum_{j=0}^{\infty}\frac{(x-s)^{2j+2}}{[(j+1)!]^2}\left(\frac{\alpha}{2}\right)^{2j+2}[\psi(j+2)+\gamma]ds- \pi/2 \int_{-1}^{1}\alpha^2 A_2(s)\ln 2 J_2(\alpha|x-s|)ds -$$

$$1/\pi \int_{-1}^{1}\alpha^2 A_2(s)\frac{4}{\alpha^2 |x-s|^2}ds - 1/\pi \int_{-1}^{1}\alpha^2 A_2(s) \sum_{j=0}^{\infty}\frac{(-1)^j\left(\frac{\alpha|x-s|}{2}\right)^{2+2j}}{j!(2+j)!}[\psi(j+1)+\psi(j+3)]$$

Eq. 2.13a can be manipulated in exactly the same way.

APPENDIX B

CALCULATION of INTEGRAL TERMS in EQUATION 2.20

The problem is to change the x^m and $\ln|x-s|$ into the Chebyshev Polynomial, with $-1 \le x \le 1$, $-1 \le s \le 1$. Suppose that $x = \cos\beta$ and $s = \cos\delta$, $0 \le \beta, \delta \le \pi$. From Rivlin (1974), we have:

$$\int_{-1}^{1} \frac{U_n(s)}{(x-s)^2}(1-s^2)^{1/2}\,ds = -(n+1)\pi U_n = -\pi T'_{n+1}(x)$$

and $x^q = \sum_{j=0}^{q} B_j^{(q)} T_j(x)$, with $\begin{cases} B_{q-2k}^{(q)} = 2^{1-q}\left[\dfrac{q!}{(q-k)!k!}\right] & k=0,1,2,\ldots\left[\dfrac{q}{2}\right] \\ B_j^{(q)} = 0 & \text{if } j \ne q-2k \end{cases}$

where $T_n(x)$ is the first kind of Chebyshev Polynomials

Thus $A_{mn} = -4/\pi \int_{-1}^{1} U_m(x)(1-x^2)^{1/2} \cdot -\pi T'_{n+1}(x)\,dx = \begin{cases} 0 & m \ne n \\ 2(n+1)\pi & m = n \end{cases}$

So, $\int_{-1}^{1} U_m(x)(1-x^2)^{1/2} x^q\,dx = \sum_{j=0}^{q} B_j^{(q)} \int_0^{\pi} \sin(m+1)\theta \sin\theta \cos j\theta\,d\theta$

$$= \frac{1}{2}\sum_{j=0}^{q} B_j^{(q)} \left[\int_0^{\pi} \cos m\theta \cos j\theta\,d\theta - \int_0^{\pi} \cos(m+2)\theta \cos j\theta\,d\theta\right]$$

$$= \frac{1}{2}\sum_{j=0}^{q} B_j^{(q)} \begin{cases} \frac{\pi}{2} & m = j \ne 0 \\ \pi & m = j = 0 \\ 0 & \text{other} \end{cases} - \begin{cases} \frac{\pi}{2} & m - j = -2 \\ 0 & \text{other} \end{cases}$$

and $\int_{-1}^{1} U_m(x)(1-x^2)^{1/2} \ln|x-s| x^q\,dx = \int_{-1}^{1} U_m(x)(1-x^2)^{1/2} \ln|x-s| \sum_{j=0}^{q} B_j^{(q)} T_j(x)\,dx$

$$= \sum_{j=0}^{q} B_j^{(q)} \int_0^{\pi} \ln|s-\cos\beta| \sin\beta \sin(m+1)\beta \cos j\beta\,d\beta$$

and $1/\pi \int_0^\pi \ln|s-\cos\beta|\sin\beta\sin r\beta d\beta = \begin{cases} -\frac{1}{2}\ln 2+\frac{1}{4}T_2(s) & r=1 \\ \frac{1}{2}\frac{T_{r+1}(s)}{r+1}-\frac{T_{r-1}(s)}{r-1} & r\geq 2 \end{cases}$ let $r = m+j+1$

then $\int_{-1}^{1} U_m(x)(1-x^2)^{1/2}\ln|x-s|x^q dx = \frac{\pi}{2}\sum_{j=0}^{q} B_j^{(q)} w_{mj}$, and w_{mj} is defined as following:

$$\begin{cases} -\frac{1}{2}\ln 2+\frac{1}{4}T_2(s) & m=j=0 \\ \frac{1}{2}\frac{T_{m+j+2}(s)}{m+j+2}-\frac{T_{m+j}(s)}{m+j} & m+j\geq 1 \\ -\frac{1}{2}\ln 2+\frac{1}{4}T_2(s) & m-j=0 \\ \frac{1}{2}\frac{T_{m-j+2}(s)}{m-j+2}-\frac{T_{m-j}(s)}{m-j} & m-j\geq 1 \\ 0 & m+1-j=0 \\ \frac{1}{2}\ln 2-\frac{1}{4}T_2(s) & m-j=-2 \\ \frac{1}{2}\frac{T_{j-m}(s)}{j-m}-\frac{T_{j-m-2}(s)}{j-m-2} & j-m\geq 3 \end{cases}$$

then $\int_{-1}^{1} U_m(x)(1-x^2)^{1/2}s^i T_g(s)ds = \sum_{b=0}^{i} B_b^{(i)} \int_{-1}^{1} U_m(x)(1-x^2)^{1/2}T_b(s)T_g(s)ds$

$$= \sum_{b=0}^{i} B_b^{(i)} \begin{cases} \frac{\pi}{8} & g+b=m\neq 0 \\ \frac{\pi}{4} & g+b=m=0 \\ -\frac{\pi}{8} & g+b-m=2 \\ 0 & \text{other} \end{cases} + \begin{cases} \frac{\pi}{8} & |g-b|=m\neq 0 \\ \frac{\pi}{4} & |g-b|=m=0 \\ -\frac{\pi}{8} & |g-b|-m=2 \\ 0 & \text{other} \end{cases}$$

Substitute above equations into $\int_{-1}^{1}[\frac{2}{\pi}J\ln(\alpha|x-s|)+f(x,s)]U_n(s)(1-s^2)^{1/2}ds$ and

$\int_{-1}^{1} JU_n(s)(1-s^2)^{1/2}dsdx$, B_{mn} and C_{mn} can be solved.

APPENDIX C

CALCULATION of DYNAMIC SIF (EQUATION 2.26)

Knowing that $|K_{III}| = |\lim_{x\to 1}[2(x-1)^{1/2}\sigma^{*}|$, all factors with the regular parts can be neglected because of the limiting progress, except $\frac{1}{\pi}\sum_{j=0}^{1}\frac{(1-j)!}{j!}(\frac{2}{\sigma|x-s|})^{2-2j}$ in Y. The Eq. 2.23 may be expressed by:

$$\lim_{x\to 1}[2(x-1)]^{1/2}(-4/\pi)\int_{-1}^{1}\frac{1}{|x-s|^2}[A_1(s)\sin\omega t + A_2(s)\cos\omega t]ds$$

$$=\lim_{x\to 1}[2(x-1)]^{1/2}(-4/\pi)\int_{-1}^{1}\sum_{n=0}^{5}[a_n U_n(s)\frac{(1-s^2)^{1/2}}{|x-s|^2}\sin\omega t + \sum_{n=0}^{5}b_n U_n(s)\frac{(1-s^2)^{1/2}}{|x-s|^2}\cos\omega t]\,ds$$

Substituting the Eq. 2.25 into above equation. we can get the Eq. 2.26.

APPENDIX D

NISA COMPUTER PROGRAM

The dislocation model of a surface crack discussed in Chapter 2 has been simulated using a different software tool to compare the analytical results. The NISA for a "family of general purpose finite element program" has been used for the simulation purpose. The data (geometry, displacement, force) required for simulation stored in a file named FRACTURE.nis, so that it can be supplied to the program before running ENDURE analysis. In earlier work, extensive refinement around the crack tip was the only technique used to capture the high stress distribution. Subsequently, several special crack tip elements incorporating the singularities are developed. While some of these special elements provide accurate estimates of the stress intensity factors, they need special treatment and modification of standard finite elements. In this research. the methods of Barsoum (1976) and Henshell and Shaw (1975) are applied to develop a scheme of generating singularities in elastic elements by simply relocating the side nodes shown in Fig. D.1. All outputs from FRACTURE.nis are saved in two binary files : the basic data file (geometry, boundary conditions) and the post data file (displacement. stress. temperature, etc.). The post results are show in Figs. D.2 to D.5. Fig. D.2 and D.3 show the shear stress singularity at the crack tip. The flow chart shown in Fig. D.6 indicates the path of ENDURE analysis. From the viewpoint of execution, Endure may be divided into two main parts. The first part involves input of all the necessary information such as the execution mode, stress file names from FEA (FRACTURE.nis). stress locations for fatigue analysis, material file name, load history file names, scale factor, output filename.

etc. This part will be referred to as "the input stage". The second part involves the actual fatigue damage calculations and output of results, and it will be referred to as "the execution stage". Furthermore, the comparison of normalized stress intensity factor is made between the presented dislocation model and NISA simulation program at very low frequency ($\alpha \approx 0$) as shown in D.7. It show that the dislocation model is in a good agreement with NISA simulation. Following are the NISA input file (*.nis), NISA output file (*.out), NISA ENDURE input file (*. end) and NISA ENDURE output file(*.eou).

APPENDIX D
(Continued)

D.1 NISA Input File (*.nis)

```
ANALYSIS =DYNAMIC
BLANK COMMON = 53410
FILE = FRACTURE
SAVE=26,27
*TITLE
3-D EDGE CRACK SUBJECTED TO PURE SHEAR LOAD
*ELTYPE
 1, 4, 11
 2, 4,  2
*NODES
   1,,,, 3.50000E+00, 8.00000E+00, 0.00000E+00,   0
   2,,,, 3.50000E+00, 8.00000E+00, 1.00000E+00,   0
   3,,,, 3.50000E+00, 8.00000E+00, 2.00000E+00,   0
   4,,,, 3.50000E+00, 8.00000E+00, 3.00000E+00,   0
   5,,,, 3.50000E+00, 8.00000E+00, 4.00000E+00,   0
   .
   .
   .
   .
 6421,,,, 2.10000E+01,-1.43000E+01, 1.00000E+01,   0
 6422,,,, 2.10000E+01,-1.43000E+01, 1.10000E+01,   0
 6423,,,, 1.92500E+01,-1.43000E+01, 9.00000E+00,   0
 6424,,,, 1.92500E+01,-1.43000E+01, 1.10000E+01,   0
*ELEMENTS
   1,  1,  2,  1,  0
   1,  2,  3,  7, 11, 10,  9,  6, 22, 23,
  26, 25, 31, 32, 33, 37, 41, 40, 39, 36,
   2,  1,  2,  1,  0
   3,  4,  5,  8, 13, 12, 11,  7, 23, 24,
  27, 26, 33, 34, 35, 38, 43, 42, 41, 37,
   3,  1,  2,  1,  0
   9, 10, 11, 15, 19, 18, 17, 14, 25, 26,
  29, 28, 39, 40, 41, 45, 49, 48, 47, 44,
   4,  1,  2,  1,  0
  11, 12, 13, 16, 21, 20, 19, 15, 26, 27,
  30, 29, 41, 42, 43, 46, 51, 50, 49, 45,
   5,  1,  2,  1,  0
  31, 32, 33, 37, 41, 40, 39, 36, 52, 53,
  56, 55, 61, 62, 63, 67, 71, 70, 69, 66,
```

```
6,  1,  2,  1,  0
   .
   .
   .
   .
 1486,  1,  2,  1,  0
 6398, 6399, 6400, 6402, 6406, 6405, 6404, 6401, 6409, 6410,
 6412, 6411, 6414, 6415, 6416, 6418, 6422, 6421, 6420, 6417,
 1487,  1,  2,  1,  0
 6383, 6403, 6404, 6407, 6306, 6305, 6288, 6384, 6386, 6411,
 6317, 6293, 6391, 6419, 6420, 6423, 6322, 6321, 6296, 6392,
 1488,  1,  2,  1,  0
 6404, 6405, 6406, 6408, 6308, 6307, 6306, 6407, 6411, 6412,
 6318, 6317, 6420, 6421, 6422, 6424, 6324, 6323, 6322, 6423,
*MATERIAL
EX ,    1,0, 2.06850E+05,
NUXY,   1,0, 3.00000E-01,
*LDCASE, ID=    1
 0, 1, 1, 0,-1, 2, 0,  0.000,  0.000
*SPDISP
** SPDISP SET =     1
 4616,UX  , 0.00000E+00,,,,,,,   0
 4616,UY  , 0.00000E+00,,,,,,,   0
 4616,UZ  , 0.00000E+00,,,,,,,   0
 4617,UX  , 0.00000E+00,,,,,,,   0
 4617,UY  , 0.00000E+00,,,,,,,   0
 4617,UZ  , 0.00000E+00,,,,,,,   0
 4618,UX  , 0.00000E+00,,,,,,,   0
 4618,UY  , 0.00000E+00,,,,,,,   0
 4618,UZ  , 0.00000E+00,,,,,,,   0
 4619,UX  , 0.00000E+00,,,,,,,   0
 4619,UY  , 0.00000E+00,,,,,,,   0
 4619,UZ  , 0.00000E+00,,,,,,,   0
   .
   .
   .
   .
 6391,UY  , 0.00000E+00,,,,,,,   0
 6391,UZ  , 0.00000E+00,,,,,,,   0
 6392,UX  , 0.00000E+00,,,,,,,   0
 6392,UY  , 0.00000E+00,,,,,,,   0
 6392,UZ  , 0.00000E+00,,,,,,,   0
 6413,UX  , 0.00000E+00,,,,,,,   0
 6413,UY  , 0.00000E+00,,,,,,,   0
 6413,UZ  , 0.00000E+00,,,,,,,   0
```

```
6414,UX  , 0.00000E+00,,,,,,,   0
6414,UY  , 0.00000E+00,,,,,,,   0
6414,UZ  , 0.00000E+00,,,,,,,   0
6415,UX  , 0.00000E+00,,,,,,,   0
6415,UY  , 0.00000E+00,,,,,,,   0
6415,UZ  , 0.00000E+00,,,,,,,   0
6416,UX  , 0.00000E+00,,,,,,,   0
6416,UY  , 0.00000E+00,,,,,,,   0
6416,UZ  , 0.00000E+00,,,,,,,   0
6417,UX  , 0.00000E+00,,,,,,,   0
6417,UY  , 0.00000E+00,,,,,,,   0
6417,UZ  , 0.00000E+00,,,,,,,   0
6418,UX  , 0.00000E+00,,,,,,,   0
6418,UY  , 0.00000E+00,,,,,,,   0
6418,UZ  , 0.00000E+00,,,,,,,   0
6419,UX  , 0.00000E+00,,,,,,,   0
6419,UY  , 0.00000E+00,,,,,,,   0
6419,UZ  , 0.00000E+00,,,,,,,   0
6420,UX  , 0.00000E+00,,,,,,,   0
6420,UY  , 0.00000E+00,,,,,,,   0
6420,UZ  , 0.00000E+00,,,,,,,   0
6421,UX  , 0.00000E+00,,,,,,,   0
6421,UY  , 0.00000E+00,,,,,,,   0
6421,UZ  , 0.00000E+00,,,,,,,   0
6422,UX  , 0.00000E+00,,,,,,,   0
6422,UY  , 0.00000E+00,,,,,,,   0
6422,UZ  , 0.00000E+00,,,,,,,   0
6423,UX  , 0.00000E+00,,,,,,,   0
6423,UY  , 0.00000E+00,,,,,,,   0
6423,UZ  , 0.00000E+00,,,,,,,   0
6424,UX  , 0.00000E+00,,,,,,,   0
6424,UY  , 0.00000E+00,,,,,,,   0
6424,UZ  , 0.00000E+00,,,,,,,   0
*PRESSURE
** PRESSURE SET =     1
 117,,,4,0,  0,1.0,   0
 119,,,4,0,  0,1.0,   0
 121,,,4,0,  0,1.0,   0
 123,,,4,0,  0,1.0,   0
 125,,,4,0,  0,1.0,   0
 157,,,4,0,  0,1.0,   0
 159,,,4,0,  0,1.0,   0
 161,,,4,0,  0,1.0,   0
 163,,,4,0,  0,1.0,   0
 165,,,4,0,  0,1.0,   0
```

```
 167,,,4,0, 0,1.0,  0
 169,,,4,0, 0,1.0,  0
 171,,,4,0, 0,1.0,  0
 173,,,4,0, 0,1.0,  0
 175,,,4,0, 0,1.0,  0
 192,,,4,0, 0,1.0,  0
 194,,,4,0, 0,1.0,  0
 196,,,4,0, 0,1.0,  0
 198,,,4,0, 0,1.0,  0
 200,,,4,0, 0,1.0,  0
 217,,,4,0, 0,-1.0,  0
 219,,,4,0, 0,-1.0,  0
 221,,,4,0, 0,-1.0,  0
 223,,,4,0, 0,-1.0,  0
 225,,,4,0, 0,-1.0,  0
 257,,,4,0, 0,-1.0,  0
 259,,,4,0, 0,-1.0,  0
 261,,,4,0, 0,-1.0,  0
 263,,,4,0, 0,-1.0,  0
 265,,,4,0, 0,-1.0,  0
 267,,,4,0, 0,-1.0,  0
 269,,,4,0, 0,-1.0,  0
 271,,,4,0, 0,-1.0,  0
 273,,,4,0, 0,-1.0,  0
 275,,,4,0, 0,-1.0,  0
 292,,,4,0, 0,-1.0,  0
 294,,,4,0, 0,-1.0,  0
 296,,,4,0, 0,-1.0,  0
*ENDDATA
```

D.2 NISA Output File (*.out)

*** EMRC NISA *** -- Version 94.0 (12/31/94-80387/32MEG) LOAD CASE ID
NO. 1 OCT/28/1996 16:48: 0
-D EDGE CRACK SUBJECTED TO PURE SHEAR LOAD

***** REACTION FORCES AND MOMENTS AT NODES
*****

LOAD CASE ID NO. 1

NODE	FX	FY	FZ	MX	MY	MZ
4617	1.54638E-03	3.22244E-03	-9.84554E-01	0.00000E+00	0.00000E+00	0.00000E+00
4618	-5.62040E-02	-1.19051E-03	5.43461E-01	0.00000E+00	0.00000E+00	0.00000E+00
4619	8.05290E-02	1.21170E-02	-1.28641E-01	0.00000E+00	0.00000E+00	0.00000E+00
4620	-1.53954E-02	-3.04430E-02	8.16139E-01	0.00000E+00	0.00000E+00	0.00000E+00
4621	8.84411E-02	3.10142E-02	-1.17558E-01	0.00000E+00	0.00000E+00	0.00000E+00
4622	1.20667E-01	2.58774E-02	-1.61549E-01	0.00000E+00	0.00000E+00	0.00000E+00
4623	4.95167E-02	9.75979E-02	-2.16326E-01	0.00000E+00	0.00000E+00	0.00000E+00
4624	-2.09988E-02	-3.91542E-02	8.18694E-01	0.00000E+00	0.00000E+00	0.00000E+00
4625	1.26482E-01	4.61431E-01	-1.63472E-01	0.00000E+00	0.00000E+00	0.00000E+00
4626	-3.85915E-02	-1.56870E-03	9.13787E-01	0.00000E+00	0.00000E+00	0.00000E+00
4627	6.34548E-02	1.70969E-01	-2.27923E-01	0.00000E+00	0.00000E+00	0.00000E+00
4628	-9.87622E-03	-4.87547E-02	1.43158E-01	0.00000E+00	0.00000E+00	0.00000E+00
4629	3.69809E-02	3.87678E-01	-1.64338E-01	0.00000E+00	0.00000E+00	0.00000E+00

4632 -2.26602E-02 -2.54808E-02 1.03231E-01 0.00000E+00 0.00000E+00
0.00000E+00
4633 2.90923E-03 2.24988E-02 -1.01270E-01 0.00000E+00
0.00000E+00 0.00000E+00
4634 -1.93575E-02 -9.79027E-02 5.20309E-01 0.00000E+00
0.00000E+00 0.00000E+00
4635 5.02326E-03 7.30489E-02 -1.53369E-01 0.00000E+00
0.00000E+00 0.00000E+00
4636 -7.76024E-03 -3.37274E-02 8.24684E-01 0.00000E+00
0.00000E+00

.

.

.

.

****** DISPLACEMENT SOLUTION ******

LOAD CASE ID NO. 1

NODE UX UY UZ ROTX ROTY ROTZ

1 -2.31846E-07 -8.26611E-08 3.15523E-06 0.00000E+00 0.00000E+00
0.00000E+00
2 -1.80581E-08 -5.25978E-08 3.16287E-06 0.00000E+00 0.00000E+00
0.00000E+00
3 -1.36021E-08 -3.48556E-08 3.16296E-06 0.00000E+00 0.00000E+00
0.00000E+00
4 -9.52678E-08 -2.57397E-08 3.16623E-06 0.00000E+00 0.00000E+00
0.00000E+00
5 -5.63139E-08 -2.09374E-08 3.17547E-06 0.00000E+00 0.00000E+00
0.00000E+00
6 -2.68403E-08 -1.34512E-08 4.20086E-06 0.00000E+00 0.00000E+00
0.00000E+00
7 -1.56217E-07 -6.33820E-08 4.23048E-06 0.00000E+00 0.00000E+00
0.00000E+00
8 -6.20340E-07 -3.94051E-07 4.26488E-06 0.00000E+00 0.00000E+00
0.00000E+00
9 -2.94894E-08 -1.91580E-07 5.37647E-06 0.00000E+00 0.00000E+00
0.00000E+00
10 -2.29109E-07 -1.31073E-07 5.40224E-06 0.00000E+00 0.00000E+00
0.00000E+00
11 -1.69796E-07 -9.34940E-07 5.41625E-06 0.00000E+00 0.00000E+00
0.00000E+00
12 -1.14921E-08 -7.22868E-07 5.43493E-06 0.00000E+00 0.00000E+00
0.00000E+00

13	-6.23180E-07	-6.02289E-07	5.46461E-06	0.00000E+00	0.00000E+00	0.00000E+00
14	-3.07018E-07	-2.36028E-07	6.60221E-06	0.00000E+00	0.00000E+00	0.00000E+00
15	-1.74211E-07	-1.09618E-08	6.63611E-06	0.00000E+00	0.00000E+00	0.00000E+00
16	-5.65130E-07	-7.70058E-07	6.69138E-06	0.00000E+00	0.00000E+00	0.00000E+00
17	-3.10762E-07	-2.09571E-07	7.83373E-06	0.00000E+00	0.00000E+00	0.00000E+00
18	-2.40109E-07	-1.23115E-07	7.83592E-06	0.00000E+00	0.00000E+00	0.00000E+00
19	-1.71578E-07	-8.51011E-07	7.82520E-06	0.00000E+00	0.00000E+00	0.00000E+00
20	-1.06685E-07	-7.44983E-07	7.81984E-06	0.00000E+00	0.00000E+00	0.00000E+00
21	-4.52528E-07	-7.90113E-07	7.83218E-06	0.00000E+00	0.00000E+00	0.00000E+00
22	-2.43409E-08	-6.93721E-07	3.31795E-06	0.00000E+00	0.00000E+00	0.00000E+00
23	-1.42174E-07	-2.88783E-07	3.34731E-06	0.00000E+00	0.00000E+00	0.00000E+00
24	-5.94180E-07	-1.94250E-07	3.38588E-06	0.00000E+00	0.00000E+00	0.00000E+00
25	-3.15620E-07	-1.81132E-07	5.71360E-06	0.00000E+00	0.00000E+00	0.00000E+00
26	-1.80717E-08	-9.06909E-07	5.78398E-06	0.00000E+00	0.00000E+00	0.00000E+00
27	-6.60024E-07	-6.17307E-07	5.87596E-06	0.00000E+00	0.00000E+00	0.00000E+00
28	-3.37372E-07	-2.06290E-07	8.39627E-06	0.00000E+00	0.00000E+00	0.00000E+00
29	-1.84871E-07	-8.82094E-07	8.40840E-06	0.00000E+00	0.00000E+00	0.00000E+00
30	-4.70306E-07	-8.52321E-07	8.46156E-06	0.00000E+00	0.00000E+00	0.00000E+00
31	-2.53716E-07	-5.35596E-07	3.45721E-06	0.00000E+00	0.00000E+00	0.00000E+00
32	-1.96314E-07	-3.25029E-07	3.48753E-06	0.00000E+00	0.00000E+00	0.00000E+00
33	-1.47573E-07	-2.15601E-07	3.50763E-06	0.00000E+00	0.00000E+00	0.00000E+00
34	-1.03736E-07	-1.76175E-07	3.53460E-06	0.00000E+00	0.00000E+00	0.00000E+00

35 -6.23613E-07 -1.69262E-07 3.57435E-06 0.00000E+00 0.00000E+00
0.00000E+00
36 -2.99824E-07 -1.05775E-07 4.65440E-06 0.00000E+00

.
.
.

**** AVERAGE NODAL STRESSES - LOAD CASE ID NO. 1 ****

NODE SX SY SZ SXY SYZ SZX

1 3.61064E-04 -4.44459E-04 -1.40080E-04 4.27124E-02 -1.86503E-
03 -9.63685E-04
2 3.02158E-04 -2.81793E-04 1.41111E-03 3.12476E-02 -1.37477E-
02 -6.81472E-03
3 2.33987E-04 -1.67147E-04 1.65321E-03 2.33759E-02 -2.54405E-
02 -1.23645E-02
4 1.80555E-04 -6.82697E-04 4.66175E-03 1.76638E-02 -3.09432E-
02 -1.41091E-02
5 1.21286E-04 5.41158E-04 6.82684E-03 1.32437E-02 -3.72387E-
02 -1.64839E-02
6 2.28258E-04 -4.61731E-04 -1.94391E-03 5.41859E-02 -2.07813E-
03 -6.22596E-04
7 1.66035E-04 -1.35444E-04 2.35230E-03 2.90749E-02 -3.47010E-
02 -1.19844E-02
8 8.57967E-04 6.09425E-04 1.06766E-02 1.54915E-02 -5.17352E-
02 -1.62986E-02
9 1.00543E-04 -3.88123E-04 -2.08247E-03 6.89730E-02 -4.35058E-
03 -1.08511E-03
10 1.21695E-04 -1.89226E-04 2.08800E-03 4.91806E-02 -
2.54475E-02 -6.45380E-03

APPENDIX D
(Continued)

D.3 NISA Endure Input File (*.end)

```
**
************* Start EXECUTIVE cards **************
**
PROBLEM=FRACTURE
FILE=FRACTURE.eou
APPROACH=SIFS,7
FEATYPE=NISA2,STATIC,LINEAR
UNIT=MM
*TITLE
papertest
**
*********** Start MATERIAL data group ************
**
*MATERIAL,steel
E,206850.0
POE,0.3
SY,324.0
AKC,121.0
**
*********** Start STRSDATA data group ************
**
*STRSDATA
1,fracture26.dat,fracture27.dat,1
**
*********** Start FMODEL data group ************
**
*FMODEL,1
FULL,QNODE,SOLID
**
*** start FRCRACK data ****
**
*FRCRACK,ID=1
*ANGLEA
0.0,90,90
*ANGLEB
90,90,0.0
*NTIP,1786
*JCFRONT
1801,0
```

APPENDIX D
(Continued)

D.4 NISA Endure Output File (*.eou)

NUMBER OF LOAD STEPS..= 1

COMPUTING FRACTURE PARAMETERS FOR STEP NO.= 1

CRACK SLIDING, OPENING AND TEARING DISPLACEMENTS:

0.7532E-11 0.8527E-12 0.1149E-04

TITLE FOR THE PROBLEM: THE STRESS INTENSITY FACTOR OF A MODE
III
SURFACE CRACK FOR L=3.5

FILES USED IN THIS RUN ARE :
INPUT DATA FILE (FINPUT) .... = FRACTURE.NIS
OUTPUT FILE (FOUT) .... = FRACTURE.EOU
MATERIAL FILE (FMAT) .... =

Names of FILE26 and FILE27 :
FILE26 .... = FRACTURE26.DAT
FILE27 .... = FRACTURE27.DAT

LOAD CASE NUMBER .... = 1

LAYER NUMBER .... = 1

VALUE OF THE MODEL SYMMETRIC CONTROL VARIABLE : ISYM = 1
1, FULL MODEL USED
2, ONE HALF SYMMETRIC MODEL USED

VALUE OF THE MID-NODE/QUARTER-NODE CONTROL VARIABLE : INQM
= 1
1, QUARTER-POINT NODE MODEL USED
2, MID-POINT NODE MODEL USED

THE DIMENSION OF THE ANALYSIS : NDIM = 3
1, AXISYMMETRIC
2, 2-D PLANE STRESS OR PLANE STRAIN
3, 3-D GENERAL SOLID

VALUE OF NTAN = 7 ; MEANING AS FOLLOWS :
1...Mode I analysis only
2...Mode II analysis only
3...Mode III analysis only
4...Mixed Modes I and II
5...Mixed Modes I and III
6...Mixed Modes II and III
7...Mixed Modes I, II, and III

OTHER CONTROL VARIABLES ARE...:
NSTR.............= 2
NLOCS............= 1

VALUE OF NCAL = 1 ; MEANING :
1.... SIFS ONLY
2.... J-INTEGRALS ONLY
3.... SIFS AND J-INTEGRALS

MATERIAL PROPERTIES
****
YOUNGS MODULUS............... E = 0.20685E+06
POISSONS RATIO............. ANU = 0.30000
YIELD STRENGTH.............. SY = 0.32400E+03
FRACTURE TOUGHNESS......... AKC = 121.00000

ELEMENT OR NODAL DATA FOR LOCATION NO.= 1

ANGLES OF LOCAL x1 AXIS WRT GLOBAL AXES...:
0.00000E+00 0.15708E+01 0.15708E+01

ANGLES OF LOCAL x3 AXIS WRT GLOBAL AXES...:
0.15708E+01 0.15708E+01 0.00000E+00

THE FOLLOWING INFORMATION IS FOR CTOD CALCULATION :

CRACK TIP NODE NUMBER USED IN CTOD CALCULATION : 1786

NODE NUMBERS OF LOWER CRACK FACE : 1782 1833 1780 1835 1781

NODE NUMBERS OF UPPER CRACK FACE : 931 1799 929 1803 930

ETA value in CTOD calculations : -0.10000E+01

THE FOLLOWING INFORMATION IS FOR EDI CALCULATION :

CRACK TIP NODE NUMBER FOR EDI CALCULATION : 1786

NO. OF ELEMENTS ARROUND THE CRACK FOR LOCATION 1 = 8

ELEMENT NUMBERS INVOLVING EDI CALCULATIONS :
304 309 314 319 324 329 334 339

NO. OF QUARTER-POINT NODES ON EDI CALCULATION = 9

QUARTER-POINT NODE NUMBERS ON EDI CALCULATION :
1800 1799 1815 1814 1822 1833 1832 1840 1846

NO. OF ELEMENTS USED FOR AREA CALCULATION : 1

ELEMENT NUMBERS FOR AREA CALCULATION : 304

CRACK FRONT NODES FOR AREA CALCULATION : 1786
CRACK FRONT NODES FOR AREA CALCULATION : 1801
CRACK FRONT NODES FOR AREA CALCULATION : 1802

UNITS OF QUANTITIES.................: MM

**** OUTPUT FOR LOCATION NO. = 1 , STEP NO. = 1 ****

STRESS INTENSITY FACTORS:
FROM DISPLACEMENT-BASED CTOD CALCULATIONS

0.15426E-06 0.13628E-07 0.18114E+01

J-INTEGRAL VALUES:
FROM DISPLACEMENT-BASED CTOD CALCULATIONS

0.30793E-10 -0.23026E-11 0.20622E-04

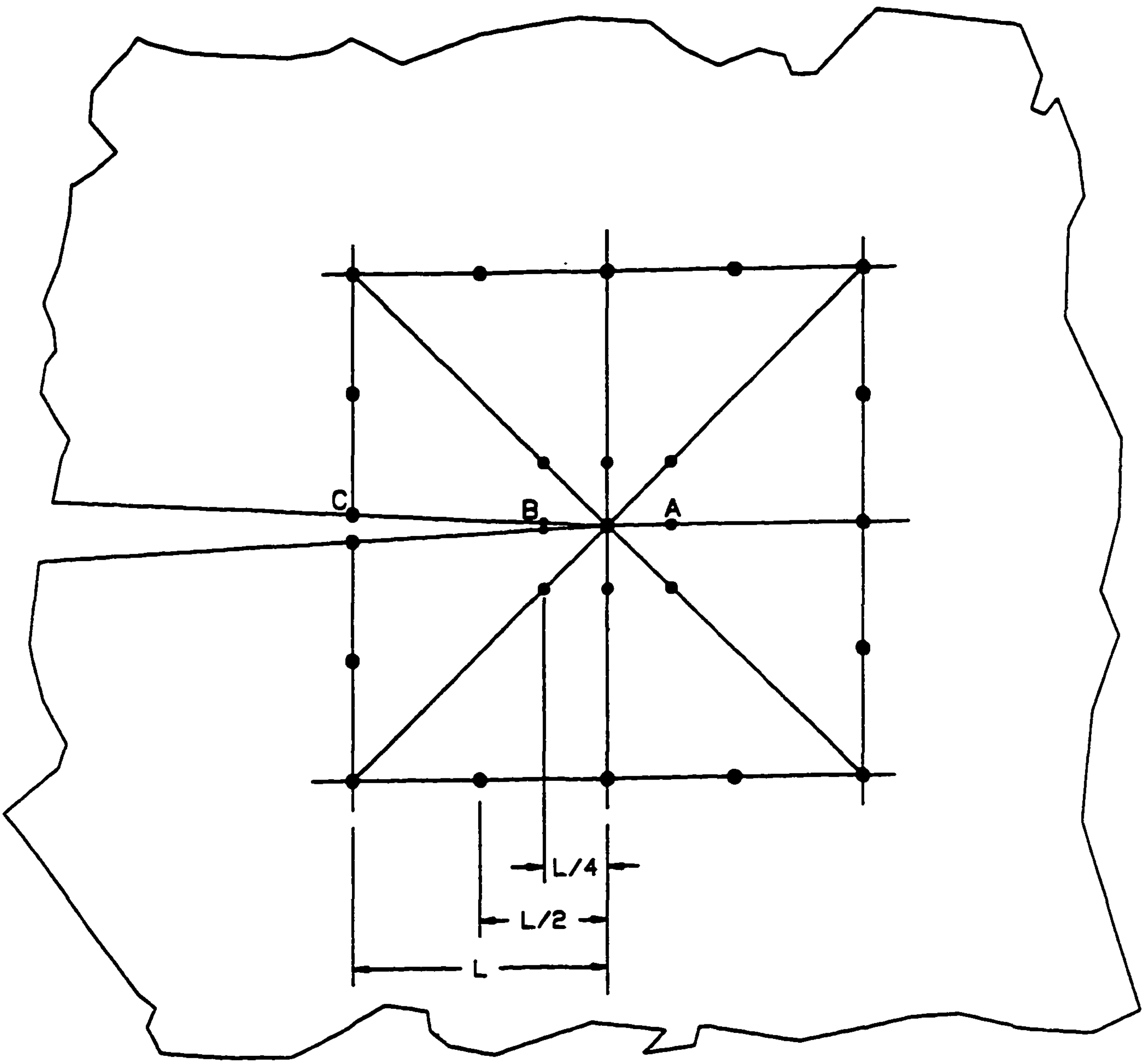

Figure D.1 Modeling a crack tip

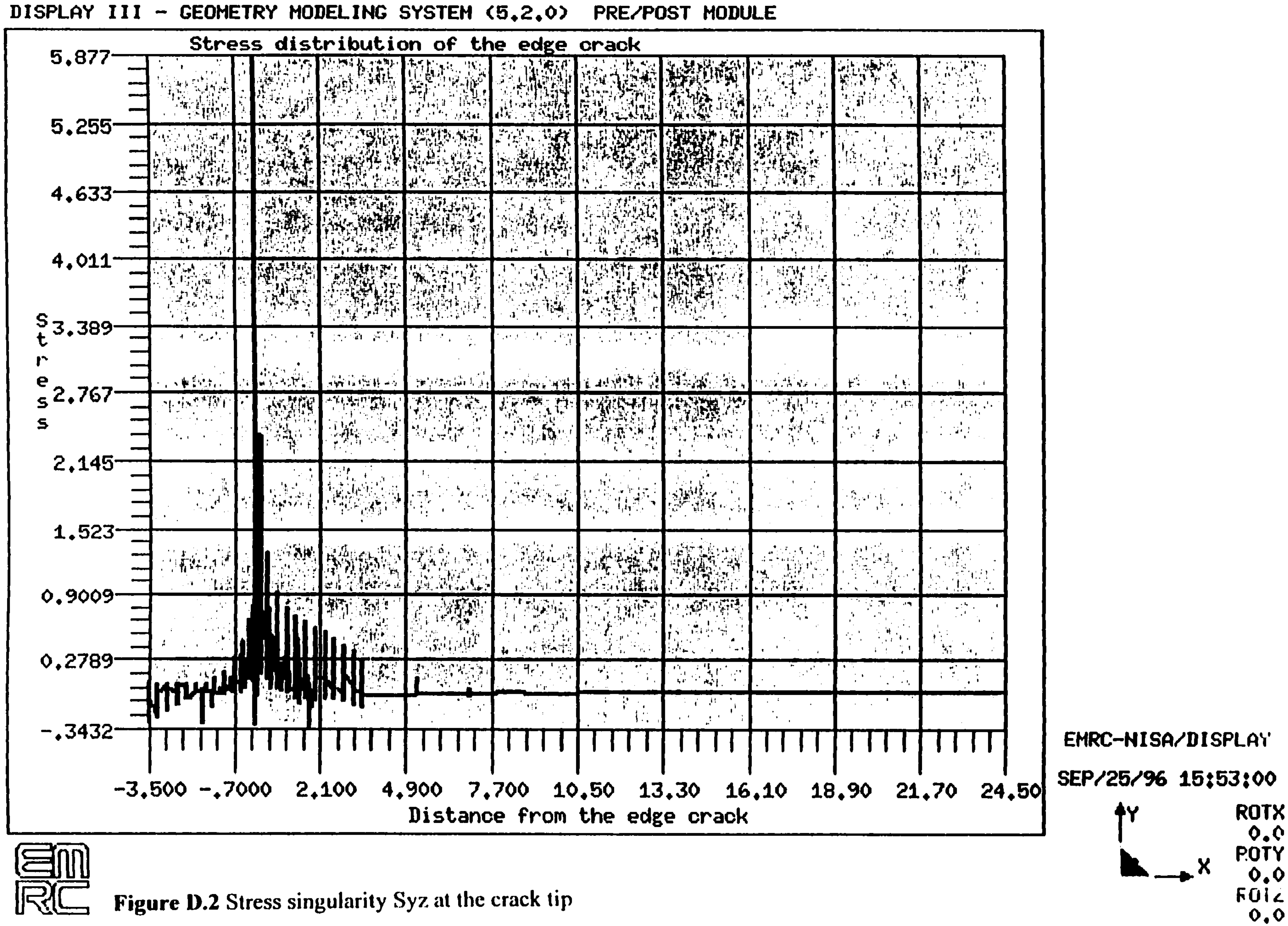

Figure D.2 Stress singularity Syz at the crack tip

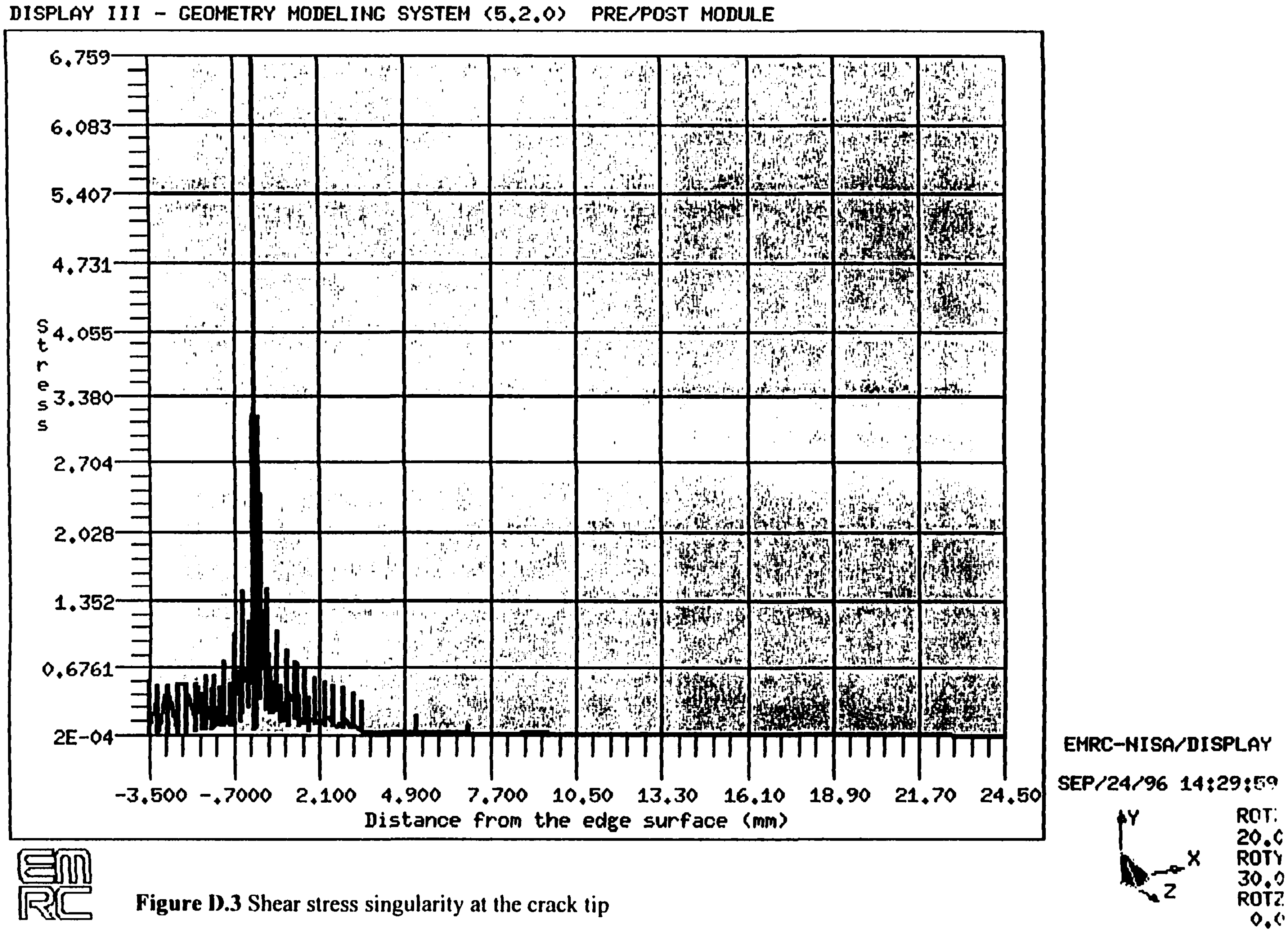

Figure D.3 Shear stress singularity at the crack tip

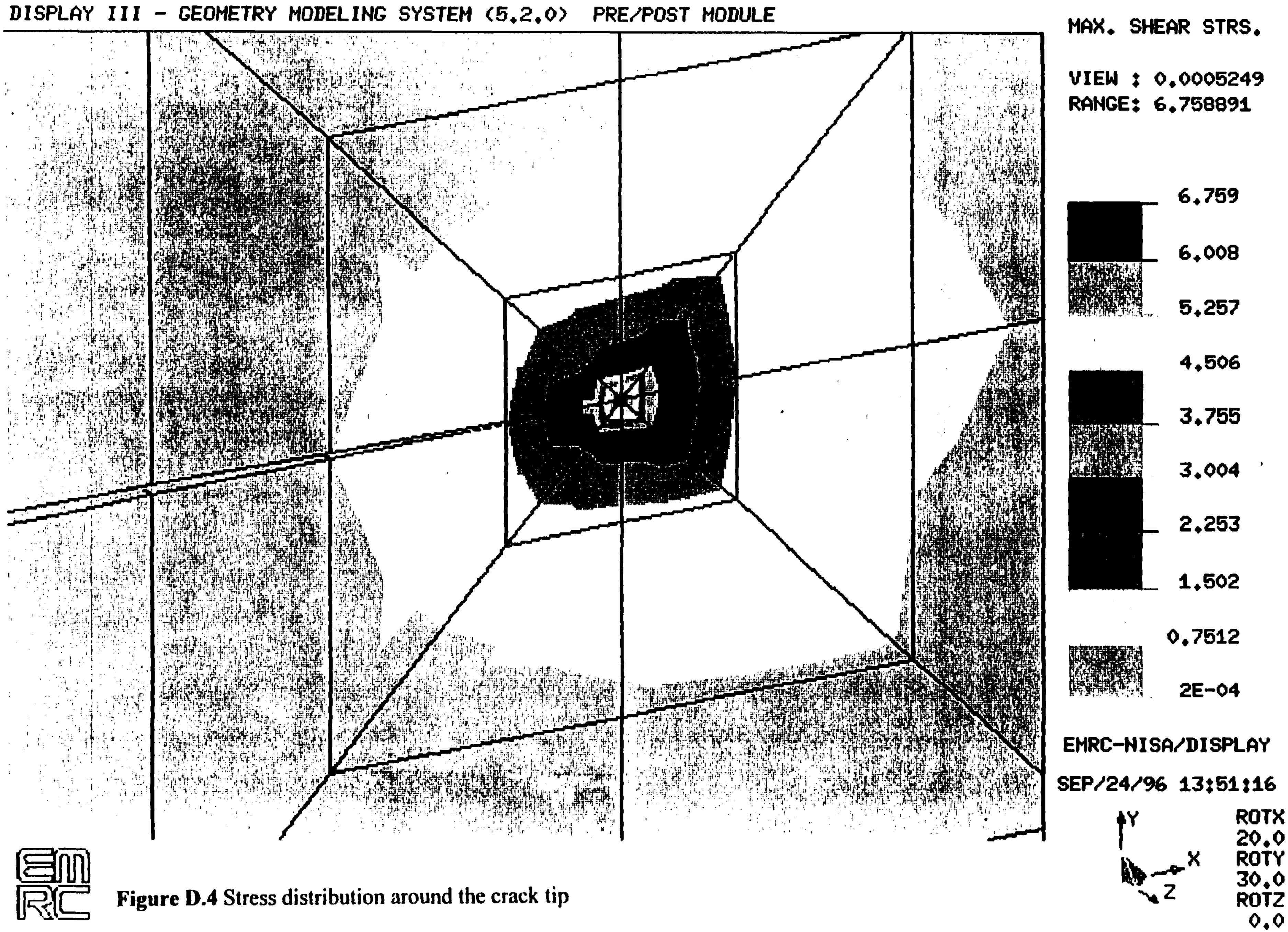

Figure D.4 Stress distribution around the crack tip

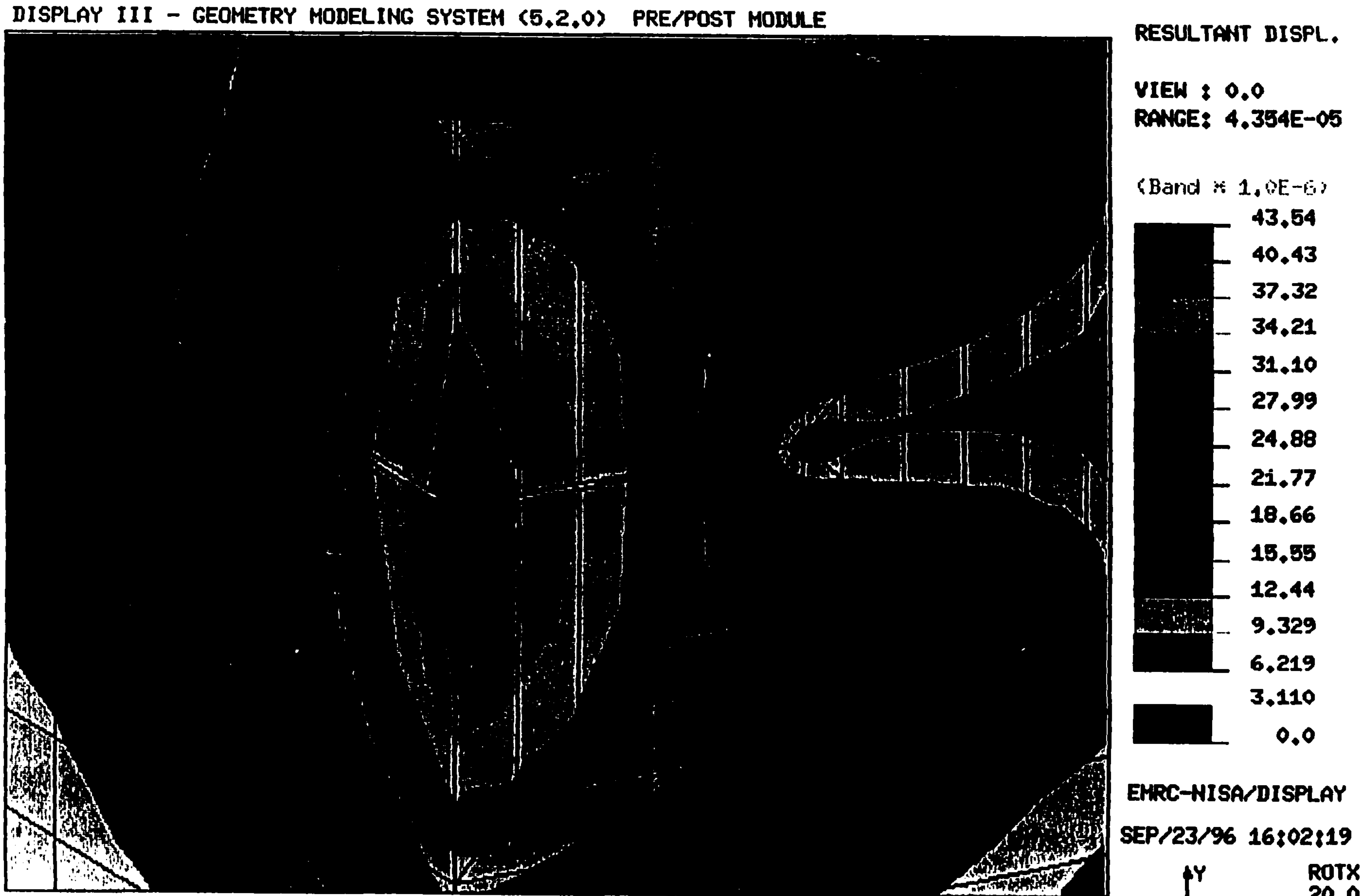

Figure D.5 Resultant displacement around a surface crack

INPUT - OUTPUT DIAGRAM

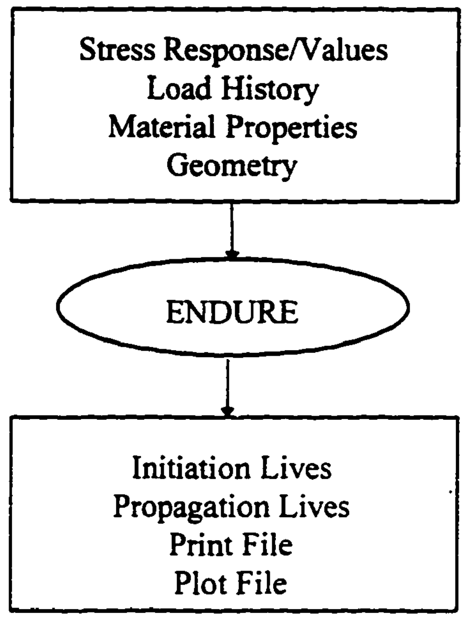

Figure D.6 Schematic input/output diagram - ENDURE

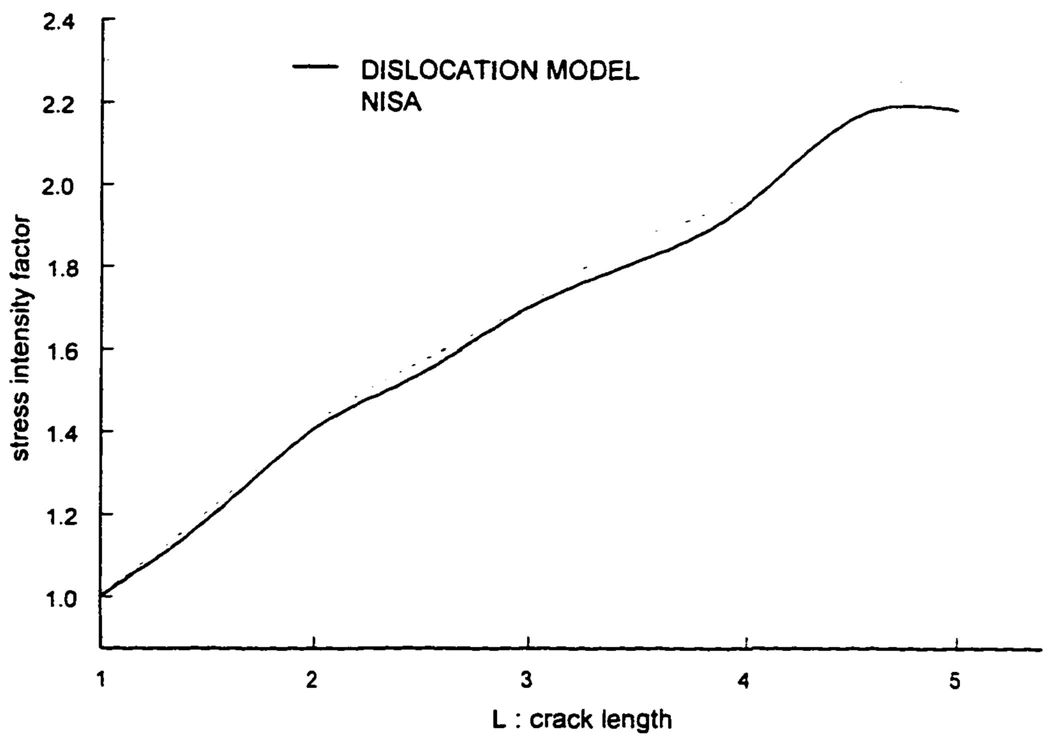

Figure D.7 Comparison of dislocation model and NISA simulation at $\alpha \approx 0$

APPENDIX E

MATHCAD PROGRAM

The analytical model discussed in Chapter 2 and 5 have been solved with the help of MathCad. As discussed in the Appendix A, B, and C, the integral equations and data required for simulation are stored in *.mcd file. Following are the MathCad functions and data file.

E.1 MATHCAD Program for a Finite Crack

The stress intensity factors of a crack located in an elastic infinite isotropic soli
to harmonic shear waves

$$n \cdot 0\ 5 \qquad \theta\ \frac{\pi}{2} \qquad L\ 1 \qquad \sigma \cdot 1 \qquad \alpha\ 0.4$$

$$A := \begin{bmatrix} 2\cdot\pi\cdot L^2 & 0 & 0 & 0 & 0 & 0 \\ 0 & 4\cdot\pi\cdot L^2 & 0 & 0 & 0 & 0 \\ 0 & 0 & 6\cdot\pi\cdot L^2 & 0 & 0 & 0 \\ 0 & 0 & 0 & 8\cdot\pi\cdot L^2 & 0 & 0 \\ 0 & 0 & 0 & 0 & 10\cdot\pi\cdot L^2 & 0 \\ 0 & 0 & 0 & 0 & 0 & 12\cdot\pi\cdot L^2 \end{bmatrix}$$

$$B = \begin{bmatrix} B_{00} & 0 & B_{02} & 0 & B_{04} & 0 \\ 0 & B_{11} & 0 & B_{13} & 0 & B_{15} \\ B_{20} & 0 & B_{22} & 0 & B_{24} & 0 \\ 0 & B_{31} & 0 & B_{33} & 0 & B_{35} \\ B_{40} & 0 & B_{42} & 0 & B_{44} & 0 \\ 0 & B_{51} & 0 & B_{53} & 0 & B_{55} \end{bmatrix}$$

$$B_{00} = \cdot 1.481492\cdot\alpha^2\cdot L^4 - .0587599\cdot\alpha^4\cdot L^6 + .0119351\cdot\alpha^6\cdot L^8 - 5.9201\cdot 10^{-4}\cdot\alpha^8\cdot L^{10} + 2.3205\cdot 10^{-5}\cdot\alpha^{10}\cdot L^{12}$$

$$\cdot .9675027\cdot\alpha^2\cdot L^4 + .1341\cdot\alpha^4\cdot L^6 - 9.1149\cdot 10^{-3}\cdot\alpha^6\cdot L^8 + 3.8671\cdot 10^{-4}\cdot\alpha^8\cdot L^{10} - 1.1252\cdot 10^{-5}\cdot\alpha^{10}\cdot L^{12}$$

$$+ \frac{2\ln(\alpha L)}{\pi} C_{00}$$

$$B_{20} = .7853982\cdot\alpha^2\cdot L^4 + .0197076\cdot\alpha^4\cdot L^6 + .010776\cdot\alpha^6\cdot L^8 - 4.1084\cdot 10^{-4}\cdot\alpha^8\cdot L^{10} + 1.4488\cdot 10^{-5}\cdot\alpha^{10}\cdot L^{12}$$

$$+ .06705\cdot\alpha^4\cdot L^6 - 8.2034\cdot 10^{-3}\cdot\alpha^6\cdot L^8 + 4.6405\cdot 10^{-4}\cdot\alpha^8\cdot L^{10} - 1.6074\cdot 10^{-5}\cdot\alpha^{10}\cdot L^{12} + \frac{2\ln(\alpha L)}{\pi} C_{20}$$

$$B_{40} = -4.0906\cdot 10^{-3}\cdot\alpha^4\cdot L^6 + 1.3585\cdot 10^{-3}\cdot\alpha^6\cdot L^8 - 1.1743\cdot 10^{-4}\cdot\alpha^8\cdot L^{10} + 5.4453\cdot 10^{-6}\cdot\alpha^{10}\cdot L^{12}$$

$$-9.1149\cdot 10^{-4}\cdot\alpha^6\cdot L^8 + 1.1048\cdot 10^{-4}\cdot\alpha^8\cdot L^{10} - 5.741\cdot 10^{-6}\cdot\alpha^{10}\cdot L^{12} + \frac{2\ln(\alpha L)}{\pi} C_{40}$$

$$B_{11} = -1.8325958\cdot\alpha^2\cdot L^4 + .1242094\cdot\alpha^4\cdot L^6 - .0117654\cdot\alpha^6\cdot L^8 + 7.4239\cdot 10^{-4}\cdot\alpha^8\cdot L^{10} - 2.6978\cdot 10^{-5}\cdot\alpha^{10}\cdot L^{12}$$

$$-.1341\cdot\alpha^4\cdot L^6 + .145839\cdot\alpha^6\cdot L^8 - 7.7292\cdot 10^{-4}\cdot\alpha^8\cdot L^{10} + 2.5689\cdot 10^{-5}\cdot\alpha^{10}\cdot L^{12} + \frac{2\ln(\alpha L)}{\pi} C_{11}$$

$$B_{31} = 3.646\cdot 10^{-3}\cdot\alpha^6\cdot L^8 - 3.5356\cdot 10^{-4}\cdot\alpha^8\cdot L^{10} + 1.6068\cdot 10^{-5}\cdot\alpha^{10}\cdot L^{12} + \frac{2\ln(\alpha L)}{\pi} C_{31}$$

$$+ .5235988\cdot\alpha^2\cdot L^4 + .0253618\cdot\alpha^4\cdot L^6 - 3.5932\cdot 10^{-3}\cdot\alpha^6\cdot L^8 + 8.309\cdot 10^{-5}\cdot\alpha^8\cdot L^{10} - 7.7505\cdot 10^{-6}\cdot\alpha^{10}\cdot L^{12}$$

$$B_{51} = -1.6363\cdot 10^{-3}\cdot\alpha^4\cdot L^6 - 1.7291\cdot 10^{-3}\cdot\alpha^6\cdot L^8 + 2.9047\cdot 10^{-5}\cdot\alpha^8\cdot L^{10} - 2.9449\cdot 10^{-6}\cdot\alpha^{10}\cdot L^{12}$$

$$-3.3412\cdot 10^{-5}\cdot\alpha^8\cdot L^{10} + 3.0715\cdot 10^{-6}\cdot\alpha^{10}\cdot L^{12} + \frac{2\ln(\alpha L)}{\pi} C_{51}$$

$$B_{02} = .06705\cdot\alpha^4\cdot L^6 - 8.2034\cdot 10^{-3}\cdot\alpha^6\cdot L^8 + 4.6405\cdot 10^{-4}\cdot\alpha^8\cdot L^{10} - 1.6074\cdot 10^{-5}\cdot\alpha^{10}\cdot L^{12} + \frac{2\ln(\alpha L)}{\pi} C_{20}$$

$$+.392699\cdot\alpha^2\cdot L^4 + 3.3451\cdot 10^{-3}\cdot\alpha^4\cdot L^6 + 9.3506\cdot 10^{-3}\,\alpha^6\cdot L^8 - 7.4002\cdot 10^{-4}\cdot\alpha^8\cdot L^{10} + 3.1957\cdot 10^{-5}\cdot\alpha^{10}\cdot L^{12}$$

$$B_{22} = -.9817478\cdot\alpha^2\cdot L^4 - .0404972\cdot\alpha^4\cdot L^6 + 6.2847\cdot 10^{-3}\cdot\alpha^6\cdot L^8 - 4.5629\cdot 10^{-4}\cdot\alpha^8\cdot L^{10} + 1.9495\cdot 10^{-5}\cdot\alpha^{10}\cdot L^{12}$$

$$-5.4689\cdot 10^{-3}\cdot\alpha^6\cdot L^8 + 4.972\cdot 10^{-4}\cdot\alpha^8\cdot L^{10} - 2.1701\cdot 10^{-5}\cdot\alpha^{10}\cdot L^{12}$$

$$B_{42} = 3.2868\cdot 10^{-5}\cdot\alpha^8\cdot L^{10} - 6.6975\cdot 10^{-6}\cdot\alpha^{10}\cdot L^{12} + \frac{2\ln(\alpha L)}{\pi} C_{42}$$

$$+.392699\cdot\alpha^2\cdot L^4 + .0323159\cdot\alpha^4\cdot L^6 - 2.3744\cdot 10^{-4}\cdot\alpha^6\cdot L^8 - 8.4898\cdot 10^{-5}\cdot\alpha^8\cdot L^{10} + 8.342\cdot 10^{-6}\cdot\alpha^{10}\cdot L^{12}$$

$$B_{13} = .2617994\cdot\alpha^2\cdot L^4 + .0212712\cdot\alpha^4\cdot L^6 - 3.8489\cdot 10^{-3}\cdot\alpha^6\cdot L^8 + 2.9795\cdot 10^{-4}\cdot\alpha^8\cdot L^{10} - 1.5767\cdot 10^{-5}\cdot\alpha^{10}\cdot L^{12}$$

$$+3.646\cdot 10^{-3}\cdot\alpha^6\cdot L^8 - 3.5356\cdot 10^{-4}\cdot\alpha^8\cdot L^{10} + 1.6068\cdot 10^{-5}\cdot\alpha^{10}\cdot L^{12} + \frac{2\ln(\alpha L)}{\pi} C_{13}$$

$$B_{33} = -1.1048\cdot 10^{-4}\cdot\alpha^8\cdot L^{10} + 8.5732\cdot 10^{-6}\cdot\alpha^{10}\cdot L^{12} + \frac{2\ln(\alpha L)}{\pi} C_{33}$$

$$-.6806784\cdot\alpha^2\cdot L^4 - .0114537\cdot\alpha^4\cdot L^6 - 1.7532\cdot 10^{-3}\cdot\alpha^6\cdot L^8 + 7.4518\cdot 10^{-5}\cdot\alpha^8\cdot L^{10} - 1.8524\cdot 10^{-6}\cdot\alpha^{10}\cdot L^{12}$$

$$B_{53} = .3141592\cdot\alpha^2\cdot L^4 + 3.5062\cdot 10^{-3}\cdot\alpha^4\cdot L^6 + 8.1934\cdot 10^{-4}\cdot\alpha^6\cdot L^8 - 4.7929\cdot 10^{-5}\cdot\alpha^8\cdot L^{10} + 2.5555\cdot 10^{-7}\cdot\alpha^{10}\cdot L^{12}$$

$$+1.0802\cdot 10^{-6}\cdot\alpha^{10}\cdot L^{12} + \frac{2\ln(\alpha L)}{\pi} C_{53}$$

$$B_{04} = -9.1149\cdot 10^{-4}\cdot\alpha^6\cdot L^8 + 1.1048\cdot 10^{-4}\cdot\alpha^8\cdot L^{10} - 5.741\cdot 10^{-6}\cdot\alpha^{10}\cdot L^{12} + \frac{2\ln(\alpha L)}{\pi} C_{04}$$

$$+.0224985\cdot\alpha^4\cdot L^6 + 4.7644\cdot 10^{-4}\cdot\alpha^6\cdot L^8 - 1.6884\cdot 10^{-4}\cdot\alpha^8\cdot L^{10} - 8.1124\cdot 10^{-6}\cdot\alpha^{10}\cdot L^{12}$$

$$B_{24} = .1963496\cdot\alpha^2\cdot L^4 + 6.1359\cdot 10^{-3}\cdot\alpha^4\cdot L^6 + 7.5332\cdot 10^{-4}\cdot\alpha^6\cdot L^8 - 1.0109\cdot 10^{-4}\cdot\alpha^8\cdot L^{10} + 6.7978\cdot 10^{-6}\cdot\alpha^{10}\cdot L^{12}$$

$$+ 3.2868\cdot 10^{-5}\cdot\alpha^8\cdot L^{10} - 6.6975\cdot 10^{-6}\cdot\alpha^{10}\cdot L^{12} + \frac{2\ln(\alpha L)}{\pi} C_{24}$$

$$B_{44} = -1.3395\cdot 10^{-6}\cdot\alpha^{10}\cdot L^{12} + \frac{2\ln(\alpha L)}{\pi} C_{44}$$

$$+.3141592\cdot\alpha^2\cdot L^4 + 3.5062\cdot 10^{-3}\cdot\alpha^4\cdot L^6 + 8.1934\cdot 10^{-4}\cdot\alpha^6\cdot L^8 - 4.7929\cdot 10^{-5}\cdot\alpha^8\cdot L^{10} + 2.5555\cdot 10^{-7}\cdot\alpha^{10}\cdot L^{12}$$

$$B_{15} = -8.181\cdot 10^{-4}\cdot\alpha^4\cdot L^6 - 1.3879\cdot 10^{-4}\cdot\alpha^6\cdot L^8 + 1.0663\cdot 10^{-5}\cdot\alpha^8\cdot L^{10} - 2.8634\cdot 10^{-8}\cdot\alpha^{10}\cdot L^{12}$$

$$-3.3412\cdot 10^{-5}\cdot\alpha^8\cdot L^{10} + 3.0715\cdot 10^{-6}\cdot\alpha^{10}\cdot L^{12} + \frac{2\ln(\alpha L)}{\pi} C_{15}$$

$$B_{35} = 1.0802\cdot 10^{-6}\cdot\alpha^{10}\cdot L^{12} + \frac{2\ln(\alpha L)}{\pi} C_{35}$$

$$+ .1570796\cdot\alpha^2\cdot L^4 + 2.6681\cdot 10^{-3}\cdot\alpha^4\cdot L^6 + 9.135\cdot 10^{-5}\cdot\alpha^6\cdot L^8 + 6.4375\cdot 10^{-6}\cdot\alpha^8\cdot L^{10} - 1.7028\cdot 10^{-8}\cdot\alpha^{10}\cdot L^{12}$$

$$B_{55} = \frac{2\ln(\alpha L)}{\pi} C_{55}$$

$$-.426359\cdot\alpha^2\cdot L^4 - 2.6297\cdot 10^{-3}\cdot\alpha^4\cdot L^6 + 4.1019\cdot 10^{-4}\cdot\alpha^6\cdot L^8 - 7.2087\cdot 10^{-5}\cdot\alpha^8\cdot L^{10} + 4.3102\cdot 10^{-7}\cdot\alpha^{10}\cdot L^{12}$$

$$C = \begin{bmatrix} C_{00} & 0 & C_{02} & 0 & C_{04} & 0 \\ 0 & C_{11} & 0 & C_{13} & 0 & C_{15} \\ C_{20} & 0 & C_{22} & 0 & C_{24} & 0 \\ 0 & C_{31} & 0 & C_{33} & 0 & C_{35} \\ C_{40} & 0 & C_{42} & 0 & C_{44} & 0 \\ 0 & C_{51} & 0 & C_{53} & 0 & C_{55} \end{bmatrix}$$

$$C_{00} = .1542126\cdot\alpha^4\cdot L^6 + 8.0319\cdot 10^{-3}\cdot\alpha^6\cdot L^8 - 2.9283\cdot 10^{-4}\cdot\alpha^8\cdot L^{10} + 7.6868\cdot 10^{-6}\cdot\alpha^{10}\cdot L^{12}$$

$$C_{20} = -.0771063\cdot\alpha^4\cdot L^6 + 7.2287\cdot 10^{-3}\cdot\alpha^6\cdot L^8 - 3.514\cdot 10^{-4}\cdot\alpha^8\cdot L^{10} + 1.0981\cdot 10^{-5}\cdot\alpha^{10}\cdot L^{12}$$

$$C_{40} = 3.0319\cdot 10^{-4}\cdot\alpha^6\cdot L^8 - 8.3666\cdot 10^{-5}\cdot\alpha^8\cdot L^{10} + 3.9219\cdot 10^{-6}\cdot\alpha^{10}\cdot L^{12}$$

$$C_{11} = .1542126\cdot\alpha^4\cdot L^6 - .012851\cdot\alpha^6\cdot L^8 + 5.8526\cdot 10^{-4}\cdot\alpha^8\cdot L^{10} - 1.755\cdot 10^{-5}\cdot\alpha^{10}\cdot L^{12}$$

$$C_{31} = -3.2128\cdot 10^{-3}\cdot\alpha^6\cdot L^8 + 2.6773\cdot 10^{-4}\cdot\alpha^8\cdot L^{10} - 1.0977\cdot 10^{-5}\cdot\alpha^{10}\cdot L^{12}$$

$$C_{51} = 2.53\cdot 10^{-5}\cdot\alpha^8\cdot L^{10} - 2.0984\cdot 10^{-6}\cdot\alpha^{10}\cdot L^{12}$$

$$C_{02} = -.0771063\cdot\alpha^4\cdot L^6 + 7.2287\cdot 10^{-3}\cdot\alpha^6\cdot L^8 - 3.514\cdot 10^{-4}\cdot\alpha^8\cdot L^{10} + 1.0981\cdot 10^{-5}\cdot\alpha^{10}\cdot L^{12}$$

$$C_{22} = 4.8191\cdot 10^{-3}\cdot\alpha^6\cdot L^8 - 3.765\cdot 10^{-4}\cdot\alpha^8\cdot L^{10} + 1.4824\cdot 10^{-5}\cdot\alpha^{10}\cdot L^{12}$$

$$C_{42} = -6.275\cdot 10^{-5}\cdot\alpha^8\cdot L^{10} + 4.5755\cdot 10^{-6}\cdot\alpha^{10}\cdot L^{12}$$

$$C_{13} = -3.2128\cdot 10^{-3}\cdot\alpha^6\cdot L^8 + 2.6773\cdot 10^{-4}\cdot\alpha^8\cdot L^{10} - 1.0977\cdot 10^{-5}\cdot\alpha^{10}\cdot L^{12}$$

$$C_{33} = 3.3666\cdot 10^{-5}\cdot\alpha^8\cdot L^{10} - 5.8566\cdot 10^{-6}\cdot\alpha^{10}\cdot L^{12}$$

$$C_{53} = -7.3793\cdot 10^{-7}\cdot\alpha^{10}\cdot L^{12}$$

$$C_{04} = 3.0319\cdot 10^{-4}\cdot\alpha^6\cdot L^8 - 8.3666\cdot 10^{-5}\cdot\alpha^8\cdot L^{10} + 3.9219\cdot 10^{-6}\cdot\alpha^{10}\cdot L^{12}$$

$$C_{24} = -6.275\cdot 10^{-5}\cdot\alpha^{8}\cdot L^{10} + 4.5755\cdot 10^{-6}\cdot\alpha^{10}\cdot L^{12}$$

$$C_{44} = 9.1509\cdot 10^{-7}\cdot\alpha^{10}\cdot L^{12}$$

$$C_{15} = 2.53\cdot 10^{-5}\cdot\alpha^{8}\cdot L^{10} - 2.0984\cdot 10^{-6}\cdot\alpha^{10}\cdot L^{12}$$

$$C_{35} = -7.3793\cdot 10^{-7}\cdot\alpha^{10}\cdot L^{12}$$

$$C_{55} = 0$$

$$\eta = \begin{bmatrix} 0 \\ \eta_{10} \\ 0 \\ \eta_{30} \\ 0 \\ \eta_{50} \end{bmatrix}$$

$$\eta_{10} = \sigma\cdot\alpha\cdot L^{3}\cdot\sin(\theta)\cdot\cos(\theta) *$$

$$\left[-.785398 + .0654498\cdot(L\cdot\alpha)^{2}\cdot\cos(\theta)^{2} - 2.042\cdot 10^{-3}\cdot(L\cdot\alpha)^{4}\cdot\cos(\theta)^{4} + 3.4127\cdot 10^{-5}\cdot(L\cdot\alpha)^{6}\cdot\cos(\theta)^{6}\right]$$

$$\eta_{30} = \sigma\cdot\alpha\cdot L^{3}\cdot\sin(\theta)\cdot\cos(\theta)$$

$$\left[.0327249\cdot(L\cdot\alpha)^{2}\cdot\cos(\theta)^{2} - 1.6362\cdot 10^{-3}\cdot(L\cdot\alpha)^{4}\cdot\cos(\theta)^{4} + 3.4127\cdot 10^{-5}\cdot(L\cdot\alpha)^{6}\cdot\cos(\theta)^{6}\right]$$

$$\eta_{50} = \sigma\cdot\alpha\cdot L^{3}\cdot\sin(\theta)\cdot\cos(\theta) * \left[4.1233\cdot 10^{-4}\cdot(L\cdot\alpha)^{4}\cdot\cos(\theta)^{4} + 1.4492\cdot 10^{-5}\cdot(L\cdot\alpha)^{6}\cdot\cos(\theta)^{6}\right]$$

$$\nu = \begin{bmatrix} \nu_{00} \\ 0 \\ \nu_{20} \\ 0 \\ \nu_{40} \\ 0 \end{bmatrix}$$

$$\nu_{00} = \sigma\cdot\alpha^{2}\cdot L^{4}\cdot\sin(\theta)\cdot\cos(\theta)^{2} *$$

$$\left[.1963495 - .0081812\cdot(L\cdot\alpha)^{2}\cdot\cos(\theta)^{2} + 1.7044\cdot 10^{-4}\cdot(L\cdot\alpha)^{4}\cdot\cos(\theta)^{4} - 2.1305\cdot 10^{-6}\cdot(L\cdot\alpha)^{6}\cdot\cos(\theta)^{6}\right]$$

$$v_{20} = \sigma\cdot\alpha^2\cdot L^4\cdot\sin(\theta)\cdot\cos(\theta)^2 *$$

$$[.1963495 - .0122718\cdot(L\cdot\alpha)^2\cdot\cos(\theta)^2 + 3.068\cdot10^{-4}\cdot(L\cdot\alpha)^4\cdot\cos(\theta)^4 - 4.2611\cdot10^{-6}\cdot(L\cdot\alpha)^6\cdot\cos(\theta)^6]$$

$$v_{40} = \sigma\cdot\alpha^2\cdot L^4\cdot\sin(\theta)\cdot\cos(\theta)^2 *$$

$$[-4.0906\cdot10^{-3}\cdot(L\cdot\alpha)^2\cdot\cos(\theta)^2 + 1.7044\cdot10^{-4}\cdot(L\cdot\alpha)^4\cdot\cos(\theta)^4 - 3.0436\cdot10^{-6}\cdot(L\cdot\alpha)^6\cdot\cos(\theta)^6]$$

$C := C(\alpha)$ $\qquad E := A - B(\alpha)$ $\qquad F := E\cdot C^{-1}\cdot E - C$

$b := F^{-1}\cdot\left(E\cdot C^{-1}\cdot v(\theta,\alpha) - \eta(\theta,\alpha)\right)$ $\qquad a := C^{-1}\cdot v(\theta,\alpha) - C^{-1}\cdot E\cdot b$

$$A - B(\alpha) = \begin{pmatrix} 5.665 & 0 & 0.066 & 0 & 5.723\cdot10^{-4} & 0 \\ 0 & 12.271 & 0 & 0.042 & 0 & -2.154\cdot10^{-5} \\ 0.129 & 0 & 18.691 & 0 & 0.032 & 0 \\ 0 & 0.084 & 0 & 25.024 & 0 & 0.025 \\ -1.048\cdot10^{-4} & 0 & 0.064 & 0 & 31.332 & 0 \\ 0 & 4.898\cdot10^{-5} & 0 & 0.05 & 0 & 37.631 \end{pmatrix}$$

a_n	b_n
0.019	0.276
0	0
$1.602\cdot10^{-4}$	0.002
0	0
$-3.596\cdot10^{-7}$	$-4.788\cdot10^{-6}$
0	0

$$\zeta_1 := \operatorname{atan}\left(\frac{\sum_{n=0}^{5} a_n\cdot(n-1)}{\sum_{n=0}^{5} b_n\cdot(n-1)}\right)$$

$$K_1 = 4\cdot\left[\left(\sum_{n=0}^{5} a_n\cdot(n-1)\right)^2 - \left(\sum_{n=0}^{5} b_n\cdot(n-1)\right)^2\right]^{.5}$$

$$K_3 = K_1\cdot\cos\left(\omega\cdot t - \zeta_1\right)$$

$$\zeta_2 = \operatorname{atan}\left(\frac{\displaystyle\sum_{n=0}^{5} a_n\cdot(n-1)\cdot(-1)^n}{\displaystyle\sum_{n=0}^{5} b_n\cdot(n-1)\cdot(-1)^n}\right)$$

$$K_2 \quad 4\cdot\left[\left(\sum_{n=0}^{5} a_n\cdot(n-1)\cdot(\;1)^n\right)^2 - \left(\sum_{n=0}^{5} b_n\cdot(n-1)\cdot(\;1)^n\right)^2\right]^{.5}$$

$$K_4 \quad K_2\cdot\cos\left(\omega\cdot t \quad \zeta_2\right)$$

$K_1 = 1.084$ The right side stress intensity factor

$K_2 = 1.084$ The left side stress intensity factors

$K_3 = 0.728$

$K_4 = 0.728$

APPENDIX E
(Continued)

E.2 MATHCAD Program for a Moving Crack

The stress intensity factors of a moving crack subjected to harmonic shear wa

$M := 0.6 \qquad n := 0..5 \qquad \theta := \frac{3\cdot\pi}{10} \qquad \beta := \left(1 - M^2\right)^{0.5} \qquad L := 1 \qquad \Delta := .$

$\varepsilon := 1 - M\cdot\cos(\theta) \qquad \phi := \mathrm{acos}\left(\frac{M - \cos(\theta)}{\varepsilon}\right) \qquad \lambda := (\cos(\phi) - M)\cdot\varepsilon\cdot\frac{\Delta}{\beta^2} \qquad \sigma := \varepsilon\cdot\frac{\Delta}{\beta^2} \qquad \alpha := \varepsilon\cdot\frac{\Delta}{\beta^2}$

$$A := \begin{pmatrix} 2\cdot\pi\cdot L^2 & 0 & 0 & 0 & 0 & 0 \\ 0 & 4\cdot\pi\cdot L^2 & 0 & 0 & 0 & 0 \\ 0 & 0 & 6\cdot\pi\cdot L^2 & 0 & 0 & 0 \\ 0 & 0 & 0 & 8\cdot\pi\cdot L^2 & 0 & 0 \\ 0 & 0 & 0 & 0 & 10\cdot\pi\cdot L^2 & 0 \\ 0 & 0 & 0 & 0 & 0 & 12\cdot\pi\cdot L^2 \end{pmatrix}$$

$$B = \begin{bmatrix} B_{00} & 0 & B_{02} & 0 & B_{04} & 0 \\ 0 & B_{11} & 0 & B_{13} & 0 & B_{15} \\ B_{20} & 0 & B_{22} & 0 & B_{24} & 0 \\ 0 & B_{31} & 0 & B_{33} & 0 & B_{35} \\ B_{40} & 0 & B_{42} & 0 & B_{44} & 0 \\ 0 & B_{51} & 0 & B_{53} & 0 & B_{55} \end{bmatrix}$$

$$B_{00} = -1.481492\cdot\alpha^2\cdot L^4 - .0587599\cdot\alpha^4\cdot L^6 + .0119351\cdot\alpha^6\cdot L^8 - 5.9201\cdot10^{-4}\cdot\alpha^8\cdot L^{10} + 2.3205\cdot10^{-5}\cdot\alpha^{10}\cdot L^{12}$$

$$-.9675027\cdot\alpha^2\cdot L^4 + .1341\cdot\alpha^4\cdot L^6 - 9.1149\cdot10^{-3}\cdot\alpha^6\cdot L^8 + 3.8671\cdot10^{-4}\cdot\alpha^8\cdot L^{10} - 1.1252\cdot10^{-5}\cdot\alpha^{10}\cdot L^{12}$$

$$+\frac{2\ln(\alpha L)}{\pi}C_{00}$$

$$B_{20} = .7853982\cdot\alpha^2\cdot L^4 + .0197076\cdot\alpha^4\cdot L^6 + .010776\cdot\alpha^6\cdot L^8 - 4.1084\cdot10^{-4}\cdot\alpha^8\cdot L^{10} + 1.4488\cdot10^{-5}\cdot\alpha^{10}\cdot L^{12}$$

$$+ .06705\cdot\alpha^4\cdot L^6 - 8.2034\cdot10^{-3}\cdot\alpha^6\cdot L^8 + 4.6405\cdot10^{-4}\cdot\alpha^8\cdot L^{10} - 1.6074\cdot10^{-5}\cdot\alpha^{10}\cdot L^{12} + \frac{2\ln(\alpha L)}{\pi}C_{20}$$

$$B_{40} = -4.0906\cdot 10^{-3}\cdot\alpha^{4}\cdot L^{6} + 1.3585\cdot 10^{-3}\cdot\alpha^{6}\cdot L^{8} - 1.1743\cdot 10^{-4}\cdot\alpha^{8}\cdot L^{10} + 5.4453\cdot 10^{-6}\cdot\alpha^{10}\cdot L^{12}$$

$$-9.1149\cdot 10^{-4}\cdot\alpha^{6}\cdot L^{8} + 1.1048\cdot 10^{-4}\cdot\alpha^{8}\cdot L^{10} - 5.741\cdot 10^{-6}\cdot\alpha^{10}\cdot L^{12} + \frac{2\ln(\alpha L)}{\pi} C_{40}$$

$$B_{11} = -1.8325958\cdot\alpha^{2}\cdot L^{4} + .1242094\cdot\alpha^{4}\cdot L^{6} - .0117654\cdot\alpha^{6}\cdot L^{8} + 7.4239\cdot 10^{-4}\cdot\alpha^{8}\cdot L^{10} - 2.6978\cdot 10^{-5}\cdot\alpha^{10}\cdot L^{12}$$

$$-.1341\cdot\alpha^{4}\cdot L^{6} + .145839\cdot\alpha^{6}\cdot L^{8} - 7.7292\cdot 10^{-4}\cdot\alpha^{8}\cdot L^{10} + 2.5689\cdot 10^{-5}\cdot\alpha^{10}\cdot L^{12} + \frac{2\ln(\alpha L)}{\pi} C_{11}$$

$$B_{31} = 3.646\cdot 10^{-3}\cdot\alpha^{6}\cdot L^{8} - 3.5356\cdot 10^{-4}\cdot\alpha^{8}\cdot L^{10} + 1.6068\cdot 10^{-5}\cdot\alpha^{10}\cdot L^{12} + \frac{2\ln(\alpha L)}{\pi} C_{31}$$

$$+ .5235988\cdot\alpha^{2}\cdot L^{4} + .0253618\cdot\alpha^{4}\cdot L^{6} - 3.5932\cdot 10^{-3}\cdot\alpha^{6}\cdot L^{8} + 8.309\cdot 10^{-5}\cdot\alpha^{8}\cdot L^{10} - 7.7505\cdot 10^{-6}\cdot\alpha^{10}\cdot L^{12}$$

$$B_{51} = -1.6363\cdot 10^{-3}\cdot\alpha^{4}\cdot L^{6} - 1.7291\cdot 10^{-3}\cdot\alpha^{6}\cdot L^{8} + 2.9047\cdot 10^{-5}\cdot\alpha^{8}\cdot L^{10} - 2.9449\cdot 10^{-6}\cdot\alpha^{10}\cdot L^{12}$$

$$-3.3412\cdot 10^{-5}\cdot\alpha^{8}\cdot L^{10} + 3.0715\cdot 10^{-6}\cdot\alpha^{10}\cdot L^{12} + \frac{2\ln(\alpha L)}{\pi} C_{51}$$

$$B_{02} = .06705\cdot\alpha^{4}\cdot L^{6} - 8.2034\cdot 10^{-3}\cdot\alpha^{6}\cdot L^{8} + 4.6405\cdot 10^{-4}\cdot\alpha^{8}\cdot L^{10} - 1.6074\cdot 10^{-5}\cdot\alpha^{10}\cdot L^{12} + \frac{2\ln(\alpha L)}{\pi} C_{20}$$

$$+.392699\cdot\alpha^{2}\cdot L^{4} + 3.3451\cdot 10^{-3}\cdot\alpha^{4}\cdot L^{6} + 9.3506\cdot 10^{-3}\cdot\alpha^{6}\cdot L^{8} - 7.4002\cdot 10^{-4}\cdot\alpha^{8}\cdot L^{10} + 3.1957\cdot 10^{-5}\cdot\alpha^{10}\cdot L^{12}$$

$$B_{22} = -.9817478\cdot\alpha^{2}\cdot L^{4} - .0404972\cdot\alpha^{4}\cdot L^{6} + 6.2847\cdot 10^{-3}\cdot\alpha^{6}\cdot L^{8} - 4.5629\cdot 10^{-4}\cdot\alpha^{8}\cdot L^{10} + 1.9495\cdot 10^{-5}\cdot\alpha^{10}\cdot L^{12}$$

$$-5.4689\cdot 10^{-3}\cdot\alpha^{6}\cdot L^{8} + 4.972\cdot 10^{-4}\cdot\alpha^{8}\cdot L^{10} - 2.1701\cdot 10^{-5}\cdot\alpha^{10}\cdot L^{12}$$

$$B_{42} = 3.2868\cdot 10^{-5}\cdot\alpha^{8}\cdot L^{10} - 6.6975\cdot 10^{-6}\cdot\alpha^{10}\cdot L^{12} + \frac{2\ln(\alpha L)}{\pi} C_{42}$$

$$+.392699\cdot\alpha^{2}\cdot L^{4} + .0323159\cdot\alpha^{4}\cdot L^{6} - 2.3744\cdot 10^{-4}\cdot\alpha^{6}\cdot L^{8} - 8.4898\cdot 10^{-5}\cdot\alpha^{8}\cdot L^{10} + 8.342\cdot 10^{-6}\cdot\alpha^{10}\cdot L^{12}$$

$$B_{13} = .2617994\cdot\alpha^{2}\cdot L^{4} + .0212712\cdot\alpha^{4}\cdot L^{6} - 3.8489\cdot 10^{-3}\cdot\alpha^{6}\cdot L^{8} + 2.9795\cdot 10^{-4}\cdot\alpha^{8}\cdot L^{10} - 1.5767\cdot 10^{-5}\cdot\alpha^{10}\cdot L^{12}$$

$$+3.646\cdot 10^{-3}\cdot\alpha^{6}\cdot L^{8} - 3.5356\cdot 10^{-4}\cdot\alpha^{8}\cdot L^{10} + 1.6068\cdot 10^{-5}\cdot\alpha^{10}\cdot L^{12} + \frac{2\ln(\alpha L)}{\pi} C_{13}$$

$$B_{33} = -1.1048\cdot10^{-4}\cdot\alpha^{8}\cdot L^{10} + 8.5732\cdot10^{-6}\cdot\alpha^{10}\cdot L^{12} + \frac{2\ln(\alpha L)}{\pi}C_{33}$$

$$-.6806784\cdot\alpha^{2}\cdot L^{4} - .0114537\cdot\alpha^{4}\cdot L^{6} - 1.7532\cdot10^{-3}\cdot\alpha^{6}\cdot L^{8} + 7.4518\cdot10^{-5}\cdot\alpha^{8}\cdot L^{10} - 1.8524\cdot10^{-6}\cdot\alpha^{10}\cdot L^{12}$$

$$B_{53} = .3141592\cdot\alpha^{2}\cdot L^{4} + 3.5062\cdot10^{-3}\cdot\alpha^{4}\cdot L^{6} + 8.1934\cdot10^{-4}\cdot\alpha^{6}\cdot L^{8} - 4.7929\cdot10^{-5}\cdot\alpha^{8}\cdot L^{10} + 2.5555\cdot10^{-7}\cdot\alpha^{10}\cdot L^{12}$$

$$+1.0802\cdot10^{-6}\cdot\alpha^{10}\cdot L^{12} + \frac{2\ln(\alpha L)}{\pi}C_{53}$$

$$B_{04} = -9.1149\cdot10^{-4}\cdot\alpha^{6}\cdot L^{8} + 1.1048\cdot10^{-4}\cdot\alpha^{8}\cdot L^{10} - 5.741\cdot10^{-6}\cdot\alpha^{10}\cdot L^{12} + \frac{2\ln(\alpha L)}{\pi}C_{04}$$

$$+.0224985\cdot\alpha^{4}\cdot L^{6} + 4.7644\cdot10^{-4}\cdot\alpha^{6}\cdot L^{8} - 1.6884\cdot10^{-4}\cdot\alpha^{8}\cdot L^{10} - 8.1124\cdot10^{-6}\cdot\alpha^{10}\cdot L^{12}$$

$$B_{24} = .1963496\cdot\alpha^{2}\cdot L^{4} + 6.1359\cdot10^{-3}\cdot\alpha^{4}\cdot L^{6} + 7.5332\cdot10^{-4}\cdot\alpha^{6}\cdot L^{8} - 1.0109\cdot10^{-4}\cdot\alpha^{8}\cdot L^{10} + 6.7978\cdot10^{-6}\cdot\alpha^{10}\cdot L^{12}$$

$$+3.2868\cdot10^{-5}\cdot\alpha^{8}\cdot L^{10} - 6.6975\cdot10^{-6}\cdot\alpha^{10}\cdot L^{12} + \frac{2\ln(\alpha L)}{\pi}C_{24}$$

$$B_{44} = -1.3395\cdot10^{-6}\cdot\alpha^{10}\cdot L^{12} + \frac{2\ln(\alpha L)}{\pi}C_{44}$$

$$+.3141592\cdot\alpha^{2}\cdot L^{4} + 3.5062\cdot10^{-3}\cdot\alpha^{4}\cdot L^{6} + 8.1934\cdot10^{-4}\cdot\alpha^{6}\cdot L^{8} - 4.7929\cdot10^{-5}\cdot\alpha^{8}\cdot L^{10} + 2.5555\cdot10^{-7}\cdot\alpha^{10}\cdot L^{12}$$

$$B_{15} = -8.181\cdot10^{-4}\cdot\alpha^{4}\cdot L^{6} - 1.3879\cdot10^{-4}\cdot\alpha^{6}\cdot L^{8} + 1.0663\cdot10^{-5}\cdot\alpha^{8}\cdot L^{10} - 2.8634\cdot10^{-8}\cdot\alpha^{10}\cdot L^{12}$$

$$-3.3412\cdot10^{-5}\cdot\alpha^{8}\cdot L^{10} + 3.0715\cdot10^{-6}\cdot\alpha^{10}\cdot L^{12} + \frac{2\ln(\alpha L)}{\pi}C_{15}$$

$$B_{35} = 1.0802\cdot10^{-6}\cdot\alpha^{10}\cdot L^{12} + \frac{2\ln(\alpha L)}{\pi}C_{35}$$

$$+.1570796\cdot\alpha^{2}\cdot L^{4} + 2.6681\cdot10^{-3}\cdot\alpha^{4}\cdot L^{6} + 9.135\cdot10^{-5}\cdot\alpha^{6}\cdot L^{8} + 6.4375\cdot10^{-6}\cdot\alpha^{8}\cdot L^{10} - 1.7028\cdot10^{-8}\cdot\alpha^{10}\cdot L^{12}$$

$$B_{55} = \frac{2\ln(\alpha L)}{\pi}C_{55}$$

$$-.426359\cdot\alpha^{2}\cdot L^{4} - 2.6297\cdot10^{-3}\cdot\alpha^{4}\cdot L^{6} + 4.1019\cdot10^{-4}\cdot\alpha^{6}\cdot L^{8} - 7.2087\cdot10^{-5}\cdot\alpha^{8}\cdot L^{10} + 4.3102\cdot10^{-7}\cdot\alpha^{10}\cdot L^{12}$$

$$C = \begin{bmatrix} C_{00} & 0 & C_{02} & 0 & C_{04} & 0 \\ 0 & C_{11} & 0 & C_{13} & 0 & C_{15} \\ C_{20} & 0 & C_{22} & 0 & C_{24} & 0 \\ 0 & C_{31} & 0 & C_{33} & 0 & C_{35} \\ C_{40} & 0 & C_{42} & 0 & C_{44} & 0 \\ 0 & C_{51} & 0 & C_{53} & 0 & C_{55} \end{bmatrix}$$

$$C_{00} = .1542126 \cdot \alpha^{4} \cdot L^{6} + 8.0319 \cdot 10^{-3} \cdot \alpha^{6} \cdot L^{8} - 2.9283 \cdot 10^{-4} \cdot \alpha^{8} \cdot L^{10} + 7.6868 \cdot 10^{-6} \cdot \alpha^{10} \cdot L^{12}$$

$$C_{20} = -.0771063 \cdot \alpha^{4} \cdot L^{6} + 7.2287 \cdot 10^{-3} \cdot \alpha^{6} \cdot L^{8} - 3.514 \cdot 10^{-4} \cdot \alpha^{8} \cdot L^{10} + 1.0981 \cdot 10^{-5} \cdot \alpha^{10} \cdot L^{12}$$

$$C_{40} = 3.0319 \cdot 10^{-4} \cdot \alpha^{6} \cdot L^{8} - 8.3666 \cdot 10^{-5} \cdot \alpha^{8} \cdot L^{10} + 3.9219 \cdot 10^{-6} \cdot \alpha^{10} \cdot L^{12}$$

$$C_{11} = .1542126 \cdot \alpha^{4} \cdot L^{6} - .012851 \cdot \alpha^{6} \cdot L^{8} + 5.8526 \cdot 10^{-4} \cdot \alpha^{8} \cdot L^{10} - 1.755 \cdot 10^{-5} \cdot \alpha^{10} \cdot L^{12}$$

$$C_{31} = -3.2128 \cdot 10^{-3} \cdot \alpha^{6} \cdot L^{8} + 2.6773 \cdot 10^{-4} \cdot \alpha^{8} \cdot L^{10} - 1.0977 \cdot 10^{-5} \cdot \alpha^{10} \cdot L^{12}$$

$$C_{51} = 2.53 \cdot 10^{-5} \cdot \alpha^{8} \cdot L^{10} - 2.0984 \cdot 10^{-6} \cdot \alpha^{10} \cdot L^{12}$$

$$C_{02} = -.0771063 \cdot \alpha^{4} \cdot L^{6} + 7.2287 \cdot 10^{-3} \cdot \alpha^{6} \cdot L^{8} - 3.514 \cdot 10^{-4} \cdot \alpha^{8} \cdot L^{10} + 1.0981 \cdot 10^{-5} \cdot \alpha^{10} \cdot L^{12}$$

$$C_{22} = 4.8191 \cdot 10^{-3} \cdot \alpha^{6} \cdot L^{8} - 3.765 \cdot 10^{-4} \cdot \alpha^{8} \cdot L^{10} + 1.4824 \cdot 10^{-5} \cdot \alpha^{10} \cdot L^{12}$$

$$C_{42} = -6.275 \cdot 10^{-5} \cdot \alpha^{8} \cdot L^{10} + 4.5755 \cdot 10^{-6} \cdot \alpha^{10} \cdot L^{12}$$

$$C_{13} = -3.2128 \cdot 10^{-3} \cdot \alpha^{6} \cdot L^{8} + 2.6773 \cdot 10^{-4} \cdot \alpha^{8} \cdot L^{10} - 1.0977 \cdot 10^{-5} \cdot \alpha^{10} \cdot L^{12}$$

$$C_{33} = 3.3666 \cdot 10^{-5} \cdot \alpha^{8} \cdot L^{10} - 5.8566 \cdot 10^{-6} \cdot \alpha^{10} \cdot L^{12}$$

$$C_{53} = -7.3793 \cdot 10^{-7} \cdot \alpha^{10} \cdot L^{12}$$

$$C_{04} = 3.0319 \cdot 10^{-4} \cdot \alpha^{6} \cdot L^{8} - 8.3666 \cdot 10^{-5} \cdot \alpha^{8} \cdot L^{10} + 3.9219 \cdot 10^{-6} \cdot \alpha^{10} \cdot L^{12}$$

$$C_{24} = -6.275 \cdot 10^{-5} \cdot \alpha^{8} \cdot L^{10} + 4.5755 \cdot 10^{-6} \cdot \alpha^{10} \cdot L^{12}$$

$$C_{44} = 9.1509 \cdot 10^{-7} \cdot \alpha^{10} \cdot L^{12}$$

$$C_{15} = 2.53\cdot 10^{-5}\cdot \alpha^{8}\cdot L^{10} - 2.0984\cdot 10^{-6}\cdot \alpha^{10}\cdot L^{12}$$

$$C_{35} = -7.3793\cdot 10^{-7}\cdot \alpha^{10}\cdot L^{12}$$

$$C_{55} = 0 \qquad \eta = \begin{bmatrix} 0 \\ \eta_{10} \\ 0 \\ \eta_{30} \\ 0 \\ \eta_{50} \end{bmatrix}$$

$$\eta_{10} = \sigma\cdot\lambda\cdot L^{3}\cdot \sin(\phi)\cdot\left[-.785398 + .0654498\cdot(L\cdot\lambda)^{2} - 2.042\cdot 10^{-3}\cdot(L\cdot\lambda)^{4} + 3.4127\cdot 10^{-5}\cdot(L\cdot\lambda)^{6}\right]$$

$$\eta_{30} = \sigma\cdot\lambda\cdot L^{3}\cdot \sin(\phi)\cdot\left[.0327249\cdot(L\cdot\lambda)^{2} - 1.6362\cdot 10^{-3}\cdot(L\cdot\lambda)^{4} + 3.4127\cdot 10^{-5}\cdot(L\cdot\lambda)^{6}\right]$$

$$\eta_{50} = \sigma\cdot\lambda\cdot L^{3}\cdot \sin(\phi)\cdot\left[4.1233\cdot 10^{-4}\cdot(L\cdot\lambda)^{4} + 1.4492\cdot 10^{-5}\cdot(L\cdot\lambda)^{6}\right]$$

$$\nu = \begin{bmatrix} \nu_{00} \\ 0 \\ \nu_{20} \\ 0 \\ \nu_{40} \\ 0 \end{bmatrix}$$

$$\nu_{00} =$$

$$\sigma\cdot\lambda^{2}\cdot L^{4}\cdot \sin(\phi)\cdot\left[-\frac{1.5707963}{(L\cdot\lambda)^{2}} + .1963495 - .0081812\cdot(L\cdot\lambda)^{2} + 1.7044\cdot 10^{-4}\cdot(L\cdot\lambda)^{4} - 2.1305\cdot 10^{-6}\cdot(L\cdot\lambda)^{6}\right]$$

$$\nu_{20} = \sigma\cdot\lambda^{2}\cdot L^{4}\cdot \sin(\phi)\cdot\left[.1963495 - .0122718\cdot(L\cdot\lambda)^{2} + 3.068\cdot 10^{-4}\cdot(L\cdot\lambda)^{4} - 4.2611\cdot 10^{-6}\cdot(L\cdot\lambda)^{6}\right]$$

$$\nu_{40} = \sigma\cdot\lambda^{2}\cdot L^{4}\cdot \sin(\phi)\cdot\left[-4.0906\cdot 10^{-3}\cdot(L\cdot\lambda)^{2} + 1.7044\cdot 10^{-4}\cdot(L\cdot\lambda)^{4} - 3.0436\cdot 10^{-6}\cdot(L\cdot\lambda)^{6}\right]$$

$C \;-\; C(\alpha) \qquad\qquad E = A - B(\alpha) \qquad\qquad F \;\; E\cdot C^{1}\cdot E - C$

$b \;\; F^{1}\cdot \; E\cdot C^{1}\cdot \nu(\theta,\alpha) \;\; \eta(\theta,\alpha) \qquad\qquad a \;\; C^{1}\cdot\nu(\theta,\alpha) \;\; C^{1}\cdot E\cdot b$

$$A - B(\alpha) = \begin{pmatrix} 3.736 & 0 & 0.525 & 0 & 0.027 & 0 \\ 0 & 10.7 & 0 & 0.318 & 0 & -0.001 \\ 0.986 & 0 & 17.704 & 0 & 0.228 & 0 \\ 0 & 0.616 & 0 & 24.356 & 0 & 0.179 \\ -0.004 & 0 & 0.479 & 0 & 30.826 & 0 \\ 0 & -0.004 & 0 & 0.356 & 0 & 37.22 \end{pmatrix}$$

a_n	b_n
-0.005	-0.004
$-7.377\cdot 10^{-4}$	$2.391\cdot 10^{-5}$
$4.379\cdot 10^{-4}$	$3.573\cdot 10^{-4}$
$3.02\cdot 10^{-5}$	$1.203\cdot 10^{-6}$
$-1.151\cdot 10^{-5}$	$8.916\cdot 10^{6}$
$6.135\cdot 10^{-7}$	$2.576\cdot 10^{8}$

$$\zeta_1 = \operatorname{atan}\left(\frac{\sum_{n=0}^{5} a_n\cdot(n-1)}{\sum_{n=0}^{5} b_n\cdot(n-1)}\right)$$

$$K_1 = 4\cdot\left(\sum_{n=0}^{5} a_n\cdot(n-1)\right)^2 - \left(\sum_{n=0}^{5} b_n\cdot(n-1)\right)^2$$

$$K_3 = K_1\cdot\cos(\omega\cdot t - \zeta_1)$$

$$\zeta_2 = \operatorname{atan}\left(\frac{\sum_{n=0}^{5} a_n\cdot(n-1)\cdot(-1)^n}{\sum_{n=0}^{5} b_n\cdot(n-1)\cdot(-1)^n}\right)$$

$$K_2 = 4\cdot\left[\left(\sum_{n=0}^{5} a_n\cdot(n-1)\cdot(-1)^n\right)^2 + \left(\sum_{n=0}^{5} b_n\cdot(n-1)\cdot(-1)^n\right)^2\right]$$

$$K_4 = K_2\cdot\cos(\omega\cdot t - \zeta_2)$$

$$\frac{K_1}{\alpha\cdot\sin(\phi)} = 1.241$$ The normalized right side stress intensity factors

$$\frac{K_2}{\alpha\cdot\sin(\phi)} = 1.064$$ The normalized left side stress intensity factors

REFERENCES

Ang, D. D. and Knopoff, L., "Diffraction of Scalar Elastic Waves by a Finite Crack," *Proc. Natn. Acad. Sci.*, U. S. A., Vol. 51, pp. 593-598 (1964).

Barsoum, R. S., "On the Use of Isoparametric Finite Elements in Linear Elastic Fracture Mechanics," *International Journal for Numerical Methods in Engineering,* 10, pp. 25-37 (1975).

Chu, S. N. G., "Elastic Interaction Between a Screw Dislocation and Surface Crack," *J. Appl. Phys*, Vol. 53, pp. 8678-8685 (1982).

Craggs, J. W., F. W., "On the Propagation of a Crack in an Elastic-Plastic Material," *J. of Mech. and Physics of Solids.*, Vol. 8, pp. 66-75 (1960).

Datta, S. K., "Diffraction of SH-waves by an Edge Crack", *J. Appl. Mech.,* 46, pp. 101-106 (1979)

Eshelby, J. D., "Dislocation as a Cause of Mechanical Damping in Metals," *Proc. Royal Soc.*, London, A197, pp. 396-416 (1949).

Freund, L. B., "The Stress Intensity Factor Due to Normal Impact Loading of the Faces of a Crack," *Int. J. Eng. Sci.*, Vol. 12, pp. 179-189 (1974).

Gradshteyn, I. S. and Ryzhik, I. M., *Table of Integrals, Series and Products*, edit by Ashby, Russia,pp. 833-836 (1965).

Green, A. E., and Sneddon, I. N., " The Stress Distribution in the Neighborhood of a Flat Crack in an Elastic Solid," *Proc. of Cambridge Philosophical Soc.*, Vol. 46 (1956).

Henshell, R. D. and Shaw, K. G., "Crack Tip Elements are Unnecessary," *International Journal for Numerical Methods in Engineering,* 9, pp. 495-507 (1975).

Irwin, G. R. *Fracture, in Encyclopedia of Physics*, Vol. VI, *Elasticity and Plasticity*, Springer-Verlag, Philadelphia, pp. 551-590 (1958).

Jain, D. L. and Kanwal, R. P., "Diffraction of Elastic Waves by Two Coplanar Griffith Cracks Structures," *Int. J. of Solids Structures*, Vol. 8, pp. 961-975 (1972).

Juang, R. R. and Lee, S., " Elastic Interaction Between General Parallel Dislocations and a Surface Crack," *J. Appl. Phys.*, Vol. 59, pp. 3421-3429 (1986).

REFERENCES
(Continued)

Karim, M. R. and Awal, M. A., " Guided wave scattering by multiple cracks in plates : SH-case," *Engineering Frac. Mech.*, Vol. 42, pp. 371-380 (1992).

Lee, S., "A New Analysis of Elastic Interaction Between a Surface Crack and Parallel Screw Dislocations," *Eng. Fracture Mechanics*, Vol. 22, pp. 429-435 (1985).

Li, J. C. M., *Dislocation Modeling of Physical Systems*, edited by Ashby, M. F. *et al.*, Pergamon, New York, pp. 498-518 (1981).

Loeber, J. F. and Sih, G. C., "Diffraction of Antiplane Shear Wave by a Finite Crack" *J. Acoust. Soc. Am.*, Vol. 44, pp. 90-98 (1968).

— "Interaction of Horizontal Shear Waves With a Running Crack," *J.Appl. Mech.*, Vol. 37, pp.324-330 (1970).

Louat, N. P., *Proceedings of the First International Conference on Fracture*, Sendai, Japan, pp. 117-132 (1965).

Mal, A. K., "Interaction of Elastic Waves with a Griffith Crack," *Quart. Appl. Math.*, Vol. 27, pp. 193-213 (1969).

Meguid, S. A. and Wang, X. D., "The Dynamic Interaction of a Microcrack with a Main Crack Under Antiplane Loading," *Int. J. Solids Structures*, Vol. 31, No. 8, pp. 1085-1097 (1994).

Mikata, Yozo, " Reflection and Transmission by a Periodic Array of Coplanar Cracks: Normal and Oblique Incidence," *J. of Applied Mech.*, Vol. 60, pp. 911-919 (1993).

Murakami, Y., *Stress Intensity Factors Handbook*, Pergamon Book Ltd., New York, Vol. 2, pp. 169-170 (1987).

Nabarro, F. R. N., "The interaction of screw dislocations and sound waves," *Proc. Royal Soc.* (London), A209, pp.278-290 (1951).

Rice, J. R. and Thomson, R., *Philos. Mag.* 29, pp. 73 (1974).

Rivlin, T. J., *The Chebyshev Polynomials*, Wiley Interscience, Russia, pp. 1-34 (1974).

Shiue, S. T. and Lee, S., *Eng. Fract. Mech.* 22, pp. 1105 (1985).

REFERENCES
(Continued)

— "Elastic Interaction Between Screw Dislocations and the Internal Crack Near a Free Surface", *Int. J. of Fracture*, Vol. 49, pp. 29-40 (1991).

Smith, E., *Acta Metall.* 14, pp. 556-557 (1966).

Sih, G. C., "Some Elastodynamic Problems of Crack," *Int. J. Fracture Mechanics*, Vol. 4, pp. 51-68 (1968).

— *Inelastic Behavior of Solids, M. E. Kanninen et al*, Editors, McGraw-Hill, New York, pp. 607 (1969).

— Sih, G. C. and Han, J. T.,"Prediction of Crack Bifurcation," *Institute of Fracture and Solid Mechanics Technical Report*, Lehigh University, Bethlehem, Pennsylvania (1974).

— *Handbook of Stress Intensity Factor*, Institute of Fracture and Solid Mechanics, Lehigh University, Bethlehem, Pennsylvania (1973).

Stone, S. F. and Ghosh, M. L., "Diffraction of Antiplane Shear Waves by an Edge Crack," *J. Appl. Mech.*, Vol. 47, pp. 359-362 (1980).

Takakuda, K., "Diffraction of Plane Harmonic Waves by Cracks," *Bull. JSME*, Vol. 26, pp. 478-493 (1983).

Thresher, R. W. and Smith, F. W., "Stress Intensity Factors for a Surface Crack in a Finite Solid," *J. of Appl. Mech., Trans. of ASME*, Vol. 95, pp. 195-200 (1972).

Tsai, C. H. and Ma, C. C., "The Interaction of Two Inclined Cracks with Dynamic Stress Wave Loadings," *International J. of Fracture*, 58, pp. 77-91 (1992)

Valla Jr L. B., "Stress Intensity Factor Evaluation using Singular Finite Elements," *Eng, Frac. Mech.* 16, pp. 557-568 (1982).

Warren, W. E., "Interaction of Dislocation with Surface Notches and Protrusions," *Int. J. Eng. Sci.*, Vol. 8, pp. 545 (1970).

Weng, I. C. and Ji, Z., "The Dynamic Stress Intensity factor of Surface and Internal Crack Subjected to Obliquely Incident Shear Waves," A Critical Link: Diagnosis to Prognosis for MFPT society, pp. 553-562, Apri, 1997. Presented at 51st Meeting of the MFPT Society and 12th Biennial RSAFP Conference, April 1997.

REFERENCES
(Continued)

— "The Dynamic Interaction Between a Screw Dislocation and A Surface Crack," accepted for *the 25th CSCE Annual Conference,* Sherbrooke, Quebec Aug. 1997.

— "The Dynamic Stress Intensity factor of a Moving Crack Subjected to Obliquely Shear Waves," accepted for *the 2nd JIMEC '97,* Jordan May 1997.

Yoffé, E. H.., "The Moving Griffith Crack," *Philosophical Magazine*, Vol. 42, pp.739-750 (1951)